UCLA
UCLA Electronic Theses and Dissertations

Title

Transcriptional Targets of CREB-Regulated Transcription Coactivator 1 (CRTC1) During Hippocampal Plasticity

Permalink

https://escholarship.org/uc/item/25z6v06g

Author

Bonanno, Shivan Luca

Publication Date

2018

Peer reviewed|Thesis/dissertation

UNIVERSITY OF CALIFORNIA

Los Angeles

Transcriptional Targets of CREB-Regulated Transcription Coactivator 1 (CRTC1) During

Hippocampal Plasticity

A dissertation submitted in partial satisfaction of the requirements for the degree Doctor

of Philosophy in Neuroscience

by

Shivan Luca Bonanno

2018

ABSTRACT OF THE DISSERTATION

Transcriptional Targets of CREB-Regulated Transcription Coactivator 1 (CRTC1) During

Hippocampal Plasticity

by

Shivan Luca Bonanno

Doctor of Philosophy in Neuroscience

University of California, Los Angeles, 2018

Professor Kelsey C. Martin, Chair

Synaptic plasticity, the change in number, position, and strength of synapses, requires

the synthesis of new cellular components that contribute to changes in synaptic composition,

and it has long-been appreciated that there is an important role for *de novo* transcription in the

maintenance of long-term potentiation (LTP). As plasticity-inducing signals are received at

synapses that can be hundreds of microns away from the cell's nucleus, which contains its

transcriptional machinery, a signal must be faithfully communicated from synapse to nucleus.

CREB-Regulated Transcription Coactivator 1 (CRTC1) acts as a retrograde signaling molecule

that travels from stimulated synapses to the nucleus, where it alters gene expression through

interactions with bZIP transcription factors such as CREB. CRTC1 has been shown to be

necessary for the maintenance of long-term potentiation in the hippocampus, and undergoes

dramatic and complex post-translational modifications that correlate with its nuclear transport

following synaptic activity. There is little known, however, about the transcriptional targets of

CRTC1 after plasticity-induction, and whether it may play a role in modulating specific programs

of gene expression during different types of long-term plasticity. To address this question, I first investigated the nuclear translocation of CRTC1 in response to different plasticity-induction protocols. Next, I optimized a Chromatin Immunoprecipitation-sequencing (ChIP-seq) protocol to investigate the genomic targets of CRTC1 following dihydroxyphenylglycine (DHPG)-induced long-term depression (LTD) in CA1 cells of the hippocampus, and found that CRTC1-containing protein complexes occupy loci including transcriptional start sites, promoters, enhancers, gene bodies, and intergenic regions. The genes associated with these loci include, but are not limited to, immediate-early genes, as well as other important neuronal genes. Finally, I conducted ChIP-seq and RNA-seq on a wider set of stimulations, including an LTP and a different LTD protocol in addition to control and DHPG-LTD samples. Data analysis for this work is ongoing and will allow correlation of transcript level with the genomic targets of CRTC1. Through this work emerges a clearer view of the genomic targets of CRTC1 during the induction of bidirectional synaptic plasticity in the hippocampus, as well as a modified protocol for conducting ChIP-seq from rodent adult brain tissue.

The dissertation of Shivan Luca Bonanno is approved.

Matteo Pellegrini

Felix Erich Schweizer

James Akira Wohlschlegel

Thomas J O'Dell

Kelsey C Martin, Committee Chair

University of California, Los Angeles

2018

This thesis is dedicated to my parents

Table of Contents

Figure Table of Contents

ACKNOWLEDGEMENTS

The composition of this thesis is dedicated to the many people who have supported and nurtured me, past and present in my life. Though I generally abstain from declarations of universal truth, I am certain that in every life there are difficult times. It is my belief that in the darkest nights, it is the love of those that care for us that supports us through to dawn. I have been extremely fortunate to be supported through my own struggles to be able to submit this work today.

In particular, I dedicate this work to my parents, without whom I very literally would not be here. Although through the course of an entire life, one may perhaps never fully understand all that has been done for them, I am grateful for the endless sacrifices my parents have made to enrich my life and to guide me towards integrity, goodness, and happiness. Both of them uprooted all familiarity and comfort to create a new life on the other side of the globe, and endured the hardships of their own lives with a grace that has inspired me to do my best in the face of my own.

The gifts I have received from my father are as tangibly relevant to a career in academic research as they are innumerable. His strength in the face of difficult circumstances and faith in his ability to produce good work without sacrificing ethicality are qualities I strive to uphold and improve in myself for the rest of my life. I owe my academic achievement, great or small, to my father's guidance from the time I was born. It was his endless personal sacrifice that ensured I received the best education I could, and that I believed I was capable of working through the

most taxing intellectual endeavors – it was his humility in his own work that inspired me and his constant engagement in my academic progress that gave me the discipline and endurance required to complete my education from elementary through graduate school. I am forever grateful for my father's guidance and support, financially and otherwise.

My mother remains the kindest and most compassionate person I have encountered in 29 years on this earth. Through my own journey, I have come to believe that these qualities are synonymous with love and therefore at the core of human existence. Like the moon, they may be impossible to discern through direct sunlight and the chaos of life that engulfs the world. But during the night, which comprises half of our lives, the moon provides our only conduit to the light of the sun, and she reflects it without failure. Like moonlight, kindness and compassion are reminders that love is eternal, and that when night inevitably returns in metaphor, their light is undeniable.

If it takes a village to raise a child, it takes at least a neighborhood to get a young adult through graduate school. In addition to my mother and father, I would like to thank my sister for her constant understanding and kindness, my parents' partners for their support, home-cooked meals, and caring through the years. I am deeply grateful for countless friendships, formed at times anywhere between childhood and yesterday, that have supported me, shown me kindness, and enjoyed life with me through many years, despite my disposition or "weather of the soul". I am also grateful, every day, for my girlfriend – for her love, which softens even the hardest days.

I would like to extend a deep and heartfelt thanks to my scientific mentors, past and present, for all they have taught me from molecular biology to navigating the human aspects of working as a scientist. A graduate student's advisor is always a unique mentor in their lives, and I count myself amongst the luckiest to have spent five years in Dr. Kelsey Martin's lab. At institutions of such high academic stature, it can be easily taken for granted that we are

surrounded by work of the highest quality. Dr. Martin upholds the very highest scientific rigor, and I have grown immensely in my time at UCLA, from philosophies of scientific approach to the technical, practical, and bureaucratic aspects of carrying out scientific research. Moreover, Dr. Martin is a beacon of grace and a testament, not unlike my father's, that achievement at the highest level does not preclude such precious human characteristics as kindness, compassion, patience, devotion, and *joie de vivre*. She is an inspiration to all that have the fortune of working with her, in the many different capacities in which she serves her communities, and I am deeply grateful for such a role model of integrity and passion for one's work.

I am grateful for the contributions of each of my thesis committee members to the maturation of my scientific approach and the refinement of the work presented in this thesis. I would like to thank Dr. James Wohlschelegl for his approachability, availability, and wisdom about the practical aspects of experiments and publication. I would like to thank Dr. Felix Schweizer for his constant open-door policy to welcome students and their struggles into his office for advice in lab and career-related matters, as well as his insights about synaptic signaling. I would also like to thank Dr. Matteo Pellegrini for joining my committee at a very late stage as I tackled next generation sequencing data analysis, for which he was so agreeable and helpful in providing me with expertise, collaborators, and confidence to fill the resources I lacked. Finally, I would like to extend a heartfelt thank you to Dr. Tom O'Dell, who welcomed me into his office repeatedly in my hours of desperation, and provided mentoring with humility and passion for research so unadulterated, it is woven into my heart as closely as any thread has ever been.

I would also like to thank the many lab members in the Martin Lab, past and present, who have taught me an invaluable toolset of scientific methods and provided deeply-appreciated lunch breaks, cookie breaks, ice cream breaks, coffee breaks, goofiness, laughter, and camaraderie. I would like to specifically thank Drs. Jenny McGrady-Achiro and Toh Hean

Ch'ng, both of whom provided understanding and support regarding the mental challenges of lab work as well as the practical, and sacrificed a great deal of their time to teach me experimental techniques with care.

In many ways, the completion of this work is built on the alignment of many fortunate circumstances from my undergraduate training until now, and I feel indebted to a universe that seems to coordinate people, places, and things, to nudge people along their journeys despite setbacks and challenges. Without the training I received at UC Berkeley as an undergraduate in Dr. Ehud Isacoff's lab, I would never have found my way into a career in science. His approachability, love for molecular neurobiology, and staggering charisma instilled in me a level of inspiration I thought impossible for a young and confused undergraduate. Several postdocs in the Isacoff Lab took me under their wing and nurtured me from scientific infancy to a functional and independent lab member. In particular, I want to thank Dr. Guillaume Sandoz for his creativity, passion for scientific discovery, confidence in navigating scientific and political environments, and holistic care for his friends and colleagues. Without Guillaume, I would never have learned half of my toolset in molecular biology or believed in my work enough continue its growth through challenging setbacks. Equally, I would like to thank Dr. Andreas Reiner for investing time and belief in me, given a sparse CV as a young undergraduate, and for trusting me to create important molecular biological reagents. Through his dedication to rigorous science and training students, Andreas taught me molecular biology and neurophysiology with German precision and patience that remains among the most precious gifts I have ever received.

Finally, I would like to reiterate a final "thank you" to everyone who has known and cared for me in any capacity, through the last six years at UCLA. Graduate school is a very challenging time and one friend referred to us as "weird creatures" after a few grueling years of lab work. Thank you to my friends, family, and colleagues for putting up with me, in so many

ways, through many years so that I can be here today and submit this thesis. I sincerely hope

that this chapter of my life gives rise to fruitful contributions and progress in this world, and my

deepest prayer is that I might pay forward all that has been done for me with love.

VITA

EDUCATION

University of California Berkeley, Berkeley, California   August 2007 – May 2011

B.A. in Molecular and Cellular Biology – Neurobiology   GPA: 3.318

RELEVANT WORK HISTORY

Ph.D. Candidate, UC Los Angeles   April 2013 – May 2018

Department of Biological Chemistry   *Dr. Kelsey Martin*

Staff Research Associate, UC Berkeley   April 2011 – May 2012

Department of Molecular and Cellular Biology   *Dr. Ehud Isacoff*

Undergraduate Researcher, UC Berkeley   April 2010 – August 2011

Department of Molecular and Cellular Biology   *Dr. Ehud Isacoff*

RESEARCH GRANTS/HONORS/SCHOLARSHIPS

NIMH F31 NRSA Fellowship (MH107210-01)   May 2015 – May 2018

PRESENTATIONS AND POSTERS

Poster: "Synaptically-generated changes in CRTC1 and its role in activity-dependent transcription"

- Society for Neuroscience conference, San Diego, CA, November 2016

Talk: "Transcriptional targets of CRTC1 during hippocampal plasticity"

- Synapse to Circuits journal club, UCLA, January 2018

PUBLICATIONS

1. Octeau JC, Chai H, Jiang R, Bonanno SL, Martin KC, Khakh BS. An optical neuron-astrocyte proximity assay at synaptic distance scales. *Neuron* **98**(1) 49-66 (2018).

Chapter 1

Introduction

The ability to learn is arguably the most important function of the brain, beyond its ability to control motor functions. We learn from the time we are born; we learn to crawl, walk, ride bikes, as well as academic material in school. In this sense, we think of "learning" as the encoding of new bits of information or behaviors in our brain, almost like little packets – in vernacular speech, one would say "I'm learning algebra" or "I'm learning to play the xylophone", and often imply an intentionality to learning. The molecular foundations of learning, however, reveal that it is a process that we do not always have supreme control over. Life experience is in a sense comprised of endless stimulation - some of which sticks, becomes associated with other things, and learned, and most of which does not. In many ways, learning processes are simply encoding or modifying a brain-representation of physical or non-physical phenomena that exist in the world, based on updated information. This capacity to learn is mediated by the neurons and circuits that develop into a functional brain by the time of birth; what is learned through life experience can be accessed and utilized at a later time to inform behavior, recalling information that is relevant to a present circumstance. Described in this way, it appears that the brain is a plastic holder of information that can be filled with information and "protocols" to help interpret present situations and appropriate responses, utilizing facts about the world around us and predicting outcomes – it seems like a system that eagerly awaits training. This is, in my view, a fair simplification. While the intricacies and implications may be up for debate, there is little debate that how we train our brains essentially defines our skillset – the things we are able and unable to compute, the behaviors we are able and unable to execute. But before diving into the molecular mechanisms that underlie the formation of memory, I want to draw attention to what I consider to be the humanistic implications of a plastic brain.

"Learning", per se, does not actually care about the truth – and it certainly doesn't care about right and wrong. Simply living and experiencing the world through time leads to the encoding of new information; whether an individual is purposefully isolated in a study booth memorizing flashcards, or whether they go to a coffee shop and order a coffee that makes them

feel ill, the brain is undergoing constant activity and small rearrangements in its wiring as it associates new information with causality. If this individual has never had coffee anywhere else and they drink a coffee that makes them ill, they may assume that coffee beans make them sick, when in fact there could simply be a disgruntled barista pouring concentrated broccoli extract into lattes in a misguided attempt at revenge against a particularly nasty customer. On a more positive note, if a student repeats the act of studying flashcards ten times, they are likely to remember the key concepts associated with the vocabulary words they are studying and recall them well when they take their exam. Whatever the molecular underpinnings of memory, they seem to create a system in which whatever a living thing is subjected to and ingrained in them, is likely to be learned and believed to be true. Depending on context and the brain in question, this could take only one or two times or hundreds. In any case, this brings attention to the fact that learning is not dependent on the information itself – a naïve subject can equally be taught that the Midwestern United States is largely agricultural or that it is inhabited by lizard aliens, if the teacher is trusted and their words believed. Discernment of truth, then, is not written into the molecular biology that underlies the fundamental process of learning; it is created through the analysis of new information against what is already known. We are at our own hands, and the hands of others, to create a world that can be trusted and that bears truth; we must be careful how we rewire our brains and those of others – with a humble acceptance that our control over what is put into us is limited, and our control over what we put out into the world is of utmost importance. In any case, the subtle (or sometimes drastic) rewiring and establishment of stable connections between neurons is the fundamental process that underlies information processing and learning in the brain, and the subject of this thesis.

The change in number, position, and strength of synapses between neurons, is termed "synaptic plasticity" and is the focus of many neuroscience research laboratories. It underlies learning and memory – even many processes that are not so clearly regarded as "conscious learning" in the sense that a mouse learns to find a submerged platform in a Morris water maze

3

or learns to associate a foot shock with particular cage decorations, all of which involve the changing of connections between neurons. These include the changing of receptive fields in developing animals whose sensory organs have been impaired[1,2,3,4,5] and subtle environmental perturbations that modify the brain states of animals[6] among many other phenomena. Pioneering investigations into the cellular mechanisms of synaptic plasticity were first conducted by Bliss and Lømo in the 1970s, showing that high frequency simulation (15 Hz for 10 seconds) is capable of potentiating of synapses between perforant path fibers and dentate granule cells in the hippocampi of anesthetized rabbits[7]. This phenomenon lasted for hours, and became known and long-term potentiation (LTP), the first electrophysiologically-described form of activity-dependent synaptic plasticity. These findings launched a flurry of investigations into the mechanisms of induction and maintenance of changes in synaptic strength, yielding major insights over the subsequent 45 years, but leaving many unanswered questions. Shortly after Bliss and Lømo's work, it was established that there are many forms of plasticity that can be induced in different ways, that utilize different intracellular mechanisms, and that trigger different consequences for the cell that expresses them. Most importantly, it was established that changes in synaptic strength can last from very short timescales (milliseconds) to very long ones (multiple days) and that plasticity is bidirectional; synapses can also be weakened, termed long-term depression (LTD). Though the molecular details of changes that give rise to these phenomena are vastly complex, they can be summarized as the alteration of synaptic composition, which yields synapses that are more or less responsive to stimulation. This requires modification of the number and type of crucial glutamate receptors on the postsynaptic membrane, many intracellular signaling molecules downstream of these receptors, and neurotransmitter release from presynaptic terminals. Some of these changes are achieved by degrading existing proteins or recruiting and repositioning them from other subcellular locations, but in order to support the longer timescales of some forms of plasticity, neurons require careful regulation of *de novo* gene expression. A brief overview of gene regulation in neurons reveals

that dynamic gene expression is crucial to the normal function of a neuron, and that acute changes in gene expression underlie its ability to adapt to, and maintain such adaptations to, extracellular signals.

Regulation of gene expression in neurons, CREB, and synaptic plasticity

Signaling between mature neurons, even outside the phenomenon of synaptic plasticity, is a vastly complex phenomenon. It requires the expression of genes that endow a neuron with appropriate membrane receptors, molecules that comprise intracellular signaling pathways, and a host of other proteins and RNAs that allow many levels of information processing between and within cells. Once neurons are properly formed and interconnected through development, with proteins targeted to specific subcellular locations, subcompartments created into mini functional domains, and poised to undergo electrochemical signaling, much of the gene expression profile changes from that of an immature neuron; there is no longer a great need for proteins that play important roles in processes like axon guidance and instead the cells require components that underlie adult neuron functions. Adult neurons, however, are far from static in gene expression. In fact, many decades of research have revealed that adult neurons undergo many levels of regulation of gene expression in order to achieve their remarkable capabilities. In the early 1980's, polyribosomes were discovered at the base of dendritic spines[8], and it was later shown that they participate in local translation to supply microdomains with *de novo* synthesized protein to properly fulfill demands of a dynamic microenvironment[9,10,11,12]. Local translation was found to be critical and sufficient for the expression of long-term facilitation (LTF) in *Aplysia Californica*[13] and later shown to play crucial roles in some forms of mammalian LTP (Kang & Schuman 1996, Kang et al. 1997, Bradshaw et al. 2003) and LTD (Huber et al. 2000). The translation of localized mRNAs provides a fast solution to provide new protein beyond what is available from pre-existing stores, yet even this is not enough to fully support a neuron's need for new gene products. In the 1990's, Uwe Frey and colleagues showed convincingly that

preincubating rat hippocampal slices with actinomycin-D (Act-D) to shut down *de novo* transcription did not interfere with the induction of LTP or its maintenance over short timescales, but caused significant degradation of LTP by approximately 5 hours post-induction[14]. Interestingly, incubating slices in Act-D after LTP induction did not lead to impaired LTP maintenance, suggesting that the synaptic stimulation quickly triggers transcription in the nucleus that supports LTP over very long timescales. These findings revealed a role for new gene transcription in the maintenance of LTP and motivated investigation into the molecular mechanisms and specific gene products necessary for the expression of plasticity.

Seminal work in this field was conducted in the laboratory of Eric Kandel, where it was shown that LTF underlying gill-sensitization in *Aplysia californica* relies upon cyclic adenosine monophosphate (cAMP) signaling, which impinges upon the cAMP response element-binding protein (CREB) to induce transcription of new genes. CREB-mediated transcription was shown to be necessary for long-term, but not short-term plasticity in *Aplysia*[15,16], and similar evidence was obtained in mammals[17,18]. Virally-mediated genetic manipulations of CREB function in medium spiny neurons of the nucleus accumbens showed that it promotes intrinsic neuronal excitability[19], and parallel studies in neurons of the locus coeruleus[20] and the amygdala[21] showed similar effects. In particularly important demonstrations to the work that follows in this thesis, it was shown that stimuli capable of inducing LTP at CA3-CA1 hippocampal synapses also induced robust cAMP-responsive element (CRE)-mediated gene expression in CA1 cells[22], and that the intrinsic capacity of CA1 neurons to undergo plasticity is greatly affected by CREB activity[23]. CREB is one of the most important of many transcription factors that binds as a dimer at CRE (5'-TGACGTCA-3'), half-CRE, or CRE-similar motifs. Through many years of research, converging data indicate that CREB is usually pre-bound to chromatin, where it rests and does not basally activate transcription[24,25]. Upon neuronal excitation and activation of particular types of G-protein Coupled Receptors (GPCRs), adenylyl cyclase (AC) stimulates production of cAMP, catalyzing dissociation of PKA catalytic subunits from regulatory subunits, with the

catalytic subunits undergoing translocation to the nucleus, where they phosphorylate chromatin-poised CREB at S133 within the kinase inducible domain (KID)[26]. Phosphorylation of S133 recruits CBP to acetylate nearby histones, and the CREB complex promotes recruitment of RNA Polymerase II (Pol II) and transcription. Such a strictly defined CREB signaling pathway, however, has been challenged by many studies, and phosphorylation of CREB may in fact recruit it to genomic loci at which it was not previously present[27]. It has also been shown that S133 regulation does not mediate non-cAMP-stimulated CREB expression[26]; its ability to induce transcription can also be modulated by calcium, a host of kinases sensitive to many factors[28,29], and receptor tyrosine kinases[30]. Moreover, decades of research since the discovery of activity-dependent CREB-mediated gene expression have now revealed that its regulation of transcription is a far more complex process than originally appreciated and involves the concert of many interacting proteins, each of which bears its own important levels of regulation.

Some calculations have estimated over 10,000 CRE sites in the mammalian genome[31], a number too large to presume that CREB interacts with each location in all cell types. This is, of course, dramatically and effectively reduced by alternative chromatin states in different cell types; stretches of DNA containing CRE-regulated genes relevant to hepatic cells will be exposed in hepatic cells, though many of these stretches may be occluded in neurons where there is no need for the genes contained within. The alternative exposure of genetic material in different cell types is obviously not a direct modulation of CREB activity, yet it greatly influences CREB's ability to bind and activate different genes – this probably explains a good portion of how the thousands of putative CRE sites are reduced to a smaller functional subset in a given cell. Further investigations into the specificity of CREB targeting within single cells types, however, and its regulation by a spectrum of different factors, have revealed that its binding to DNA and transcriptional activity may be directly regulated at many levels within a given cell and respond dynamically to different signals.

The CREB gene itself contains 11 exons, alternatively spliced to yield CREBα, CREBΔ, or CREBβ - with the α isoform predominant (and the subject of all previous and subsequent studies mentioned here), though all are ubiquitously expressed in all tissues and several tissue-specific isoforms also exist[32]. Though not the primary focus of work discussed in this thesis, it bears mentioning that CREB-related genes such as cAMP-Regulated Element Modulator (CREM) and Activating Transcription Factor-1 (ATF-1) are highly similar in primary structure to CREB and play modulatory roles in activating or repressing transcription at CRE sites as well, through direct binding to DNA, imposing an important and complex level of regulation to CRE-containing promoters and enhancers. As mentioned earlier, initial hypotheses included regulation of CREB-DNA interaction through post-translational modification (PTM) of CREB, most notably S133, though *in vitro* gel-mobility studies indicated that CREB phosphorylation does not significantly alter its ability to bind naked DNA[33]. Earlier studies, however, observed increased affinity for certain CRE-sites with phosphorylation[34], though in either case it did not seem that PTM of CREB could fully explain the regulation of its transcriptional activity. CREB binds to DNA as a dimer, where both dimerization and DNA-binding are mediated through its C-terminal basic leucine zipper (bZIP) domain[35]. The presence of a bZIP domain places CREB within a broad family of bZIP transcription factors, including ATF1, CREM, c-Jun, c-Myc, c-Fos, and C/EBP. CREB, CREM, and ATF-1 have been found to heterodimerize at CRE sites *in vitro* and in cell lines[36], and it has been postulated that binding of CREB to distinct bZIP-containing partners may modulate the duration of its transcriptional activity at particular sites. Though the canonical view of basally-poised CREB, PKA-mediated phosphorylation at S133, and CBP recruitment leading to transcriptional activation remains an important aspect of CREB signaling, evidence that CREB interacts with other proteins to regulate various aspects of its activity at different genomic targets brings us to a new picture of CREB-dependent transcription. It is likely that CREB-mediated gene

expression integrates convergent signaling pathways through its post-translational modification and interaction with distinct binding partners to dynamically activate and repress different genes with different durations of transcriptional activation.

Identification of CRTCs as modulators of CREB activity

Through the aforementioned studies, it became clear that CREB is regulated through its direct interaction with other proteins. In fact, the previous picture of CREB as a stand-alone transcription factor regulated mostly through phosphorylation of a single residue left holes in our understanding of CREB-mediated transcription, though until recently there was no convincing evidence of any single protein that plays a major role in modulating CREB activity. An early study employing a high-throughput screen of nearly 21,000 cDNA clones to identify proteins that modulate an IL-8 promoter-luciferase construct (a cAMP-inducible promoter) revealed a new family of transcriptional modulators[37], originally termed Transducers Of Regulated CREB (TORCs) and later renamed as CREB-Regulated Transcription Coactivators (CRTCs). CRTCs were found to potentiate CRE-element-mediated transcription by up to 1500-fold. This study identified a family of three CRTC family members in mammals, defined a transactivation domain of CRTC1 responsible for its potentiation of CREB-mediated transcription, and established a functional CRTC homolog in drosophila. The Iourgenko et al (2003) study thus paved the road for over a decade of research that has established CRTCs as important modulators of CREB in many cell types, including neurons.

The CRTCs were first described in molecular detail by Marc Montminy and colleagues researching insulin and glucagon-mediated metabolic signaling and their regulation of transcription in pancreatic β-islet and hepatic cells. They showed that intracellular increases in calcium/cAMP levels caused translocation of CRTC1, 2, and 3 from cytoplasm to nucleus of many different cell types, regulating their interaction with CREB[38,39,40]. Through luciferase assays conducted in Human Embryonic Kidney (HEK) cells, they showed that CRTC1

translocation was capable of dramatically potentiating expression of a CRE-driven reporter, that this could be recapitulated by mutating a key residue (S151) to a phospho-incompetent alanine that rendered CRTC1 constitutively nuclear in HEK cells, and that transcriptional activity of the luciferase construct could be shut down by co-expression of an inhibitory form of CREB[41]. These initial studies established the basic behavior of the CRTC family of proteins. CRTCs are sequestered in the cytoplasm at rest in a highly phosphorylated state. Increases in intracellular calcium and cAMP trigger CRTC dephosphorylation and translocation to the nucleus, where CRTC binds CREB to activate expression of target genes. These findings stimulated studies that elucidated further details of CRTC signaling.

CRTC1 is predicted to be an intrinsically disordered protein. The Pymol Protein structure prediction software predicts that CRTC1 is 96% unstructured, with only one predicted primary structural component--an alpha helix corresponding to the CREB-binding domain (CBD). XStalPred crystallization prediction software (Slabinski et al. 2009, Jaroszewski et al. 2008, Jahandideh et al. 2014) also predicts that CRTC1 is nearly impossible to crystallize, due to its disordered primary structure, which raises interesting questions about the regulation of its structure, PTM, and binding to other proteins. In accordance with such predictions, a structural study of CRTC2 employing x-ray crystallography and circular dichroism found that the CBD is a 28-residue helix responsible for its interaction with the bZIP domain of CREB. This CBD peptide/CREB/DNA complex was found to exist in 2:2:1 stoichiometry, consistent with one molecule of CRTC2 bound to one molecule of CREB within a CREB homodimer, and exhibits micromolar affinity on palindromic and variant half-site CREs *in vitro*[42]. Interestingly, mutating residues in the bZIP interface between CRTC2 and CREB disrupted their interaction, but did not disrupt CREB-DNA binding, consistent with the view of pre-chromatin-bound CREB whose transcriptional activity could be activated by binding of a transcriptional co-activator. Structural studies of CRTC1 have been hindered by its intractability for classical assays such as

crystallography, though the behavior of CRTCs across many cell types has been, and continues to be investigated in great detail.

The CRTC family of proteins, from *C. elegans* to *Drosophila melanogaster* to mammals, behave in a similar fashion: dephosphorylation of cytoplasmic CRTC leads to its translocation to nuclei, where it potently activates transcription. By now, a large body of literature has established that CRTC-mediated transcription is crucial in many cell types and that its dysregulation can lead to severe phenotypes. This is perhaps best illustrated in peripheral tissues involved in glucose homeostasis, a process that is underscored by transcriptional regulation of several factors that control circulating glucose levels. Chronic CRTC2 activation in hepatic cells through mutation of S171 and S245 to alanine leads to elevation of circulating glucose and insulin resistance[43]. *Crtc1*^{-/-} knockout mice are hyperphagic, obese, and infertile; in wild-type mice, leptin causes dephosphorylation of CRTC1 in hypothalamic neurons and induces expression of *Cartpt* and *Kiss1* genes, which encode neuropeptides that mediate leptin's effects on appetite and fertility[41]. In adipocytes, β-adrenergic receptor activation stimulates CRTC3 translocation, upregulating *Rgs2* expression, which inhibits AC activity and promotes obesity[39]. Though regulation of metabolism is linked to many other processes in the body, it is somewhat remarkable that CRTCs are so important across so many distinct cell types; even macrophage polarization is induced by paracrine hormone prostaglandin E2 (PGE2) through CREB/CRTC2/3[44]. Recently, it has been shown that germline knockout of CRTC2 and 3 mice are embryonic lethal, but that a single allele of either restores viability, and that the two proteins are involved in modulating bone marrow hematopoiesis[45]. In *C. elegans,* decreasing CRTC-1 activation by AMPK or calcineurin increases lifespan[46], and CRTC activation in *Drosophila* neurons induces production of short Neuropeptide F (sNPF), which is secreted by neurons and diffuses to enteric cells to increase their resistance to starvation[47]. Finally, particular and curiously common genetic mutations involving fusion of CRTC1 to MAML2 results in cancer, underscoring the ability of CRTC to alter gene transcription[48]. These findings all

situate CRTC as a crucial mediator of gene expression linked to highly important processes that span many cell types and functions. Though many of the aforementioned studies have included investigation of CRTC behavior in neurons of various subtypes, none have systematically defined CRTC regulation and function in neurons.

CRTC1 in neuronal signaling

A handful of studies have investigated the molecular details of CRTC signaling in the brain. CRTC1 is the predominant isoform present in the adult mammalian forebrain, including the hippocampus, and in fact CRTC2 and 3 are virtually absent from these brain regions[49]. At rest and in silenced neurons, in both adult brain tissue and cultured cortical and hippocampal neurons, CRTC1 is largely excluded from the nucleus. In cultured neurons, CRTC1 colocalizes with PSD95 puncta, indicating that it is localized to synapses, where it colocalizes with 14-3-3ε proteins[50,51]. Biochemical studies show that synaptically localized CRTC1 is highly phosphorylated. Upon synaptic stimulation and increases in intracellular calcium, CRTC1 is dephosphorylated by calcineurin, releasing it from 14-3-3ε followed by translocation to the nucleus. This can be blocked by chelating intracellular calcium with BAPTA-AM, or by incubating cells with cyclosporin A (CsA) to inhibit protein phosphatases (predominantly calcineurin). CRTC1 nuclear accumulation is also mediated by increases in cAMP that activate PKA, causing it to phosphorylate and deactivate SIK1/2, thus preventing the rephosphorylation of CRTC1, which is required for CRTC1 nuclear export. This suggests that CRTC1 is constantly in a state of dynamic nuclear import/export balance, and that signaling that pushes the system toward one side or the other results in different amounts CRTC1 translocating to the nucleus, for different periods of time – a finding corroborated by experiments in which blockage of nuclear export by leptomycin B was sufficient to cause CRTC1 nuclear accumulation[50]. Perhaps most fascinatingly of all, CRTC1 undergoes massive shifts in PTM in response to neuronal signaling,

as evidenced by 1 and 2-dimensional polyacrylamide gel electrophoresis experiments that reveal multiple CRTC1 species with distinct mobilities and distinct isoelectric points. Incubation of cell lysates with phosphatase results in a massive drop in PTM electrophoretic mobility and collapse to a few distinct species that migrate to high isoelectric point and low (~50kDa) molecular weight, indicating many of the different CRTC1 species may be defined by differential phosphorylation. As CRTC1 is a potent transcriptional coactivator, it is tempting to hypothesize that different stimulations lead to differential CRTC1 PTM-states that endow the protein with different capabilities to bind different interacting proteins. This may, in turn, redirect its transcriptional activity in the nucleus and provide a way to diversify the transcriptional output of a single protein.

Though many of the molecular signaling events that act upon CRTC1 have been worked out through molecular biology, there is still much to be appreciated about convergent and interacting pathways that undergo important signaling in neurons. In cultured neurons, pCREB rises and stays elevated from 0 to 360 minutes post KCl-depolarization, though CRTC1 nuclear accumulation peaks at 60 minutes, and then reduces significantly to a slightly-elevated level for the rest of the 360 minutes[52]. KCl also induces expression of *Sik1* mRNA, which could act as a negative feedback loop, in which newly synthesized SIK1 rephosphorylates CRTC1, kicks it out of the nucleus, and halts its transcriptional activity. This could then be dampened by coincident elevations in cAMP that restrict SIK1 activity, even if new protein is generated. Such a dynamic process is difficult to study in a highly controlled system; even in cultured neurons both calcium and cAMP are regulated by a vast number of processes. In any case, convergent pathways that influence the behavior of CRTC1 in the nucleus clearly exist. As with many molecular biological studies, investigation of the role of CRTC1 in neuronal signaling and plasticity has been investigated from the "top-down" of plasticity induction and the "bottom-up" of molecular pathways.

Several studies have shown that CRTC1 signaling is important for the maintenance of LTP in hippocampal slices and for modulating memory salience. One study used recombinant dominant negative CRTC1 protein fused to an 11-arginine peptide to facilitate cellular uptake, and showed that this degraded LTP maintenance by 90 minutes post-LTP induction[53], while another lab used virally transduced dominant negative CRTC1 to show a similar effect[54]. The latter study also showed that supplying excess CRTC1 through viral overexpression lowered the electrical threshold for LTP induction, while another study showed similar results *in vivo* using virally-mediated increase in CRTC1 expression to increase memory strength without compromising quality[55]. Though there are experimental concerns with these studies – 11-arginine recombinant proteins are known to sometimes have off-target effects[56] and dominant-negative forms of CRTC1 were not extensively validated in any of these studies – collectively they suggest that CRTC1 signaling is important for the maintenance of hippocampal plasticity, and may play a part in the transcriptional dependence identified by Frey at colleagues in 1996. Accordingly, CRTC activation in *drosophila* mushroom body neurons leads to a significant increase in long-term olfactory memory[57,58], and a very recent study in mice suggests that CRTC1 nuclear translocation in the hippocampus and amygdala following induction of fear memory modulates memory strength through rearrangements of chromatin complexes[59]. Taken together, these studies motivate a deeper examination of CRTC1 and its role in neuronal plasticity.

It has long been appreciated that there is a missing link between the induction of synaptic plasticity – which happens through particular patterns and types of synaptic signaling at synapses themselves, very distal to the cell body – and changes in transcription that occur in the nucleus. As mentioned in detail earlier, a signal must be communicated from synapse to nucleus to trigger changes in gene expression, and none of the "classical" forms of neurobiological signal transduction, such as changing 2nd messenger concentrations, electrochemical signaling, or regenerative calcium waves contain information about the synapse

from which plasticity was induced. While induction of plasticity at a single or a set of synapses may trigger global changes that affect all synapses on the cell, there must still be a way of informing the nucleus of the type of plasticity-inducing signal that was received, and perhaps of which synapse was responsible for this signal. Thus, a role for proteins that translocate from synapse to nucleus is highly appealing. Such proteins could carry information about their synapse of origin, could encode information about the type of plasticity induced by virtue of their electrostatic identity, and are capable of directly influencing transcription through binding of different factors in the nucleus. CRTC1 is a prime candidate to fill this role. It is known to couple extracellular signals to CREB-mediated transcription (a protein whose transcriptional activity is highly important in plasticity) in many cell types, it localizes to inactive synapses and is undergoes nuclear translocation in response to synaptic activity, and its structure bears an extraordinary capacity to encode information through its PTM. Thus, my thesis work has focused on mapping the types of plasticity-inducing stimuli that drive CRTC nuclear translocation, and on determining whether these stimuli differentially regulate CRTC1 binding to protein complexes to drive transcription of different genes, each which, in turn, could support the expression of different forms of synaptic plasticity.

Chapter 2

CRTC1 exhibits modular responses to different neuronal stimulations in cultured neurons

Introduction

At rest and in TTX-silenced cultured neurons, CRTC1 is mostly excluded from the nucleus and peri-nuclear cytoplasm. It instead fills dendrites and colocalizes with PSD95 puncta, where it is highly phosphorylated and tethered to 14-3-3ε proteins that interact with key phosphorylated residues in CTRC1[50,51]. Upon synaptic stimulation, calcium influx triggers binding of calmodulin (CaM), to the phosphatase calcineurin (CaN). This activates CaN to dephosphorylate CRTC1, releasing it from 14-3-3ε and allowing its retrograde transport from the activated synapse to the nucleus (Fig. 1). This process can be blocked by chelating intracellular calcium with BAPTA-AM, or by incubating cells with cyclosporin A (CsA) to inhibit calcineurin (and other phosphatases). Salt inducible kinases (SIK) can rephosphorylate CRTC1, promote its nuclear export, and oppose the effects of CaN. As the nucleocytoplasmic localization of SIK1 and 2 are themselves regulated by cAMP levels through phosphorylation and inactivation by PKA (with elevated intracellular cAMP promoting nuclear exclusion of SIK1 and 2), the nuclear occupancy of CRTC1 is dynamically regulated by multiple signaling modalities. This suggests that CRTC1 is constantly in a state of dynamic nuclear import/export balance, and that signaling that pushes the system toward one side or the other results in different amounts and durations of nuclear CRTC1 occupancy.

Perhaps most fascinating of all, CRTC1 undergoes massive shifts in post-translational modification (PTM) in response to neuronal signaling, as evidenced by 1 and 2-dimensional gel electrophoresis, which reveals that CRTC1 resides in multiple species that differ in electrophoretic mobility and in their isoelectric point. Treatment of cell lysates with phosphatase results in a massive drop in PTM electrophoretic mobility and collapses CRTC1 to a few distinct species that migrate to high isoelectric point and low (~70kDa) molecular weight on 2D gels, indicating many of the different CRTC1 species may be defined by differential phosphorylation (Fig. 2). Moreover, phosphatase-treated lysates collapse the panel of different CRTC1 species

observed in response to BIC or FSK to 3 distinct species at high isoelectric points; this also suggests that other modifications may also play a role in CRTC1 PTM state. As CRTC1 is a potent transcriptional coactivator[41], it is tempting to hypothesize that different stimuli lead to differential CRTC1 PTM-states that endow the protein with different electrostatic profiles, and that these distinct profiles dictate differential binding to interacting proteins, including different transcription factors in the nucleus. This may, in turn, dictate its ability to modulate transcriptional activity and provide a way to diversify the transcriptional output of a single protein. This principle has been shown for another synaptonuclear signal, Jacob, where ERK-mediated phosphorylation at S180 determines its influence on transcription in the nucleus; nuclear translocation of dephosphorylated Jacob from extrasynaptic sites leads to upregulation of cell death pathways while nuclear translocation of phosphorylated Jacob originating from synaptic sites promotes cell survival and enhancement of synaptic activity[60]. Similarly, the synaptic information received by a neuron may be encoded in the PTM state of CRTC1 and decoded at the nucleus to enable dynamic transcriptional responses by virtue of differential binding to transcriptional regulators.

Previous studies of activity-dependent nuclear translocation of CRTC1 in cultured neurons utilized bicuculline (BIC), a gamma-amino-butyric-acid A receptor (GABA$_A$R) channel blocker known to drive excitatory activity in cultured neurons by blocking inhibition. Researchers have favored this stimulation in recent years as it relies on pre- and postsynaptic activation of the preformed synaptic architecture in the dish and drives excitatory synaptic activity. In many cases, this is preferable over other ways of activating synapses, as most of those involve directly targeting and activating only certain types of postsynaptic receptors or global depolarization, which cause a myriad of intracellular changes that confound those that are truly dependent upon synaptic transmission. Most synapses harbor both α-amino-3-hydroxy-5-methyl-4-isoxazolepropionic acid (AMPA) and N-methyl-D-aspartate (NMDA) glutamate receptors (AMPAR/GluA's and NMDAR/GluN's, respectively) as well as various G-

18

protein-coupled receptors (GPCRs) and calcium channels. The composition and positioning of synaptic proteins, then, plays a large role in dictating the snapshot of intracellular calcium and other second messenger concentrations that changes in response to synaptic activation at a given synapse. In the context of BIC, synapses of different compositions will be activated repeatedly by dramatic action AP induced by the relief of GABAergic inhibition. As these synapses are variable in strength and composition, one synapse may experience a large increase in intracellular calcium and activate sufficient CaN to dephosphorylate all adjacent CRTC1, while another synapse may receive weaker activation and leave local CRTC1 incompletely dephosphorylated or modified differently than at another given synapse. Moreover, there are probably many phosphatases and kinases that induce PTM of CRTC1 in addition to CaN and SIKs, and their abundance at a particular synapse, dendrite, or the nucleus may affect the PTM state of CRTC1 molecules there. This is all to say that when cultured neurons are stimulated by increasing neuronal excitability, the heterogeneity of synapse composition leads to a heterogeneous representation of CRTC1 PTM states. This may explain the smear of CRTC1 immunoreactivity (IR) on a western blot (WB) loaded with a lysate from neurons that have been stimulated heterogeneous synaptic activation.

In order to probe the specific receptors involved in CRTC1 signaling, subsequent studies utilized specific pharmacological agonists and antagonists to study the regulation of CRTC1 nuclear translocation by different calcium sources and signaling modalities. Blocking NMDARs with APV or MK-801 prevents synaptonuclear translocation of CRTC1[50,51], though specifically blocking GluN2B-containing NMDARs with ifenprodil actually increased the amount of CRTC1 found in the nucleus following NMDA application. Of note, ifenprodil also triggers significantly greater CREB phosphorylation at S133 than does NMDA alone, suggesting that activation of GluN2B receptors opposes the action of other NMDAR subtypes that promote CRTC1 and CREB activation[51]. Interestingly, blocking NMDARs with APV greatly reduced, but did not completely prevent BIC-induced CRTC1 translocation, indicating that AMPA receptors also

contribute to CRTC1 nuclear translocation. AMPA accordingly induced robust nuclear

translocation that can be blocked by the AMPAR-blocker NBQX. More interestingly, blocking L-

type voltage-gated calcium channels (VGCCs) with nimodipine also reduced AMPA-mediated

CRTC1 translocation, suggesting that AMPARS produce sufficient synaptic depolarization to

open VGCCs and that calcium influx through these sources is sufficient to trigger CRTC1

nuclear translocation[51]. As AMPAR and NMDAR signaling are closely coupled (AMPAR-

mediated synaptic depolarization contributes to calcium flux through NMDARs), it follows that

CRTC1 nuclear translocation may be regulated by a dynamic interplay between the two

glutamate receptor subtypes and the effects their activation exert on other signaling molecules

and channels at synapses.   In support of this view, preincubating neurons with NBQX greatly

reduced the NMDA-induced nuclear translocation of CRTC1, though this effect is abrogated by

reducing Mg^{2+} in the extracellular medium and artificially relieving the depolarization-

requirement for NMDAR channel opening (Ch'ng et al. 2015).

This work laid the foundation for the dissection of different synaptic signals that induce

CRTC1 synaptonuclear trafficking and persistence in the nucleus. Such signals likely integrate

several signaling pathways, many of which are highly complex themselves. Such multiple-

pathway integration has already been observed for CRTC2, which integrates hormone and

energy-sensing pathways to determine its phosphorylation status and thus its CREB-mediated

activation of hepatic gene expression[40] or to regulate incretin hormones and glucose to promote

pancreatic β-cell survival[61]. CRTC1 likely exhibits similar multi-pathway integration in neurons,

reflecting the complexity and constant regulation of neuronal responses to extracellular signals;

increasing cAMP levels leads to SIK phosphorylation and inactivation by PKA, but PKA also

targets AMPARs to increase their conductance[62], which in turn may depolarize a synapse

sufficiently to increase the probability of NMDAR opening. Intracellular calcium concentrations

are tightly regulated at both local and global levels as well, and can be affected by extracellular

calcium influx through glutamate receptors, VGCCs, intracellular calcium stores, intracellular

20

calcium-binding proteins, and other factors[63]. In fact, such complex calcium regulation has long

been appreciated to dynamically affect gene expression[64,65,66,67] and the sensitivity of CRTC1 to

multiple pathways of calcium influx may contribute to the dynamic coupling between stimulation-

induced calcium signaling and transcription.

Stimuli that induce plasticity in dissociated neuronal cultures

Cultured neurons pose several advantages to adult brain tissue for many molecular

biological experiments, including many that I planned to pursue in the course of my thesis work,

and this has led researchers to develop several chemical induction protocols to study long-term

potentiation (LTP) and long-term depression (LTD) in culture. To design studies examining the

behavior of CRTC1 in response to the induction of plasticity, I reviewed published protocols and

selected several for my experiments (Table 1).

DHPG-LTD

Work by Kim Huber, Mark Bear, and colleagues established a particular form of protein-

synthesis-dependent LTD induced by dihydroxyphenylglycine (DHPG) activation of

metabotropic group I (mGluR1/5) receptors that is distinct from NMDA-LTD[68]. DHPG targets

group 1 mGluRs, which are coupled to G_q/G_{11} and activate phospholipase C (PLC), leading to

the conversion of phosphoinositol diphosphate (PIP_2) to diacylglycerol (DAG) and inositol

triphosphate (IP_3)[69]. IP_3 then acts on IP_3 receptors on the endoplasmic reticulum to mobilize

intracellular calcium stores, and DAG leads to activation of protein kinase C (PKC). However,

further research has revealed that group 1 mGluR activation can affect additional signaling

pathways, downstream of G_q as well as those stemming from $G_{i/o}$, G_s, and others that are

completely independent of G protein effectors. Depending on the cell type, group I mGluRs can

activate a range of downstream effectors[70], including phospholipase D, casein kinase 1, cyclin-

dependent protein kinase 5, Jun kinase, components of the mitogen-activated protein kinase

21

(MAPK)/extracellular receptor kinase (ERK) pathways, and the mammalian target of rapamycin (mTOR)/p70 S6 kinase pathway[71,72,73]. The regulation of MAPK/ERK is thought to be very important in the regulation of DHPG-induced synaptic plasticity[74,75] and although there remains much to learn about the intricacies and variety of intracellular events triggered by DHPG application, it is clear that DHPG application produces a robust depression of synaptic transmission in cultured neurons[76]. As it is a highly-cited protocol, results in robust LTD, and is significantly distinct from other forms of LTD, this is a very attractive candidate form of plasticity in which to study the role of CRTC1.

NMDA-LTD

Moderate concentrations of NMDA (usually in the tens of micromolar and most commonly 20uM) are capable of inducing robust depression of synaptic transmission in cultured neurons[77]. Although NMDA application triggers NMDAR opening, calcium influx, and triggering of signaling cascades with ease in neurons, properly-recorded LTD has only been published in a few highly controlled experiments employing several key details. Lu and colleagues conducted patch-clamp recordings of cultured neurons perfused with magnesium-free extracellular solution that contained TTX to block APs, strychnine (Strych) to block glycine receptors (GlyRs), and BIC. Under these conditions, baseline spontaneous events are greatly reduced in frequency and amplitude compared to uninhibited cultures, and the inhibitors play important roles to reshape the action of pharmacological agents intended to induce plasticity. The presence of Strych and BIC to shut down glycinergic and GABAergic inhibition, respectively, and TTX to shut down AP firing focuses Lu et al.'s use of 20uM NMDA/glycine for 3 minutes mostly upon NMDARs. The moderate glycine concentration to adequately bind the glycine co-agonist site and lack of magnesium to relieve depolarization-sensitivity of NMDARs ensures that NMDA is capable of inducing significant ion flux through the channels. As these cultures are grown in normal medium, and are used at 21 days in vitro (DIV), most synapses

contain NMDARs[78,79,80] and will be affected by this treatment. Synapses thus experience a

prolonged increase in intracellular calcium in response to the 3-minute NMDA-application. This

triggers molecular events leading to decrease in AMPAR-mediated currents, removal of

AMPARs from the cell membrane, and depression of mEPSC amplitude and frequency[77]. It is

important to note that in this scenario, researchers employ the use of a pharmacological agent

that exclusively targets postsynaptic receptors (though NMDA will activate both synaptic and

extrasynaptic receptors, irrespective of subunit composition) and that the NMDARs are held

open for the duration of the treatment. The presynaptic terminals are not directly affected by

NMDA application and the inclusion of TTX prevents triggering of action potentials (APs) and

evoked presynaptic neurotransmitter release. Given that this stimulation employs such a

commonly-used pharmacological agent (NMDA) that has been shown to induce LTD in many

circumstances[81] and is known to affect CRTC1 nuclear translocation[51], this is also a very

attractive protocol to study the role of CRTC1 during plasticity.

Gly-LTP

The glycine-LTP protocol was also established by Lu et al. in their 2001 Neuron

publication. This protocol calls for the same magnesium-free extracellular solution containing

TTX, Strych, and BIC, as NMDA-LTD but instead induces LTP with 200uM glycine for 3

minutes. This induction protocol requires careful consideration, especially with regards to

calcium dynamics. In this case, the high level of glycine is still prevented from activating GlyRs

by Strych, and acts primarily on NMDARs. This is not, however, sufficient to activate NMDARs;

200uM glycine saturates the glycine co-agonist sites but the receptors still require glutamate

binding for channel opening and ion flux. As such, the opening of NMDARs in this case

requires presynaptic neurotransmitter release, and the elevated glycine and lack of magnesium

simply relieve restrictions on NMDAR activation. Thus, the saturating glycine and lack of

extracellular Mg^{2+} in this context simply renders spontaneous glutamate release capable of

inducing NMDAR-mediated currents; the coordination between presynaptic release and postsynaptic NMDAR activation may in fact be what underlies the induction of LTP at these synapses. Furthermore, the type of LTP observed is again a potentiation of mEPSC amplitude and frequency that lasts up to 40 minutes (Lu et al. 2001) and is completely independent of inhibitory signaling or APs. Though LTP is often thought to involve significant rises in intracellular calcium, even if their duration and frequency are tightly controlled, one might suppose that Gly-LTP in cultures should also involve significant increases in postsynaptic calcium. However, in neurons incubated with TTX, Strych, and BIC, calcium dynamics will be greatly dampened, and spontaneous release leading to NMDAR opening likely cause small changes in intracellular calcium that are insufficient to drive many calcium-dependent synaptic processes. Nevertheless, I included this stimulation in my experiments and the effects of Gly-LTP on CRTC1 regulation are elaborated upon further in the discussion section.

FSK/rolipram-LTP

Targeting the cAMP second messenger system in cultured neurons can also produce LTP. A 10-minute application of FSK/rolipram results in drastic increases in cAMP produced by adenylate cyclase (AC), while rolipram inhibits phosphodiesterase (PDE) to halt the breakdown of cAMP. The activation of PKA by increases in cAMP is known to affect many processes involved in plasticity, including AMPAR phosphorylation[82], CRTC1 nuclear translocation[50] and CREB activation[83]. The interpretation of FSK/rolipram-LTP requires several considerations, however. Forskolin is known to significantly increase neuronal excitability[84], and a 10-minute application of FSK/rolipram hits the critical cAMP second messenger system with a sledgehammer. It also bears distinctions from classical NMDAR-LTP; although FSK/rolipram-LTP increases surface GluR1 and S845 phosphorylation, neither are affected by preincubation with APV or TTX[85]. As this protocol is not as highly cited as others, and because it is such a drastic perturbation, I chose not to pursue this protocol for my experiments.

KCl-LTP

Brief, repeated depolarization by KCl can also result in LTP in cultured neurons in a TTX-independent manner. This stimulation results in synaptic glutamate release, which activates NMDARs, involves the insertion of AMPARs into membrane locations in which they were originally lacking[86], and is dependent on NMDARs, postsynaptic calcium, and protein interactions involving SAP97 and/or myosinIV[87]. KCl-LTP, however, only results in an increase in mEPSC frequency, with little effect on amplitude[88]. Several factors led to eventually excluding this protocol from those I tested for their action on CRTC1. Importantly, the technical limitations of implementing a system to treat large-format culture dishes with accurate 1-second uniform pulses of elevated KCl seemed impossible to control as well as is possible for small coverslips with an electrophysiology/perfusion system. Moreover, brute depolarization of cultured neurons does not specifically target receptors involved in synaptic plasticity and may exert many off-target effects not directly involved in plasticity[89].

APVpc-LTP

Preculturing neurons in APV leads to chronic silencing of NMDAR currents and homeostatic increases in sensitivity of the NMDA-signaling system. If these cultures are then treated with a 3-minute application of APV-free medium lacking magnesium, the NMDARs undergo massive activation, resulting in the expression of LTP and many associated phenomena[90]. Electrophysiological recordings show a significant increase in the amplitude of spontaneous activity lasting over 20 minutes, as well as robust spine pruning and formation. These are satisfying exhibitions of potentiation, however this protocol is also a very drastic stimulation. Growing neurons in the complete inhibition of NMDARs will have profound effects on synapse formation, type, gene expression, and many other factors[91], to the extent that comparing them to neurons grown in normal medium is probably meaningless. As this

stimulation would be too drastically different than the others selected to examine CRTC1 behavior, I chose to exclude this stimulation from my work as well.

In the following data, I compare immunocytochemistry (ICC) and WBs for three stimulations that result in different expressions of plasticity in cultured neurons, beside control stimulations already established by past studies of CRTC1[50].

Results

The nucleocytoplasmic (N:C) ratio is defined as the immunofluorescent signal from a protein within the nucleus divided by its signal from the cytoplasm. In these experiments and those to which they are compared[50,51], the nuclear area is defined as DAPI-positive and microtubule associated protein 2 (MAP2)-negative while the cytoplasmic signal is defined as the MAP2-positive signal that surrounds the nucleus. As the CRTC1 N:C ratio is dependent upon the extent and type of synaptic stimulation a neuron receives, it follows that different neuronal cultures with different levels of baseline synaptic activity may exhibit different levels of nuclear CRTC1. As the level of baseline activity in neuronal culture is sensitive to many parameters and therefore some level of variability is unavoidable[92,93], it is most important that comparisons of different conditions are done in the same batch of coverslips. Unfortunately, CRTC1 seems to be so sensitive to that even the smallest perturbation can affect its nuclear translocation; pipetting too vigorously onto the wall of a 24-well dish is sufficient to mechanically activate neurons and alter CRTC1 N:C ratio. Through careful refinement of experimental technique, I was able to diminish this effect; remaining elevated levels of nuclear CRTC1 likely indicate basal levels of activity in the neuronal cultures (Fig. S1).

Cultured rat and mouse hippocampal neurons were silenced with TTX for one hour or incubated with BIC for 10 minutes, 100uM DHPG for 10 minutes, 200uM glycine for 3 minutes, or 20uM NMDA/glycine for 5', and N:C ratios for CRTC1 immunostaining were analyzed (Fig. 3).

Basal, untreated neurons exhibited a low CRTC1 N:C ratio, while TTX triggered nuclear export of CRTC1 (decreasing the CRTC1 N:C ratio) and BIC triggered robust CRTC1 nuclear translocation (increasing CRTC1 N:C ratio), as previously reported[50]. Interestingly, DHPG triggered dramatic CRTC1 nuclear translocation, and NMDA caused a moderate increase in N:C ratio with low variance. TTX restricted CRTC1 to two high-molecular weight species (~100kDa) by Western Blot (WB), and basal CRTC1 existed as a smear of different species with more IR at higher molecular weights. DHPG produced a smear of IR similar to that of BIC, but NMDA generated a distinct low band, without the intermediate-weight bands observed in other stimulations. This may be due to the selectivity of NMDA for NMDARs in comparison to other treatments; in both DHPG and BIC conditions, neurons undergo increased excitability and each synapse may feel different levels of synaptic activation, leading to a wide breadth of differential PTMs on CRTC1. NMDA, however, specifically engages signaling pathways coupled to NMDARs, results in increases in specific calcium microdomains, and may restrict the number and type of PTM changes on CRTC1. Tantalizingly, the low-weight band generated by NMDA/gly appeared to migrate to approximately the same molecular weight as lambda phosphatase- or calf intestinal phosphatase-treated lysates, indicating that it may represent a mostly/completely dephosphorylated form of CRTC1 (Fig. 3C).

Gly-LTP, in contrast, caused no perceptible change above basal CRTC1 N:C ratio, nor a significant difference from basal in electrophoretic mobility by WB. This result was unexpected, as many previous reports have shown CRTC1 nuclear translocation in response to LTP-induction in different systems[50,55,59], however further examination of the specifics of the Gly-LTP protocol and consideration of its neurobiological foundations (outlined in the introduction and further explained in the discussion below) render this result consistent with our understanding of CRTC1 N:C regulation.

Further examination of the Gly-LTP and NMDA-LTD protocols revealed that they were originally validated using pre-perfusion of neurons with magnesium-free extracellular solution

including TTX, Strych, and BIC. I conducted ICC experiments to determine whether pre-incubating neurons with these inhibitors would change their response to subsequent glycine or NMDA application. Preincubating neurons in this cocktail of inhibitors results in nuclear export of CRTC1 and reduced N:C ratio compared to basal uninhibited neurons. Application of 200uM glycine on top of these inhibitors had no effect on CRTC1 nuclear accumulation, but 20uM NMDA/glycine was able to induce significant translocation above the inhibitor-only control (Fig. 4). This is consistent with the view that CRTC1 nuclear translocation is gated by rises in postsynaptic calcium; the 200uM glycine application probably results in minimal calcium transients due to the rarity of glutamate release events in TTX, whereas NMDA is capable of directly holding channels open and causing sustained calcium influx, even if its amplitude is lessened by pre-silencing neurons. These results showed that Gly-LTP does not drive CRTC1 nuclear translocation, while DHPG and NMDA do, with different amplitude, variance, and mechanisms of action.

While DHPG is known to engage the canonical signaling pathway of Group I mGluRs, leading to release of calcium from intracellular stores, it remained unclear whether DHPG-induced CRTC1 nuclear translocation was due to such intracellular release, or resulted from other mechanisms by which DHPG alters neuronal signaling. To probe this question, I compared nuclear translocation of CRTC1 between DHPG-treated coverslips, and those pre-incubated with NBQX to block AMPARs, TTX to block APs, or APV to block NMDARs (Fig. 5). In the course of these experiments, it became clear that, in some cases, comparing raw nuclear values for CRTC1 IR demonstrated more pronounced effects than N:C ratios (Fig. 5A,B). Although measuring the N:C ratio provides the experimenter some advantages (this serves as internal normalization against both variable immunofluorescence across experiments and cell-to-cell protein expression variability within and across experiments), some stimulations produce a significant increase in nuclear CRTC1 with a concomitant increase in perinuclear cytoplasmic

CRTC1, causing N:C ratio to dampen the measurement of CRTC1 translocation to the nucleus (Fig. 5C).

In summary, a brief (3-5 minute) application of 20 uM NMDA/glycine was sufficient to increase nuclear CRTC1 with modest amplitude and low variance, in the presence or absence of pre-incubation with TTX/Strych/BIC, though 200uM glycine alone is insufficient with our without incubators. A 10-minute application of 100uM DHPG induced robust nuclear translocation of CRTC1, with high variance and amplitude. For each stimulation protocol, there remain open questions about the exact signaling pathways engaged and the etiology of CRTC1 nuclear translocation.

Discussion

Taken together, these data indicate that several protocols known to induce plasticity in cultured neurons are capable of driving CRTC1 nuclear translocation. Further examination of the pharmacological treatments and experiments inhibiting specific receptors reveal that there are several converging pathways that regulate CRTC1. DHPG causes robust translocation of CRTC1, but this is unlikely solely dependent on mGlur1/5 activation, as it is completely abolished by pre-incubation of neurons in TTX. DHPG-mediated activation of mGlur1/5 is independent of AP firing or neuronal depolarization, though there is debate about whether mGluR-mediated intracellular calcium increases are abolished by TTX[94,95], and in acute hippocampal slices there is evidence that basal M_1 muscarinic acetylcholine receptor-mediated activation of PKC is required for the expression of DHPG-LTD[96]. Even if not completely dependent upon APs, mGluR activation may synergize with depolarization and other signals to exert its full effects. Blocking AMPARs with NBQX also completely abolished DHPG-mediated CRTC1 nuclear translocation, suggesting that increased excitability may be a key feature of DHPG in this context. Interestingly, pre-incubating neurons with APV to inhibit NMDAR signaling before DHPG application caused a decrease in CRTC1 nuclear translocation, though

it did not completely abolish it. This is similar to observations pre-incubating neurons with APV before BIC treatment[50], suggesting that both DHPG and BIC act upon CRTC1 primarily by increasing neuronal excitability, though potentially through distinct intracellular signaling pathways.

NMDA drives CRTC1 nuclear accumulation through NMDAR-coupled pathways that increase intracellular calcium. It is important to regard the NMDAR-signaling system as a complex and tightly regulated concert of many factors, almost like a system of gears; these channels are positioned carefully in the postsynaptic membrane and stabilized by scaffolding proteins in the PSD that couple them to downstream signaling molecules[97] such as calcineurin that then trigger such molecular events as CRTC1 nuclear translocation. In fact, in order to properly appreciate the synaptic consequences of NMDA application, one must have a holistic picture of synapse composition and juxtaposition of different effectors to the sources that activate them. In this example, NMDARs are tightly regulated at the postsynaptic membrane where kinases and phosphatases target their intracellular domains to modulate their conductance and interaction with other proteins. They are coupled to the postsynaptic density (PSD) through scaffolding proteins, and the architecture of the PSD ensures that other proteins are also positioned to respond to NMDAR-mediated calcium influx quickly. This colors our interpretation of NMDA-mediated CRTC1 nuclear translocation; NMDA activates only NMDA receptors, causing calcium influx primarily through these receptors (and practically solely through them, when cells are pre-incubated with TTX/Strych/BIC). This is only one route of increasing intracellular calcium, and will only activate calcineurin that is positioned next to these activated receptors; there are other routes by which to increase intracellular calcium and induce nuclear translocation of CRTC1 that are unaffected by NMDA. Thus, the population of CRTC1 that is substantially dephosphorylated to trigger its nuclear translocation is probably a small subset of the total CRTC1 in a given neuron. This complete activation of only one calcium pathway provides an explanation for the modest, yet low-variance increase in nuclear CRTC1

observed in response to NMDA. Importantly, APV dampens BIC and DHPG-induced CRTC1 nuclear translocation, implying that this pathway is engaged by stimulations such as these that increase neuronal excitability. DHPG-induced nuclear translocation of CRTC1, however, is completely abrogated by pre-incubation of cells with NBQX, suggesting that NMDAR activation that contributes CRTC1 translocation in this context is dependent upon AMPAR-mediated depolarization.

It is also logical that 200uM glycine does not drive CRTC1 nuclear accumulation on top of TTX-silencing, as in this context the only electrophysiological-detectable synaptic activity arises from spontaneous rather than evoked neurotransmitter release. There is considerable evidence that the vesicle pools engaged in these two types of release are distinct[98–103] and the plasticity that affects spontaneous excitatory postsynaptic potentials (EPSPs) versus those evoked by APs are likely substantially different. In fact, although the two types of release usually occur concurrently without significant difference in their unitary properties[104,105], they have been found to engage different populations of NMDARs with limited overlap[106]. Saturating NMDARs with glycine is insufficient to lead to much NMDAR opening with severely diminished glutamate release; while spontaneous vesicle fusion is intact in TTX-treated neurons, the frequency of release is quite low, and the quantal release is even lower[107,108]. Thus, such accordingly low-levels of glutamate release into the synaptic cleft produce insufficient calcium currents to trigger many molecular processes with higher calcium thresholds, such as appears to be the case for CRTC1 nuclear translocation.

These studies raise several tantalizing questions. The different WB bands generated by different stimulations motivates further inquiry into their PTM-definition and the enzymes that mediate their differential PTM. I did not go further trying to identify these bands due to previous work in the Martin lab that failed to isolate sufficient quantities of high-purity CRTC1 from neurons for analysis by mass-spectrometry. In addition, phospho-specific antibodies for CRTC1 are unreliable and insufficiently validated for use in ICC or WB. All of these technical issues

can, and should, be optimized to address shortcomings; at least one custom-made phospho-specific antibody has been validated for use by WB on chemiluminescent systems (data not shown), and may be useful in defining differential phosphorylation at pS64/245 in different stimulations. Of course, the PTM-regulation of CRTC1 is likely a vastly complex phenomenon, requiring appreciation of many convergent pathways. A recent study showed that the three CRTCs exhibit distinct patterns of 14-3-3 binding at three conserved sites: S64, 151, and 245 in CRTC1. The analogous residue for CRTC1-S151 in CRTC2 (S171) functions as the gatekeeper site for 14-3-3 binding and acts cooperatively with S275 (S245 in CRTC1) to stabilize this interaction[109]. These phosphorylations are mediated by SIK, which is cAMP-responsive, and MARK, which is not. The different CRTC family members carry variant AMPK recognition motifs that may also influence their regulation by other highly-expressed kinases, and provide a window by which to begin to dissect different signaling pathways and their integration by CRTCs. It is worth noting, however, that all levels of such regulation may be significantly different between different cell types, and none of these studies have yet been conducted in neurons.

Concluding Remarks

The experiments described in this chapter form a solid foundation from which to interpret results regarding CRTC1 translocation in response to the induction of neuronal plasticity. They show that pharmacological stimulations that target different pathways in cultured neurons, specifically NMDA- and DHPG-LTD, are capable of driving CRTC1 nuclear translocation and create different profiles of electrophoretic mobility by western blot. These results begin to shed light into the molecular differences between NMDA- and DHPG-LTD induction, and how these differences affect CRTC1 nuclear translocation and PTM. However, the lack of a suitable LTP-inducing stimulus that causes robust CRTC1 translocation in cultured neurons halted my original goal of comparing the transcriptional activity of CRTC1 during bidirectional (LTP and

LTD) induction of plasticity, and necessitated switching to a different model system to address these questions. Thus, the findings outlined in this chapter regarding the behavior of CRTC1 in cultured neurons informed the design of further experiments conducted in acute hippocampal slices, which are reported in detail in the next chapter.

Materials and Methods

        All experiments were performed with approval from the UCLA Institutional Animal Care and Use Committee.

Preparation of hippocampal and cortical rat and mouse cultures

        Mature hippocampal or cortical tissue was dissected from P0 or P1 rat or mouse pups, dissociated, and plated on Poly-DL-lysine (0.5 mg/ml) coated coverslips (Carolina Biologicals, Burlington, NC). Cells were cultured in a defined serum-free media: Neurobasal A medium (Invitrogen, Carlsbad, CA); β-mercaptoethanol (Sigma, St. Louis, MO); monosodium glutamate (Sigma); B27 (Invitrogen); GlutaMAX (Invitrogen).

Pharmacological treatments

        For most pharmacological treatments (except those specified in the following section), neurons were incubated with pharmacological agents in conditioned medium, in a 37°C, 5% CO_2 incubator for the specified amount of time before cells were either fixed for immunocytochemistry or lysates were collected for immunoblots. For receptor antagonist treatments (APV, NBQX, ifenprodil, etc.), unless otherwise specified, cultured neurons were pre-treated with the antagonist for 30–60 min prior to stimulation. BIC was applied to neurons for 10 min while NMDA was applied for 3 or 5 min before immediate washout and fixation for immunocytochemistry or preparation of cell lysates for immunoblot. The following pharmacological agents were used: bicuculline (BIC, 40 μM; Sigma), forskolin (FSK, 25 μM; Calbiochem, San Diego, CA), tetrodotoxin (TTX, 1 μM; Tocris, Ellisville, MO), strychnine (Strych 1 μM, Sigma), APV (100 μM; Tocris), NBQX (100 μM; Tocris); ifenprodil (IFP, 50 μM; Tocris), NMDA (20 μM; Tocris), AMPA (25 μM; Tocris).

Induction of Gly-LTP and NMDA-LTD

The induction of both Gly-LTP and NMDA-LTD were conducted in a manner that closely matched the original publication of these protocols. Conditioned medium was removed from cultured neurons (21-28 DIV) and replaced with pre-warmed extracellular solution similar to that used in patch-clamp recordings for 10 min: 140mM NaCl, 1.3 mM $CaCl_2$, 5 mM KCl, 25 mM HEPES, 33mM Glucose, pH 7.4 with TTX, BIC, and Strych. After 10 min pre-incubation, some of the extracellular solution was removed, supplemented with glycine or NMDA to the appropriate concentration, and added back onto cultured neurons for the appropriate length of time before fixation and immunocytochemistry.

Preparation of cellular lysates and immunoblotting

Neuronal cultures were lysed directly in RIPA buffer (150 mM NaCl, 1.0% NP-40, 0.5% sodium deoxycholate, 0.1% SDS, 50 mM Tris) with small-molecule protease (Roche cOmplete) and phosphatase (Roche phosSTOP) inhibitor tablets. Protein levels were quantitated using a BCA assay (BioRad), and ~15-30 µg was loaded onto SDS/PAGE gels containing 4% (stacking) and 10% (resolving) acrylamide. Protein was transferred to 0.2 µm nitrocellulose membranes, then blocked with Odyssey blocking buffer (LI-COR) for 1 hour at RT. Membranes were then incubated overnight at $4^{o}C$ in blocking buffer + antibody with agitation. Tris-buffered saline containing 0.05% Tween-20 (TBST) was used to wash membranes 3 times, for 5 min each. Fluorescent secondary antibody was incubated for 2-4 hours at room temperature, followed by 3 more 5 min TBST washes. Imaging was conducted using an Odyssey scanner (LI-COR) and analyzed using Image Studio and Image Studio Lite Software (LI-COR).

Primary antibodies: Rabbit polyclonal anti-CRTC1 (1:1000, Bethyl Labs A300-769).

Fluorescent secondary antibodies from LI-COR: IRDye 800CW Goat anti Mouse (LI-COR #926-32210), IRDye 680LT Goat anti Rabbit (LI-COR #926-68021).

Immunocytochemistry

Cells were quickly washed in PBS warmed to 37°C (unless otherwise specified), then fixed in 4% paraformaldehyde for 10 min at RT. Permeabilization of cell membranes was conducted with 0.1% Triton-X-100 (Calbiochem) for 5 min, and cells were blocked with 10% goat serum for 30 min at RT. Neurons were then incubated in primary antibodies in goat serum overnight at 4°C. Secondary antibodies and Hoechst nuclear dye (Invitrogen) were incubated 1:2000 at RT for 2 hours. Coverslips were mounted with aqua/polymount (Polysciences, Warrington, PA).

Primary antibodies: Rabbit polyclonal anti-CRTC1 (1:1000, Bethyl Labs A300-769), chicken polyclonal anti-MAP2 (Phosphosolutions, Aurora, CO).

Fluorescent secondary antibodies: Goat anti-rabbit or chicken, conjugated to Alexa dyes 488, 555, or 633 (Invitrogen).

Confocal image acquisition and analysis

Confocal images were acquired using a Zeiss LSM 700 with 405, 488, 555, and 639 nm solid-state lasers. Zen 2009 software was used for data acquisition and preliminary image analysis.

Nuclear, cytoplasmic, and N:C values were quantified using ImageJ software. Breifly, raw confocal images taken using a 63x 1.4NA oil objective were imported into ImageJ. For each neuron, masks and regions of interest (ROIs) were manually drawn around the cell nucleus (outlined by Hoechst staining) or cell body (outlined by MAP2 staining). The "XOR" function in ImageJ allowed simple subtraction of the two masks to obtain a separate mask for the cytoplasm. Pixel intensities were quantified to obtain nuclear and cytoplasmic values. The nuclear to cytoplasmic ratios for individual neurons were calculated based on the average intensity of staining in each mask. Data was then plotted using Prism Graphpad software. All

data sets are presented as mean ± SEM as scatter plots and *p*-values determined using One-Way analysis of variance (ANOVA) with Bonferroni's Correction *post-hoc* test.

Figure Legends

Figure 2-1. Schematic depicting regulation of CRTC1 subcellular localization. CRTC1 is tethered in the cytoplasm by 14-3-3ε proteins that interact with key phosphorylated residues. Increases in intracellular calcium promote calcineurin-mediated dephosphorylation of CRTC1, and allow it to translocate to the nucleus, where it affects programs of gene expression. The opposing action of SIK1/2, that rephosphorylate CRTC1 and promote its nuclear export, can be inhibited by elevated cAMP levels.

Figure 2-2. 1 and 2-dimensional gels examining CRTC1 electrophoretic mobility in response to different treatments in cultured neurons (adapted from Ch'ng et al. 2012). A) When cultured neurons are silenced with TTX, CRTC1 is restricted to high molecular weight by WB and exhibits increased pS151 IR with respect to basal cultures. BIC and FSK cause modification of CRTC1 such that it migrates to lower molecular weights with a corresponding loss in pS151 IR. BIC and FSK-induced change in CRTC1 molecular weight can be blocked by inhibition of calcineurin with CsA, and treatment of lysates with CiP results in collapse of CRTC1 IR to a low band. Together, these data suggest that BIC and FSK cause dephosphorylation of CRTC1, and that differences in phosphorylation state underly differences in CRTC1 electrophoretic mobility in response to different pharmacological treatments. B) Cultured neurons were treated as described in A), and lysates separated by molecular weight and isoelectric point (. CRTC1 (green) resides in a spectrum of different states that migrate to different isoelectric points, in TTX, BIC, and FSK-treated neurons, though the range of species differs in each case. Treatment of BIC-stimulated culture lysates with CiP reveals collapse of CRTC1 to 3 major species at high isoelectric point, revealing the importance of phosphorylation in generating CRTC1 species diversity, but that other modifications of CRTC1 play some role in generating diversity. TUJ1 anchor (red) does not change in isoelectric point with pharmacological stimulation.

Figure 2-3. CRTC1 nuclear translocation and post-translational modification in cultured neurons.
A) Cultured neurons were treated with various pharmacological agents, fixed, stained, imaged, and N:C values recorded. Basal and TTX-treated neurons exhibit low CRTC1 N:C, while this ratio is elevated to different extents by BIC, DHPG, and NMDA-treatment. Interestingly, glycine alone is insufficient to drive CRTC1 nuclear accumulation. *B)* WB for lysates that mirror the conditions in the ICC in *A)* show that TTX-silenced neurons harbor CRTC1 restricted to two high molecular weight bands, while BIC and DHPG cause a smear of CRTC1 immunoreactivity that spans from ~70 to 100 kDa. Strikingly, NMDA application causes significant (though incomplete) conversion of high-molecular weight CRTC1 to a distinct low molecular weight band that migrates to ~70kDa. Glycine application appears somewhat similar to BIC and DHPG, but more closely mirrors basal neurons in both electrophoretic mobility and N:C value. *C)* Incubation of lysates from basal neurons with lambda phosphatase (LP) or calf intestinal phosphatase (CiP) collapses CRTC1 IR to low molecular weight bands that are very close in electrophoretic mobility to that of NMDA-treated neurons. It is worth noting that there may be small differences in the electrophoretic mobility of the low band observed in LP, CiP, and NMDA lanes, though the resolution of 1D gels is insufficient to say for sure that there are salient differences between them.

Figure 2-4. Dissection of the effects of different aspects of NMDAR-dependent plasticity-
induction protocols in cultured neurons. Cultured neurons exhibit some level of nuclear CRTC1, at rest. Pre-incubation with extracellular solution supplemented with BIC/TTX/Strych (see materials and methods) causes nuclear export of CRTC1 within 10 min. Application of 200μM glycine ontop of these inhibitors does not promote CRTC1 nuclear import, though 20μM NMDA does.

Figure 2-5. Comparison of nuclear translocation of CRTC1 in cultured neurons in response to pharmacological treatments. A,B) Cultured neurons were treated with DHPG and compared to DMSO controls or coverslips that were pre-incubated with TTX, APV, or NBQX. DHPG reliably induces CRTC1 nuclear translocation that can be completely blocked by TTX or NBQX. This suggests that the ability of DHPG to drive CRTC1 translocation is due to increases in neuronal excitability that lead to increased AP firing and AMPAR activation. *C)* Careful analysis of nuclear, cytoplasmic, and N:C values for these images reveals that some treatments produce a significant increase in nuclear CRTC1 with a concomitant increase in perinuclear cytoplasmic CRTC1, causing N:C ratio to dampen its report of CRTC1 translocation to the soma.

Table 2-1. Published plasticity-induction protocols for use in cultured neurons. A brief overview of plasticity-induction protocols for cultured neurons reveals that many require careful consideration of many parameters, rendering cross-comparison hard to interpret. Bearing experimental considerations and the goal of analyzing the action of these stimulations on CRTC1, mGluR-LTD, Gly-LTP, and NMDA-LTD are the best candidates for investigation.

Supplemental Figure Legends

Figure 2-S1. Cultured neurons were prepared by SLB or SN. They were then fixed and stained for CRTC1, with or without including a PBS-wash before fixation. In all cases, the PBS wash alone causes some level of CRTC1 nuclear translocation – a consideration that must be borne in mind when analyzing the ability of a pharmacological stimulation to induce CRTC1 nucelar translocation; some of the effect observed may simply be due to (unavoidable) mechanical perturbation. That said, in all experiments in this study, neurons are treated in the same way across conditions; all neurons within an experiment were washed with PBS in the same way, or all excluded the PBS wash, and thus cross-condition comparisons are valid.
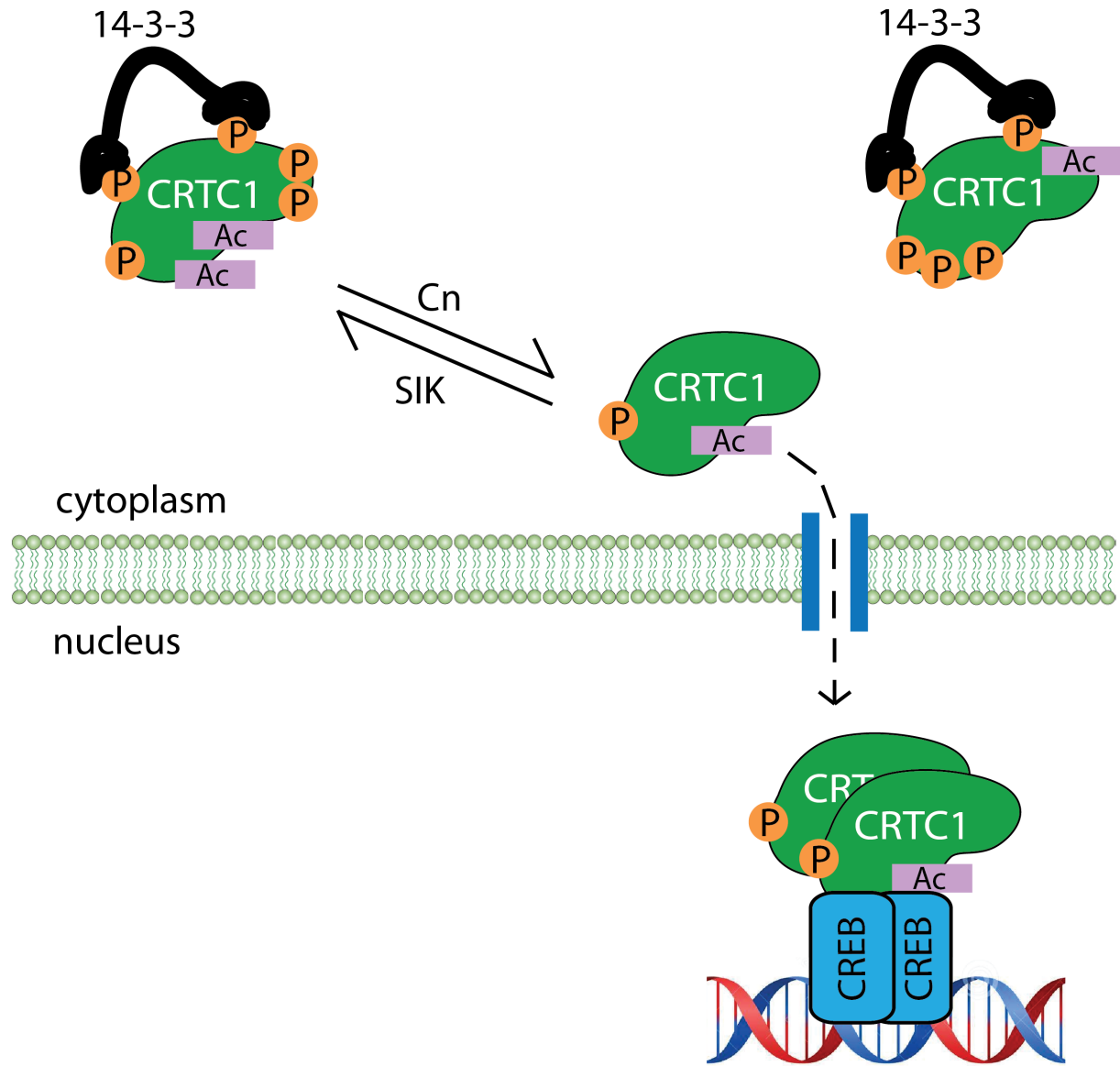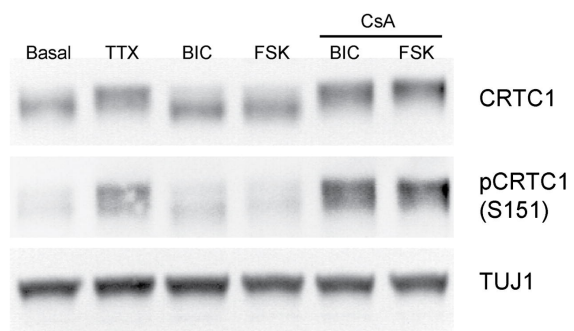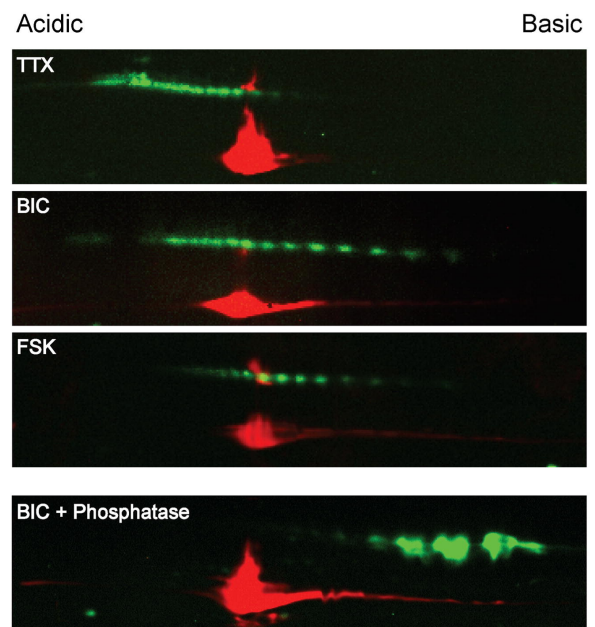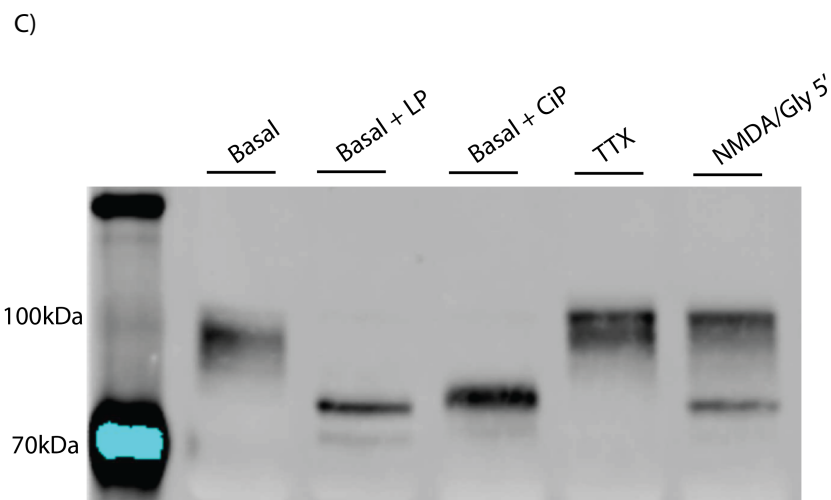
Figure 2-1

Figure 2-2

A

B

Figure 2-3

A)

B)

C)
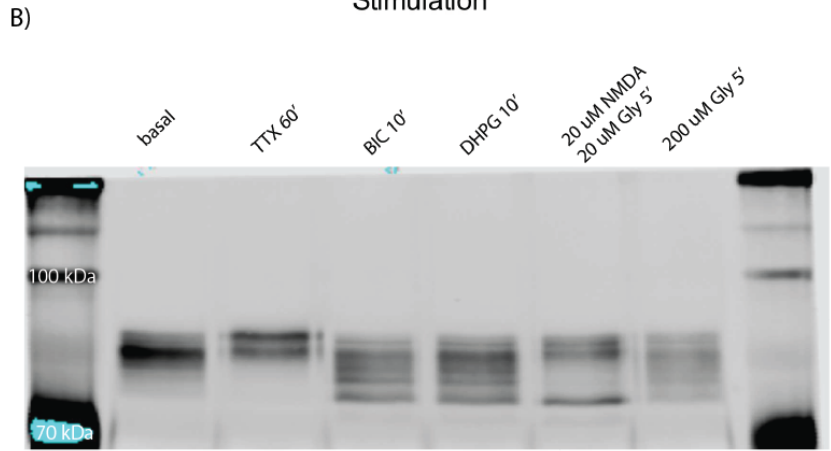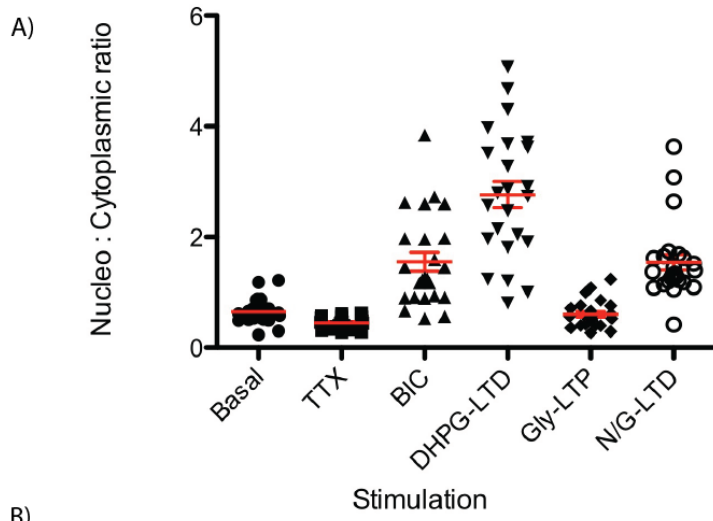
Figure 2-4

Figure 2-5

A)

B)
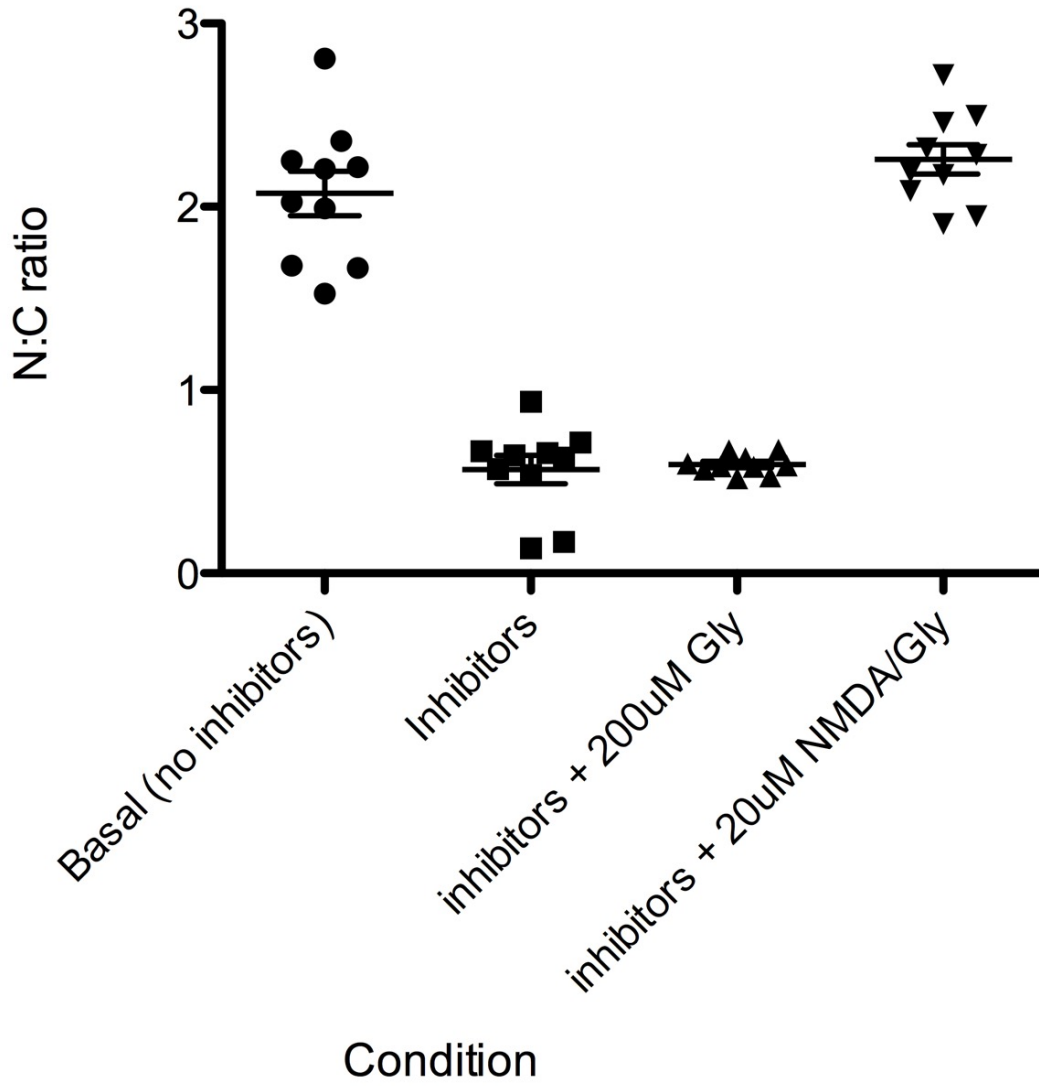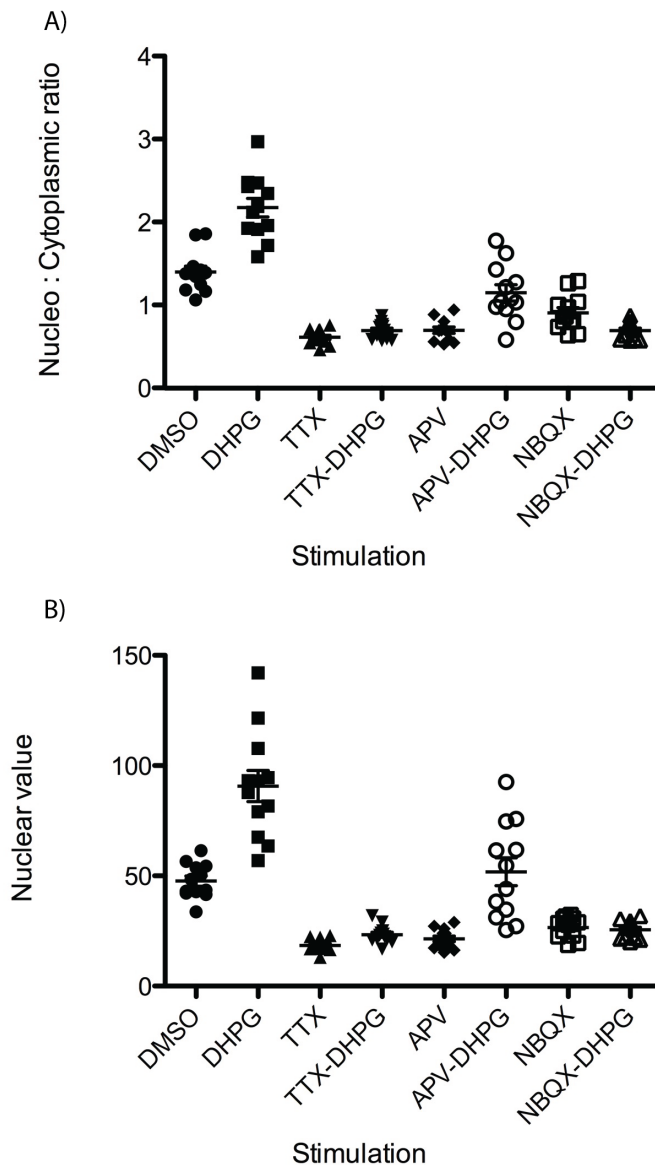
C)

Image	Nuc	Cyto	N:C ratio
APV-1	16.3	29.8	0.546979866
APV-2	15.3	22	0.695454545
APV-3	17.3	24.7	0.700404858
APV-4	20.6	21.8	0.944954128
APV-5	27.2	30.6	0.888888889
APV-6	20.7	36.8	0.5625
APV-7	23.9	34.2	0.698830409
APV-8	18.6	31.7	0.586750789
APV-9	26.1	32.4	0.805555556
APV-10	18.6	34.9	0.532951289
APV-11	28.9	41	0.704878049
APV-12	23.9	33	0.724242424

Image	Nuc	Cyto	N:C ratio
APV-DHPG-1	44.1	42.6	1.035211268
APV-DHPG-2	54.7	50.7	1.078895464
APV-DHPG-3	61.8	48.4	1.276859504
APV-DHPG-4	92.6	56.9	1.62741652
APV-DHPG-5	75.8	53	1.430188679
APV-DHPG-6	61.6	50.6	1.217391304
APV-DHPG-7	34.7	35.3	0.983002833
APV-DHPG-8	27.2	46.6	0.583690987
APV-DHPG-9	25.4	31.8	0.798742138
APV-DHPG-10	31.2	32.7	0.95412844
APV-DHPG-11	74.7	42	1.778571429
APV-DHPG-12	38.3	36.6	1.046448087

Image	Nuc	Cyto	N:C ratio
DHPG-1	63.5	40.1	1.583541147
DHPG-2	67.5	30.8	2.191558442
DHPG-3	94.6	38.1	2.482939633
DHPG-4	56.9	29.7	1.915824916
DHPG-5	79	41	1.926829268
DHPG-6	93	47.4	1.962025316
DHPG-7	81.7	47.5	1.72
DHPG-8	142	47.8	2.970711297
DHPG-9	93.2	43.9	2.123006834
DHPG-10	121.6	49.1	2.476578411
DHPG-11	87.8	36.1	2.432132964
DHPG-12	107.8	45.9	2.348583878

Table 2-1

	Induction protocol	**Observation of plasticity**	**Citation**
mGluR-LTD/DHPG-LTD	100uM DHPG, 5'	Patch clamp – decrease in freq. of mEPSCs >60'	Snyder et al. *Nat Neuroscience (*2001)
NMDAR-LTD/NMDA-LTD	Preinc. in TTX, Strych, BIC → 20uM NMDA / 20uM Glycine, 3'	Patch clamp - depression of mini amplitude lasting >20min	Lu et al. *Neuron* (2001)
NMDAR-LTP/Gly-LTP	Preinc. in TTX, Strych, BIC → 200uM Glycine, 3'	Patch clamp - increase in amplitude and frequency of minis lasting >40min	Lu et al. *Neuron* (2001)
FSK/rolipram-LTP	Preinc. In ACSF → 50uM FSK/0.1M rolipram/0 Mg^{2+}	Surface expression and phosphorylation of AMPARs	Oh et al. *JBC* (2006)
KCL-LTP	3 x 1s 90mM KCl	Increase in mEPSC freq.	Pickard et al. *Neurophys* (2001)
APVpc-LTP	Grow cultures in APV → APV/Mg^{2+}-free medium 3'	Increase in spontaneous burst amplitude, >20m, spine pruning	Goldin et al. *J Neurosci* (2001)

Figure 2-S1
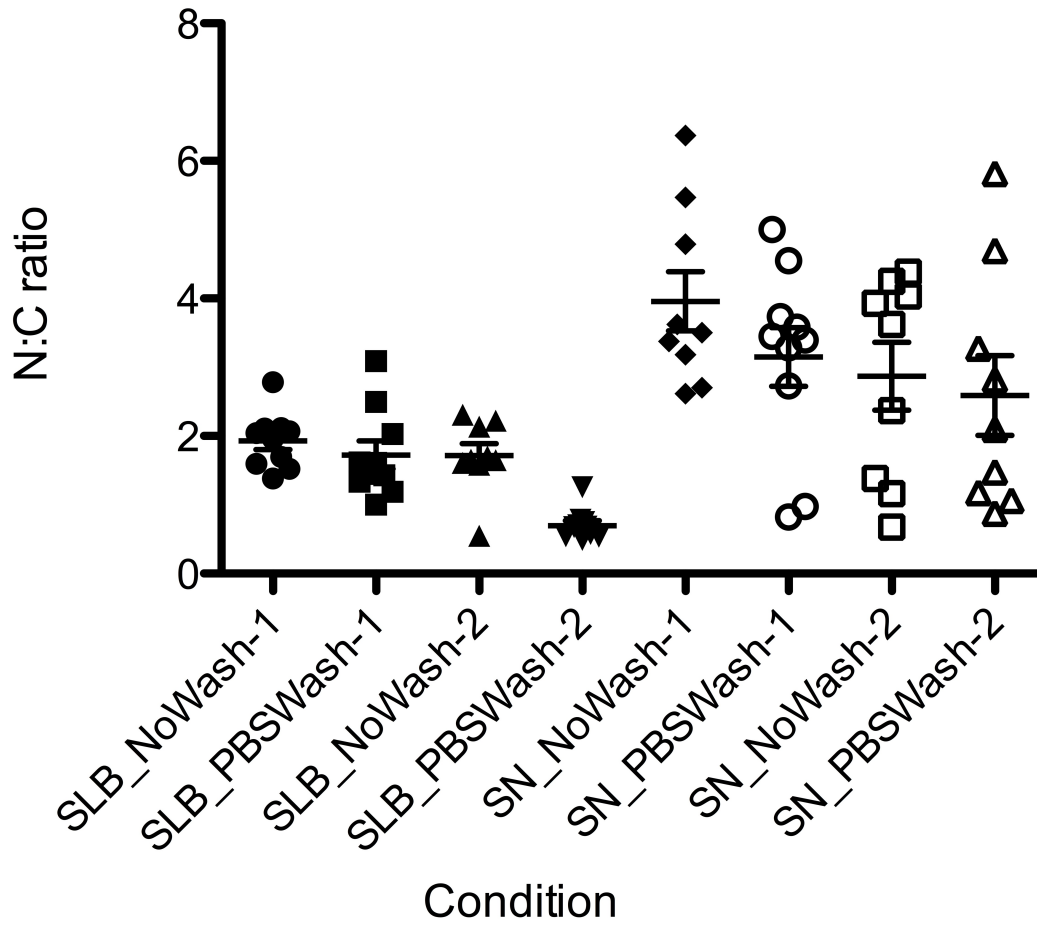
Chapter 3

CRTC1 Chromatin Immunoprecipitation-sequencing (ChIP-seq) in hippocampal slices

Introduction

Chromatin Immunoprecipitation (ChIP) as we recognize it today was developed in the 1990's as a technique to study direct interactions between protein complexes and DNA[110]. It is particularly useful for studying the regulation of genomic elements by transcription factors and other DNA-binding proteins. Preparing a sample for ChIP requires chemical cross-linking of proteins to DNA, followed by cell lysis, immunoprecipitation (IP) of the protein of interest, release of DNA fragments from IP'd material, and analysis of these nucleic acids. ChIP studies are classically performed on cultured cells, as in the original conception of the ENCODE project, and sample preparation has been optimized for many cell types in such formats. Large-scale generation of starting material and chemical access from culture medium to nuclei are easiest in such systems, as well as more precise biochemical manipulations such as cell dissociation and purification of intact nuclei. In recent years, major advances have been made in many steps of the ChIP-sequencing (ChIP-seq) workflow to enable studies bearing particular challenges that were once prohibitive. It is now possible to conduct ChIP-seq on less-abundantly expressed proteins and those that do not bind DNA directly, as well as to prepare sequencing libraries from smaller starting amounts. The aim of my ChIP-seq experiments was to study the binding of CRTC1 to genomic targets during the induction of plasticity. This required careful selection of an appropriate model system, stimulation protocols, and experimental design to circumvent technical concerns that pose significant challenges to acquiring high-quality data.

Ideally, one would research biochemical changes that underlie plasticity in behaving animals. Such experiments would show the closest reflection of such changes induced by *in vivo* learning events. However, there are technical limitations to the types of analyses that can be conducted on brains that have undergone behaviorally-induced plasticity. Though careful analysis of the profiles and percentages of activated cells following learning remains to be systematically dissected across brain regions, evidence suggests that such changes are

sparsely distributed with respect to the total cell population in a given area. Impressive

increases in immunoreactivity (IR) of proteins such as phospho-cAMP-responsive element

binding protein (CREB) or Fos are observable through immunohistochemical (IHC) staining of

animal brains after learning, but the number of cells that harbor such changes still comprises a

small portion of the total population[111]. Furthermore, there is no evidence that the cells that are

activated and involved in encoding new memory are pre-defined by a unique pattern of gene

expression that might give researchers a handle by which to manipulate such cells using classic

or intersectional genetic techniques such as CRE-lox and/or inducible systems. Instead,

learning appears to be encoded in a subset of neurons that are wired to compute the

information involved in a particular learning event. A convincing illustration of this principle is

presented by a paper from the Tonegawa Lab in 2012, wherein researchers used an adeno-

associated virus (AAV) injected into the dentate gyrus (DG) of adult c-fos-tTA transgenic mice to

manipulate cells activated by learning events[112]. The viral construct encoded channelrhodopsin-

EYFP (ChR2-EYFP) driven off of a tetracyclin-responsive-element (TRE); this approach directly

coupled the activity-dependent promoter of *c-fos* to the tetracycline transactivator (tTA),

enabling intersectional utilization of the doxycycline (Dox) system for inducible expression of

ChR2-EYFP. In this system, keeping mice on a Dox+ diet inhibits expression of ChR2-EYFP,

and moving mice to Dox-free diet is in the hands of the experimenter, giving them temporal

control of the initiation of activity-induced ChR2-EYFP expression. This is important, as cells of

the DG will be activated to some extent through life experience, and would cause leaky

expression of ChR2-EYFP before a learning event is experimentally imposed. This inducible

system allowed the Tonegawa lab to specifically mark cells that had been activated during an

experimentally-controlled learning paradigm with ChR2-EYFP (Fig. 1). Immunohistochemistry

of brain slices from fear-conditioned (FC) and control mice revealed FC only activates a small

proportion of cells within the DG. This is not due to insufficient transduction efficiency of the

viral construct, as seizure induces EYFP fluorescence in nearly 100% of cells in the DG. While

learning clearly involves activation of cells, leading to immediate early gene (IEG) induction, the particular cells within a brain region that are involved in such learning are not defined by genetic makeup but rather by their wiring; there is no particular set of cells that can be identified from animal to animal that always encodes fear memory. This poses a fundamental problem to identifying biochemical changes induced by learning: signal-to-noise is inherently low due to sparse neuronal activation.

Some labs have attempted to employ laser capture microdissection (LCM) to isolate subregions of tissue with greater accuracy than manual dissection, in order to isolate affected cells from unaffected neighbors and restrict further analysis to material obtained from relevant cells, but such methods bear their own concerns due to severe injury effects, dissatisfying strategies to mark activated cells without significant perturbation, and extremely low cell yield. Such a low cell-count is actually permissive for some analyses; a recent paper showed that LCM can be used in isolating single cells from the brain for RNA-sequencing (scRNA-seq)[113]. There are several important caveats to these types of experiments, however. Data obtained from single cells exhibit lower signal-to-noise as compared to datasets generated from larger pools of starting material[114], limiting transcript identification to those that are sufficiently abundant. Furthermore, scRNA-seq exhibits great variability from cell-to-cell and it can be hard to tease apart technical limitations from biological differences, especially in maintaining sufficient sequencing depth to enable comparison between different groups. Nevertheless, improvements in the scRNA-seq workflow have allowed at least the acquisition and analysis of this data, though there is much left to improve. Unfortunately, due to the nature of the ChIP-seq workflow, it is impossible to start with comparably little starting material. As there are only two copies of each chromosome per cell, the relative yield of ChIP-seq is inherently lower than that of RNA-seq, which captures many transcripts for a given gene. In fact, obtaining sufficient and high-quality starting material for library preparation is a central concern in ChIP-seq experiments and deserves careful consideration.

The amount and purity of ChIP DNA used to prepare a sequencing library is affected by nearly all parameters of sample preparation. Classical considerations include the input cell number, efficiency of chromatin fragmentation from the chosen cell/tissue type, abundance of protein-DNA interactions, the strength of the protein-DNA interaction, and the specificity and efficiency of the IP. For these reasons, ChIP-seq works most robustly for histones and other abundant proteins that are highly expressed and tightly associated with DNA. ChIP-seq for CRTC1 requires consideration of these parameters, as well as several others that are specific to its particular nature. As CRTC1 is a protein that does not directly bind DNA and undergoes trafficking between the cytoplasm and the nucleus, only nuclear CRTC1 that is bound to transcription factor complexes would yield ChIP DNA; this can be conceptualized as a ratio of its DNA bound and unbound states in each sample. Put simply, if after stimulation only a small portion of total cells within a tissue sample have undergone CRTC1 translocation, it is reasonable to expect that the amount of chromatin purified by a CRTC1 IP will be comparably low. In order to ensure that sufficient CRTC1-protein-DNA complexes are purified by the IP, then, it is important to choose a model system in which it is possible to induce CRTC1 translocation in a relatively uniform and robust manner.

As previous work in the Martin lab has shown that CRTC1 does not undergo robust translocation in mouse CA1 even following strong fear induction (Wendy Herbst, Martina De Salvo, Martin Lab unpublished), behavioral learning paradigms did not seem promising for ChIP-seq experiments. Although some stimulations, such as pilocarpine-induced seizure, cause extremely robust CRTC1 translocation in the hippocampus (Caroline Houser, unpublished), and some forms of learning may induce CRTC1 translocation in other structures, the focus of my experiments was to study CRTC1 in the context of hippocampal plasticity. The many experimental and technical hindrances of conducting CRTC1 ChIP-seq from the brains of behaviorally-conditioned animals drove me to explore more tractable model systems.

Acute hippocampal slices as a model system

The acute hippocampal slice preparation is an ideal system for the study of CRTC1 transcriptional targets, as its properties navigate many opposing experimental concerns. Acute hippocampal slices are an ideal system for many investigations, including next-generation sequencing (NGS) to analyze changes in RNA levels or protein-DNA interactions following the induction of plasticity. In acute hippocampal slice preparations, the synaptic wiring of the hippocampus is preserved, allowing the researcher to induce plasticity at a large number of synapses with methods that recapitulate physiological stimulations of natural circuitry[115]. In fact, a great portion of all research into the molecular basis of synaptic plasticity has been conducted on the Cornu Ammonis (CA3-CA1) synapses of the hippocampal slice, lending a rich literature to the interpretation of results. Most importantly, it is feasible to purify nucleic acids and proteins for biochemical analysis by pooling slices that have been treated with stimuli that reach a high proportion of cells in the slice.

As with any system, acute hippocampal slices bear several caveats. Preparation of the slices by removal of the hippocampus from the brain and subsequent slicing by a tissue chopper triggers a host of molecular changes and signaling cascades with large effect sizes, so that injury-effects can easily occlude experimental results unless carefully controlled[115]. To a certain extent, this confound is unavoidable – brain tissue must be dissected to prepare it for subsequent experimentation – though careful consideration of injury effects aids in the design of experiments that minimize undesired artifacts of this preparation. Using a tissue chopper rather than a vibratome, and resting the slices for 2 hours on interface chambers minimizes the persistence of injury-effects in the slice and allows the researcher to conduct biochemical and sequencing experiments on material purified from slices[115]. Chopping the tissue results in acute injury to the areas surrounding those touched by the blade including severing of dendritic and axonal processes, and though the slices are subsequently rested in a carefully controlled system, cell death progresses as time passes. Such injury effects are a particularly great

54

concern when analyzing material that is likely to be modified and retain signatures of injury effects, such as changes in gene expression[116–119], though they are ultimately impossible to avoid completely. Thus, it has become common practice for researchers to allow slices ~2 hours resting time after cutting, to minimize injury effects while preserving a large portion of living cells for experimentation[120–122].

Most studies of the effects of traumatic injury to brain tissue have examined mRNA expression. While RNA copy number exhibits a great dynamic range that contributes to the danger of confounding stimulus and injury related changes (if injury upregulates a transcript 10-fold and stimulation only 2-fold, one may never capture the effect of stimulation), ChIP-seq does not exhibit this dynamic range and is thus slightly safer from such confounds. However, it is possible that even in ChIP-seq, dead cells preserve transcription factor-DNA complexes that will be pulled down and sequenced, reflecting cell death rather than plasticity, though they will not exhibit the signal amplification that is common for RNA. In many senses, such effects are impossible to predict without prior knowledge; in our experiments, there is essentially no data to shed light on the effects of injury on CRTC1-containing protein-DNA complexes, and our experimental design is guided largely by studies in our lab and others regarding global changes in RNA expression. While one cannot be sure that sequencing data from tissue that has undergone dissection completely excludes artifacts from tissue damage, the acute hippocampal slice system is nevertheless a powerful system in which to conduct ChIP-seq experiments after the induction of plasticity. Acute hippocampal slices preserve mature brain synaptic connectivity in a highly organized structure understood through a wealth of investigative literature, and allow researchers to apply pharmacological treatments that induce plasticity in a very high proportion of cells in the total tissue area. Despite unavoidable caveats, acute hippocampal slices uniquely navigate the technical concerns of conducting ChIP-seq and the desire to study plasticity in a context that most closely recapitulates the molecular bases of plasticity-induction *in vivo*.

Development of a ChIP-seq protocol from acute hippocampal tissue

The very nature of neurons poses several particular challenges that have rendered assays such as ChIP-seq harder than in many other cell types. Neurons are post-mitotic; they cannot be expanded or passaged in a culture system and must be dissected from animals for every experiment. This renders generation of large quantities of cells much more laborious, slow, and costly than for expandable cells such as human embryonic kidney (HEK), Henrietta Lacks (HeLa), chinese hamster ovarian (CHO), neuro-2a mouse neuroblastoma (N2a), or other common cell lines. In addition, neurons grow long processes that are ensheathed in myelin, a fatty substance important for their electroconductive properties that greatly increases the lipid content of the cells. Difficulty in preparing large quantities of starting material can be addressed to some extent by patiently pooling samples over time, but the high lipid content of the cells makes some biochemical manipulations inherently problematic. Perhaps even more importantly, neurons are designed to be extremely sensitive to their extracellular environment; manipulations such as scraping cells from a dish, treating them with enzymes such as trypsin to dissociate them from each other, or even pipetting without extreme gentleness can activate neurons and confound the effects of pharmacological stimulations. Even still, at this time many studies have yielded high-quality ChIP-seq and RNA-seq data from cultured neurons by troubleshooting innovative methods by which to circumvent challenges in sample preparation. Recent work by Martina DeSalvo, Sylvia Neumann, and Kostantinos Chronis at UCLA conducted ChIP-seq targeting several proteins in rat cultured neurons. For these experiments, many 10-cm dishes, each with 1 full p0 rat brain plated, were pooled to achieve high enough input DNA (~10μg) to conduct the IP. This volume of starting material is typical for ChIP-seq studies in cultured cells of various types, and can be used with sample prep procedures and equipment that have been established for use with relatively high input material. In addition, this dataset utilized an AAV encoding a FLAG-tagged CRTC1 transduced to each plate of cultured neurons, and overexpressed at 2-3x endogenous CRTC1 expression levels. In their work,

Martina and colleagues found that the particular biochemical concerns of cultured neurons, specifically the heavy myelination/lipid content, hindered many manipulations including the nuclear preparations. By increasing the input amount to tens of dishes per sonication and omitting the nuclear preparation, these obstacles were circumvented. Neurons were treated with bicuculline (BIC), which induces robust nuclear translocation of CRTC1 in nearly all neurons in the dish, except inhibitory neurons, which comprise approximately 10-20% of the neuronal population[50]. These details have important consequences; in each BIC-treated dish, neurons were virtually homogeneous with regard to the subcellular localization of CRTC1, such that eventual IP would capture a high ratio of nuclear:cytoplasmic (N:C) CRTC1 that is putatively engaged in protein-DNA complexes. Cultured neurons were cross-linked in a two-step process using DSG (7 Å) followed by formaldehyde (2 Å), applied directly onto cultured cells in-dish, scraped, pooled, and sonicated in 0.1% SDS. It is worth mentioning that many ChIP experiments in other cell lines would first trypsinize the cells, pellet them, and include several steps to deplete the sample of extraneous cellular material by isolating nuclei before cross-linking. Since this was impossible to conduct precisely without significantly altering gene expression in cultured neurons, direct cross-linking before pelleting was preferred. Cell pellets were then pooled and sonicated to prepare protein-DNA complexes of appropriate size, and the IP was conducted using FLAG epitope, rendering differences in post-translational-modification of CRTC1 less likely to affect or bias IP efficiency than with an antibody (even a polyclonal) raised against CRTC1. The protocol used in these experiments from cultured neurons served as a guideline for my own ChIP-seq work in hippocampal slices, though the particularities of brain tissue required further revision and troubleshooting.

Selection of an appropriate antibody for IP of endogenous CRTC1

I conducted my studies on endogenous CRTC1, which may reduce the efficiency, specificity, and yield of the IP compared to that of an overexpressed epitope-tagged protein, but

has the great benefit of circumventing the many caveats of experiments utilizing

overexpression. Thus, I required use of an antibody of extremely high quality raised against

CRTC1; the success of ChIP-seq studies is highly dependent on the fidelity of the antibody used

for the IP[123,124].

Validating antibodies for ChIP-seq has the same general concerns as those of regular

IPs, though it also bears several further considerations. In general, the promiscuity of an

antibody for other proteins present in a lysate will always affect the saturation of the antibody

with the protein of interest. For example, if the antibody binds actin as well as CRTC1, it is

unlikely that the CRTC1 IP will be complete, as much of the antibody will be bound to the vastly

abundant actin. In the context of ChIP-seq, this does not directly change the identity of the

sequencing results from DNA released from CRTC1-protein-DNA complexes – actin does not

bind DNA and thus will not pull down extraneous DNA with it – but the sequencing depth and

complexity will be severely crippled by the low yield of DNA pulldown. Thus, if an off-target non-

DNA-complex-binding protein has significant affinity for the antibody, the major effect is simply

to impair the ability of the antibody to pull down sufficient DNA to be analyzed and not to

confound the actual source of DNA that is pulled down. The promiscuity of the antibody for all

cytoplasmic, and those nuclear proteins that are not cross-linked directly or indirectly to DNA,

then, would seem somewhat tolerable as long as enough target protein is purified.

In practice, ChIP-seq experiments are not so forgiving and require very high-specificity

antibodies. The likelihood of cross-reactivity with other DNA-protein-complex-binding proteins is

significant[123], and the specificity of the antibody is tantamount to obtaining high-quality

sequencing results; suboptimal antibodies generally fail to yield enough high-quality DNA

fragments to obtain robust sequencing data. In fact, academic researchers and companies

alike have developed workflows to validate "elite" antibodies for ChIP-seq, realizing the

importance of good antibodies for these experiments. That said, approaches to antibody

validation should also be considered in the specific contexts of experiments in which they will be used.

In order to ensure sufficient specificity and avidity of antibodies for ChIP-seq, researchers generally prefer to use ones that have been pre-validated and ideally produced robust sequencing results in previous studies. This is trivial for histones and other proteins that have been subjected to countless ChIP-seq studies (a great example is Histone H3K4me3 polyclonal antibody, which has been used across many studies, researchers, and labs) but is a serious concern for proteins that are not surrounded by such a wealth of previous work. It is important to note that previous ChIP-seq datasets using the same antibody offer a compelling comparison by which to validate new datasets; such comparison is a luxury that less-studied proteins are not afforded. Of course, proteins that have not yet been studied in such detail are of at least as great interest as histones, and often much greater interest in many experiments. In order to validate new antibodies for ChIP-seq, researchers sometimes carry out Western Blots (WBs), peptide dot blots, or Enzyme-Linked Immunosorbent Assays (ELISAs) on an assortment of antibodies and then test only those high in specificity for ChIP-seq. Polyclonal antibodies are generally preferred over monoclonals as they recognize multiple antigens and reduce the chance of missing key epitopes masked during the cross-linking process. Although polyclonals exhibit greater batch-to-batch variability and may sacrifice specificity compared to monoclonals, affinity-purified antibodies have greatly increased specificity and minimize cross-reactivity. The concentration of the antibody in the IP also contributes to the signal and background strength of sequencing data; if the other parameters of an experiment are permitting, researchers will often titrate the antibody from 1-10 μg to experimentally ascertain the optimal concentration for high yield without sacrificing specificity. The later steps of the ChIP protocol can also be optimized to increase specificity; in particular, the washes of the IP can be adjusted in many ways to increase the specificity of the final elution. Typically, magnetic protein-G beads are preferred over agarose ones, as the magnetic system can aid in more complete removal of wash

solutions, and washes are conducted successively with sodium chloride and lithium chloride to wash beads as stringently as possible. All of these parameters can be optimized to some degree to improve IP quality and it is clear that obtaining reliable ChIP-seq data requires consideration of nearly every step of the experimental procedure. As each experiment should be designed with the specific input material, antibody, target protein's characteristics, and eventual goal in data analysis in mind, I considered all of these parameters for my experiments on CRTC1 from acute hippocampal slices and created a design that would maximize the likelihood of success.

Especially with a protein whose behavior is as complex as that of CRTC1, it is important to consider the IP of protein-DNA-complexes with every aspect of sample preparation in mind. CRTC1 is a translocating protein, excluded from the nucleus in resting neurons and driven into the nucleus to different degrees – and possibly with different PTM profiles – by different stimulations. Its exclusion from the nucleus (as detectable by IHC) in unstimulated cells serves as an elegant control; one would expect very few or zero peaks in ChIP-seq data. As there is currently no direct evidence to indicate the particular identities of PTMs on nuclear CRTC1 species or their genomic targets in mouse hippocampal slices (other than that they likely include complexes with CREB) after any experimental stimulation, we are unable to base our antibody selection on affinity for any particular species of CRTC1. In fact, experimental determination of antibody specificity is limited for proteins such as CRTC1 that undergo such dramatic changes in PTM, as it is impossible to completely control the relative contribution of different PTM-forms of CRTC1 in a given IP from total cell lysate that contains different forms of the protein. Nevertheless, several fortuitous circumstances aligned to render the challenge of selecting an appropriate antibody for CRTC1 ChIP-seq surmountable. First, ,as the mouse genome contains 3 isoforms of CRTC (CRTC1, CRTC2, and CRTC3) with considerable homology, obtaining a highly-selective antibody for CRTC1 could be a great obstacle. Fortunately, CRTC2 and 3 are virtually absent from the adult hippocampus, and more importantly, from CA1, thus rendering

antibody cross-reactivity to the other CRTC isoforms far less concerning (Fig. 2). The capacity of CRTC1 to contain such a large number of post-translational modifications (PTMs)[51,109,125], however, is a significant concern as they can influence antibody binding dramatically. As we also have no direct evidence showing which PTM forms of CRTC1 are present in the nucleus of CA1 cells after various stimuli induce translocation (though these are likely highly-dephosphorylated forms), it behooves us to choose an antibody that recognizes as many forms of CRTC1 as possible. In this case, the antibody would IP CRTC1 that is bound to protein-DNA complexes, as well as cytoplasmic CRTC1 that will not yield ChIP-seq data. However, if there is sufficient translocation in the input sample and the IP is sufficiently complete, the irrelevant CRTC1 will simply contribute nothing to the sequencing data, and should not cause a problem in data analysis. Importantly, the selection of slice stimulation will greatly affect this parameter, as not all stimulations will induce the same N:C proportion of CRTC1 as others.

Given these considerations and a careful review of available CRTC1 antibodies, we used the TORC1 (CRTC1) A300 rabbit polyclonal antibody commercially produced by Bethyl Labs, the details of which align fortuitously with our experimental concerns. WBs that utilize this antibody, as shown in Chapter 2, reveal that the antibody is able to recognize high- and low-molecular weight species of denatured CRTC1 as well as intermediate species created by BIC or dihydroxyphenylglycine (DHPG) in lysates from cultured neurons. The antibody is also able to recognize cytoplasmic and nuclear CRTC1 by immunostaining and is raised against an immunogen between amino acids 600 and the C-terminus (630) of human CRTC1 (PLTLDGLHMLNDPDMVLADPATEDTFRMDRL), a region that bears 100% amino acid sequence identity between human, mouse, and rat. Encouragingly, standard stringency protein-BLAST of this 31-amino-acid stretch returns against the *Mus musculus* proteome returns only CRTC1, 2, and 3 isoforms, and no other proteins. This immunogen harbors only one site, T602, which has been identified as phosphorylated in N2a cells[51] and no other residues that have been reported to harbor PTMs in any cell type. Ideally, an immunogen would create an

61

antibody with high affinity, and harbor zero sites that are PTM in cells from which CRTC1 would be purified, such that it would bind all forms of CRTC1 equally within a lysate. While of course other, currently unidentified PTMs may exist within amino acids 600-630, there is no reason to assume that there are. Whether accidental or cleverly designed, this is an important feature of the Bethyl A300 antibody and a different immunogen could very likely have been susceptible to more PTMs, affecting antibody recognition of different PTM-forms of CRTC1. The Bethyl A300 CRTC1 antibody is unconjugated, affinity purified, supplied as whole IgG, and previously validated by Bethyl for IP and western blot and by the Martin Lab for immunostaining and western blot. These data are encouraging and provide evidence that the polyclonal antibody is robust in recognizing many forms of CRTC1, though we cannot conclude that every PTM-form of CRTC1 will be equally captured by IP.

Given that CRTC1 behaves very differently in a stimulation and cell-type specific manner (Fig. 3), testing antibodies should be conducted in the cell type in which eventual experiments will be conducted. My ChIP-seq studies required modification of the standard ChIP workflow due to the concerns of working with brain tissue and low input amounts, rendering concerns such as titration of antibody amount less tractable to troubleshoot; the sonicate must be diluted 10x before IP, creating large and unideal volumes that cloud the interpretation of optimal antibody-to-sonicate ratios, and tissue samples are extremely precious. The Bethyl antibody has been used for nearly a decade in the Martin Lab and extensively validated for WB, immunostaining, and IP from neurons, and recently has been validated against a CRTC1 KO mouse (Fig. 4). It is also worth noting that this antibody has been used successfully in ChIP-qPCR of CRTC1 from DG of adult mice[59], though the biased investigation of only a handful of targets as conducted in qPCR is statistically less susceptible to antibody promiscuity than unbiased ChIP-seq. Though many other antibodies against CRTC1 exist, they have been created with different antigens that may harbor more PTM sites, and have not been as

extensively validated in the Martin Lab. For these reasons, the Bethyl CRTC1 antibody seemed the best choice for my experiments.

Optimization of a ChIP-seq protocol for CRTC1 from acute hippocampal tissue

As stated briefly in the introduction, classical ChIP-seq studies on cultured cells include several steps to improve the purity of input material to the IP. In such scenarios, cells are often scraped, pelleted, and subjected to nuclear purification protocols to obtain intact nuclei that are relatively depleted of extranuclear cellular material. This is of course ideal, as it restricts cross-linking and the eventual lysate to nuclear components. In this process, cells are often treated with trypsin or other dissociation agents to assist in biochemical manipulations, and for many cell lines such processing can be highly successful[126,127]. However, due to the extreme sensitivity of neuronal gene expression to mechanical and chemical perturbations, many of these manipulations are undesirable in neurons. While several new developments have emerged to facilitate ChIP studies in lipid-dense tissues[128], they have yet to address the sensitivity of neuronal gene expression, in particular, to biochemical perturbations. Nonetheless, new techniques that utilize genetic strategies to purify nuclei and modify the cross-linking procedure such as the INTACT method have been used to purify nuclei during ChIP sample preparation from brain cells[129], though these studies have focused on histones and have yet to be proven efficacious in studying less-abundant and weaker DNA-binding proteins such as transcription factors, much less transcriptional co-activators that do not directly bind DNA such as CRTC1. Furthermore, studies that employ such strategies generally perform cross-linking during lysis and homogenization of tissue chunks, and do not perform further dissection of brain tissue after stimulation. As the pharmacological treatments in my experiments require intact hippocampal connections between CA3 and CA1, we were unable to fully dissect CA1 from hippocampal slices before snap-freezing them and storing until enough were pooled to perform the ChIP protocol; we needed to further dissect CA1 from intact hippocampal slices

after collecting samples for months at -80°C before cross-linking (to ensure dissection was feasible, and that tissue would not degrade in the process), which prevented such a clever combination of steps as other researchers have been able to employ in simpler preparations of input material.

Due to the particularities of the experiments I planned, I synthesized a ChIP-seq protocol from several sources for use with CA1 from acute hippocampal slices. Study of several ChIP-seq protocols for use in cultured cells or other tissue types (notably, liver adipose tissue which bears some of the same concerns regarding high lipid density that brain tissue does) are summarized in Table S1. From this comparison, it was clear that several parameters would need to be optimized for a new protocol that could circumvent the challenges presented by acute hippocampal slices.

The first of these challenges was achieving efficient sonication of brain tissue. It has long been recognized that the high lipid content of the brain poses challenges to biochemical analysis and often requires modification of techniques compared to more standard ones used in other cell types[130]. Using an Active Motif bath sonicator, I conducted pilot experiments to ascertain optimal sonication power and ON-time to sufficiently sonicate CA1s. Unfortunately, the bath sonicator proved incapable of sufficiently sonicating brain tissue, even when parameters were increased beyond their usual operating limits; after two seven-minute rounds of sonication (which is likely to destroy DNA residing in the target 100-500 base pair (bp) range), the material was mostly unsonicated (Fig. S1). Thus, I necessitated a new approach to shearing DNA in brain tissue, and moved to a probe-tip sonicator. While this approach was not immediately successful for CA1s using a sarkosyl-based buffer, a proprietary sonication buffer from Active Motif containing 0.1% SDS, or my own sonication buffer recipe including 0.5% SDS, I was able to achieve robust sonication of DNA from cultured neurons with any of these buffers. This indicated that the issue with sonication was likely due to the increased lipid content of brain tissue compared to cultured neurons, and provided a foothold by which to guide further

64

experiments (Fig. 5). Quadrupling ON-time was effective in shearing a greater proportion of genomic DNA, though it is likely inappropriate for sonication in a real experiment, as it is too harsh and results in oversonicated fragments and/or destruction of epitopes. A parallel sample sonicated in the same 0.5% sonication buffer, but including N-octyl-glucoside to assist in solubilizing myelin basic protein[131,132] had virtually no effect in improving sonication. Finally, correspondence with Dina Mattheos in the Wood lab at UC Irvine provided a robust method by which to sonicate DNA from brain tissue. Tissue chunks are first pooled in a 1% NP-40 lysis buffer, vortexed, and incubated on ice repeatedly to perform a light digestion of the tissue. After 3 rounds of vortexing and incubation, the lysis buffer is removed and replaced with 1% SDS for sonication. This results in a spread of genomic DNA fragment sizes that approaches the ideal range between 2-1200 bp, with reasonable (2 minute) ON-time, and allowed me to proceed in establishing other aspects of my ChIP-seq protocol.

While I conducted these experiments to optimize sonication parameters, I also researched available options to address the issue of working with low-input starting material. It was immediately apparent that the range of input material I would start with for my experiments using hippocampal CA1 subregions would be significantly less than those of classic ChIP-seq experiments. In fact, though preparing 28 CA1s is highly time-consuming and challenging, it still only yields a small amount of tissue compared to the cellular material harvested for ChIP from cultured neurons (Fig. S2). At the time of my research, there were only four commercially available low-input ChIP kits that seemed worth further examination. After comparison of input requirement, careful review of each company and customer satisfaction, and detailed examination of each protocol (Table S2), I chose to use the Active Motif Low Cell ChIP-seq kit that had just been introduced to the market. This kit does not require a nuclear prep, utilizes the highest-grade reagents available from Active Motif (which are commonly used by ChIP scientists at UCLA and referenced in ChIP publications), and introduces clever optimization techniques that do not compromise the quality of DNA for sequencing. Briefly, input material is

sonicated, pre-cleared on agarose protein-G beads, then IP'd using the antibody of interest, and bound to new protein-G beads. The use of agarose beads is counterintuitive from the perspective of reducing sample loss; usually magnetic beads are preferred for this purpose because the physical action of magnetic separation allows for more complete solution removal than low-speed centrifuge spins of agarose beads (some of the beads are usually left in the supernatant, or some supernatant is left behind to avoid accidentally pipetting beads). In this kit, however, Active Motif developed a special gravity column to retain agarose beads after IP and allow the researcher to perform thorough washes over the column without losing material in pipetting. The kit also employs siliconized low-binding microcentrifuge tubes that withstand sonication and that minimize loss of DNA to plastic binding. The kit features to increase ChIP yield and data quality, including blocking of beads with nonspecific DNA, a carrier for DNA precipitation, and highly-optimized salt concentrations and pH for IP washes, elution, de-crosslinking, and DNA retrieval. This kit also supplies all reagents necessary for library preparation and size selection to run on Illumina NGS platforms. Overall, this kit seemed extremely well designed and through personal communication with Active Motif and my own pilot experiments, I was confident it would be streamlined from tissue preparation to sequencing without question of compatibility between any steps of the process. This said, the Active Motif protocol had not been validated for use in brain tissue or even cultured neurons, and my experience with the challenges of sonicating brain tissue led me to modify the protocol slightly.

The first half of my ChIP-seq protocol from acute hippocampal slices includes optimization of cross-linking parameters bearing the particular concerns of collecting sufficient hippocampal slices, further dissecting and pooling them, and sonicating them with a Misonix 3000 sonicator. Briefly, hippocampal slices were stored at -80°C until enough were collected to pool for an experiment, then CA1s microdissected in groups of four and placed into DSG cross-linking solution for 25 minutes. This was followed by cross-linking in formaldehyde for 10 minutes, re-pooling of all CA1s per sample, lysis using the previously described 2-step method,

and sonication in 1% SDS. The high SDS concentration is key to disrupting the high lipid

content of the tissue, yet it poses a problem for IP; the high detergent concentration will prevent

antibody-antigen association. Thus, I was forced to dilute the sonicate 10-fold before

performing IP, which created large (5ml), unideal volumes for the IP. To combat this decreased

efficiency, I conducted the IP in several parallel microcentrifuge tubes to ensure better agitation

than in a larger-volume tube, and used very generous concentrations of beads and antibody.

These were the only major modifications I made to the Active Motif protocol, though the entire

custom protocol is delineated and annotated in Appendix 1. Having established this protocol

and passing checkmarks of feasibility for my planned experiments, I focused on carefully

selecting pharmacological stimulations to induce plasticity in acute hippocampal slices.

Selection of stimulation protocols to induce synaptic plasticity

A great advantage of switching model system from cultured neurons to acute

hippocampal slices is the existence of several well-established protocols for chemical induction

of long-term potentiation (LTP) and long-term depresson (LTD) in slice that more closely

recapitulate those that underlie learning and memory *in vivo*. While glycine-LTP and NMDA-

LTD in cultured neurons require preincubation of neurons with a mixture of pharmacological

agents to shut down many key signaling pathways (tetrodotoxin (TTX) to block action potentials

(APs), BIC to block $GABA_A$ receptors, strychnine (Strych) to block glycine receptors, and 0 Mg^{2+}

to artificially render depolarization unnecessary for NMDA receptor (NMDAR) activation),

chemical protocols to induce plasticity in acute hippocampal slices do not require the shutdown

of inhibitory signaling or action potentials. In fact, these differences speak strongly to the type of

plasticity that is induced in each model system; Gly-LTP and NMDA-LTD in cultured neurons

are substantially different than forms of canonical hippocampal CA3-CA1 synaptic plasticity.

Although methods of inducing plasticity in acute hippocampal slices using electrical

stimulation are the most highly studied and physiologically-relevant, conducting biochemical

analyses of the effects of electrically-induced plasticity can be challenging. This is largely

because it is hard to define exactly which Schaffer collaterals and CA1 postsynaptic cells have

been stimulated by the electrode and to what extent; the routine use of a parallel control

pathway between CA3-CA1 in which plasticity is not induced speaks to the fact that standard

electrical plasticity-induction protocols do not reach all synapses in the slice[133]. Researchers

have successfully activated a higher proportion of fibers by placing wide stimulating electrodes

that straddle stratum radiatum, but it is impossible to apply exactly the same electrical impulse

to all axons in the slice due to the decay of the stimulation pulse with distance from the

electrode tip. As the goal of my experiments was to identify stimulus-induced changes in the

binding of CRTC1 to protein-DNA complexes, I needed to maintain great control over the

stimulus provided to the cells as well as to maximize the signal-to-noise ratio of the tissue input

to the ChIP protocol. With these concerns in mind, I focused on pharmacological stimulii

capable of reaching a high proportion of synapses in every slice and that recapitulate canonical

electrically-induced synaptic plasticity in CA1.

Pharmacological agents afford the experimental advantages of directly and equally

activating all receptors of a certain subtype with some temporal control (endowed by

experimenter-controlled incubation time, but mediated for each agent by its receptor unbinding

kinetics). Pharmacology is a valuable tool towards analysis of biochemical changes in acute

slices, and using pharmacological protocols has been used successfully in conjunction with next

generation sequencing (NGS) to identify changes in RNA expression that accompany the

induction of synaptic plasticity[134,135]. It is a logical step forward to apply the same treatments to

understand the regulation of transcription that underlies such changes. I thus reviewed

pharmacological treatments that recapitulate bidirectional synaptic plasticity and selected three

from which to acquire CRTC1 ChIP datasets.

FSK-LTP

Electrically-induced LTP is usually induced by either theta-patterned stimulation or high frequency stimulation (HFS). Though low frequency stimulation is usually of insufficient strength to induce LTP, coincident increases in postsynaptic cyclic adenosine monophosphate (cAMP) can render such subthreshold electrical stimulations capable of inducing LTP[136–138]. Incubating acute hippocampal slices in standard artificial cerebrospinal fluid (ACSF) containing 50μM forskolin (FSK) for 5 minutes, followed by 5 minute incubation in a modified ACSF containing 0 Mg^{2+}, elevated K^+ and Ca^{2+}, and 50μM forskolin (FSK) induces robust LTP (FSK-LTP) that lasts at least 3 hours[139]. This treatment replaces electric stimulation of presynaptic fibers with K^+ elevation to achieve a more global synaptic activation during high-Ca^{2+} stimulation, and includes FSK to activate adenylyl cyclase (AC). This form of LTP is NMDAR-dependent, AC/cAMP and calmodulin kinase II (CaMKII) pathways, relies on synaptic activity in the form of spontaneous bursting, and causes an increase in protein levels of the IEG activity regulated cytoskeleton associated protein (Arc) one hour after induction[139,140]. Perhaps most importantly for ChIP-seq studies, the maintenance of FSK-LTP requires both mRNA and protein synthesis (Fig. 6). FSK-LTP has recently been used to identify a host of changes in in alternative polyadenylation[135], total mRNA, and ribosome-loaded mRNAs[134] induced by the protocol at early (30') and late (multiple hour) timepoints. Importantly, this protocol induces and requires bursting synaptic activity between CA3 and CA1; severing of these connections prevents LTP-induction[140]. FSK-LTP provides a fantastic chemical protocol by which to induce LTP at CA1 synapses and has recently been used to study changes in transcription, lending strong motivation to study its effect on CRTC1.

NMDA-LTD

A brief application of NMDA (usually 20μM for 3 minutes) can induce a form of LTD that overlaps substantially with LFS-LTD and spike timing-dependent plasticity (STDP)-LTD, as they

are mutually exclusive and cannot be induced on top of each other, although significant

differences do exist between them[141,142]. NMDAR-dependent LTD is relatively easy to induce in

young animals, but is more difficult to induce in brain slices from adults[143,144] or intact rodent

hippocampi *in vivo*[145–147]. Recently, however, the O'Dell Lab at UCLA established an NMDA

protocol by which to induce LTD in adult mice by slightly elevating Ca^{2+} in ACSF from 2mM to

4mM, such that NMDA application produces a stronger increase in intracellular Ca^{2+} sufficient to

trigger intracellular signaling[148]. This NMDA-LTD protocol causes α-amino-3-hydroxy-5-methyl-

4-isoxazolepropioinic acid receptor (AMPAR) endocytosis, induces phosphorylation of p38

mitogen activated protein kinase (MAPK), and dephosphorylation of GluA1 AMPA receptors at

S845 and T840. The induction of LTD and dephosphorylation of GluA1 receptors are mediated

by protein phosphatases 1 and 2 (PP1 and PP2), as inhibiting them with cantharidin prevents all

of these effects (Fig. 8). Given that this stimulation relies on specific signaling pathways

engaged by NMDARs which are known to play pivotal roles in synaptic plasticity, and that

NMDA is known to induce CRTC1 translocation in cultured neurons (see Chapter 2), there is

great motivation to include NMDA-LTD in this study.

DHPG-LTD

As in cultured neurons, activation of metabotropic group I (mGluR1/5) receptors by

DHPG induces a protein-synthesis-dependent form of LTD that is distinct from NMDA-LTD[68].

The first evidence that mGluRs are involved in LTD was presented by studies that blocked

Group I mGluRs with L(+)-2-amino-3-phosphonopropionic acid (LAP3) and observed blockade

of *de novo* LTD[149] or α-methyl-4-carboxyphenylglycine (MCPG) which blocked both

depotentiation[150] and *de novo* LTD at CA1 synapses[151]. Group 1 mGluRs are coupled to G_q/G_{11}

and activate phospholipase C (PLC) leading to conversion of phosphoinositol diphosphate

(PIP_2) to diacylglycerol (DAG) and inositol triphosphate (IP_3)[69]. IP_3 then acts on IP_3 receptors on

the endoplasmic reticulum to mobilize intracellular calcium stores, and DAG leads to activation

of protein kinase C (PKC). It has been reported many times that PKC activation is critical for the

induction of mGluR-LTD, though DHPG-application is insufficient to drive LTD-induction in CA1

without the action of basal M_1 muscarinic acetylcholine receptors (M_1 mAchRs), indicating that

DHPG-LTD may not be solely governed by the action of mGluRs[96]. Moreover, group 1 mGluR

activation can also affect additional signaling pathways, downstream of G_q as well as those

stemming from $G_{i/o}$, G_s, and others that are completely independent of G protein effectors[70],

including phospholipase D, casein kinase 1, cyclin-dependent protein kinase 5, Jun kinase,

components of the mitogen-activated protein kinase (MAPK)/extracellular receptor kinase (ERK)

pathways, and the mammalian target of rapamycin (mTOR)/p70 S6 kinase pathway[71–73]. The

regulation of MAPK/ERK is thought to be very important in the regulation of DHPG-induced

synaptic plasticity[74,75] and in fact upregulation of phospho-ERK serves as a robust marker of

DHPG-induced LTD in acute hippocampal slices (Fig. 7).

There is considerable evidence that mGluR- and NMDAR-mediated LTD are distinct

forms of synaptic plasticity. In slices, mGluR-mediated LTD is usually induced electrically by

paired-pulse LFS[152] rather than single-shock LFS used to induce NMDA-LTD. Additionally,

NMDAR-LTD, but not DHPG-LTD in CA1 was associated with a decrease in sensitivity to L-

glutamate[153]. Perhaps most important to its distinction from NMDA-LTD, DHPG can be used to

depress synapses that have been potentiated by NMDAR-dependent HFS, and this

depotentiation can be washed out by application of the group I mGluR inhibitor LY341495[74],

showing that the molecular underpinnings of LTP can persist in an occult state despite

electrophysiological depression induced by mGluR-LTD. In concordance with this, further HFS

is incapable of restoring potentiation to DHPG-depotentiated synapses, showing that the

mechanisms by which they affect synaptic strength cannot completely overlap.

Thus, DHPG-LTD is a very interesting form of synaptic plasticity that is remarkably

distinct from canonical NMDAR-induced plasticity. DHPG-LTD is mostly unstudied with regards

to its effects on gene expression, though a few pieces of evidence suggest that this is an area ripe for investigation. Though conducted in organotypic hippocampal slices rather than acute, one study found that DHPG causes a MAPK-mediated increase in nuclear phospho-ETS-domain-containing-protein (pElk-1), that Elk-1 and serum response factor (SRF) exhibit DHPG-induced binding of serum response elements (SRE) on chromatin in ternary complexes with 1:2 stoichiometry[154]. This study also utilized microarrays and qPCR to show that DHPG induces upregulation of c-fos, JunB, Egr1, and Nr4a1 IEG mRNAs in organotypic slices. As DHPG-induced LTD clearly involves the activation of many pathways, dissecting those that are necessary and sufficient for its manifestation is complicated. However sufficient evidence exists to support significant distinction between DHPG-LTD and NMDA-LTD. DHPG-LTD is also known to induce changes in transcription and is dependent on protein synthesis, rendering it a highly interesting protocol by which to study stimulus-induced nuclear translocation of CRTC1 and binding to protein-DNA complexes.

As the aim of my experiments was to examine the transcriptional targets of CRTC1 after bidirectional plasticity, I necessitated robust protocols by which to induce LTP and LTD. These three protocols (FSK-LTP, NMDA-LTD, and DHPG-LTD) are highly distinct in molecular underpinnings and seemed most likely to reveal interesting biology regarding changes in gene expression that accompany the induction of bidirectional synaptic plasticity.

Results

Experiments in cultured neurons (Chapter 2) showed that different pharmacological stimuli result in different magnitude and variance of nuclear CRTC1. Although experiments in cultured neurons and acute hippocampal slices are scarcely comparable due very significant differences in circuitry and protocols used to induce plasticity, this observation illuminates the need to examine the extent of CRTC1 translocation after each stimulation. To this end, I

conducted IHC on acute hippocampal slices after stimulation with FSK-LTP, DHPG-LTD, NMDA-LTD, or ACSF control. As CRTC1 has been shown to undergo synaptonuclear translocation at rates consistent with active transport[51], approximately 1 μm/sec, I chose to hold constant the amount of time after stimulation onset, to ensure that in every condition there was equal time for CRTC1 to accumulate in the nucleus. This was simple for FSK-LTP and DHPG-LTD, as they are both 10-minute protocols. NMDA-LTD, however, only involves a 3-minute pharmacological stimulation. Thus, for the NMDA-LTD condition, I included a 7-minute washout incubation after 3-minute NMDA-stimulation, to reach 10-minute total time after stimulus onset for CRTC1 to translocate to the nucleus.

IHC of slices after these stimulation protocols revealed that different amounts of CRTC translocated to the nucleus of CA1 cells in each condition (Fig. 9). As it seemed logical that material from CA1 that robust CRTC1 translocation would yield the highest amount of CRTC1-protein-DNA complexes for ChIP-seq, and DHPG-LTD showed the strongest CRTC1 translocation to CA1, I chose to focus initial experiments on this stimulation protocol.

In collaboration with Jenny McGrady-Achiro in the Martin Lab, I generated acute hippocampal slices treated with either ACSF control or DHPG-LTD until 40 slices were accumulated for each condition. After dissection of CA1s and pooling for each condition, they were cross-linked in DSG and formaldehyde, sonicated, and subjected to IP using half (20 CA1s) for IgG IP and the other half for CRTC1 IP. After completing the rest of the ChIP protocol outlined in Appendix 1, libraries were prepared for each sample and sequenced on the Illumina HiSeq platform (Fig. S3). After data processing and alignment to the mm9 build of the mouse genome, alignment files were analyzed using the Homer software suite[155] employing IgG as control/background comparison for peak-calling in each condition. This analysis identified 117 peaks for the DHPG-CRTC1 sample and 26 for the ACSF-CRTC1 condition. Manual examination of every peak identified across either condition and removal of uncertain peaks and false-positives resulted in a final peak count of 113 peaks for DHPG-CRTC1 (Fig. 10) and 2

peaks for ACSF-CRTC1 (Fig. 11). These manually-verified peaks appear very robust in peak shape, amplitude, enrichment over IgG controls, and largely overlap with genes identified by other datasets examining transcription factor ChIP and upregulated mRNA associated with the induction of neuronal activity and plasticity[24,25,115]. The 113 DHPG-CRTC1 peaks include IEGs such as *c-fos*, *nr4a1*, *nr4a2*, *nr4a3*, and *jun*, though they do not include all IEGs or previously-identified CRTC1 target genes. Notably, there is no DHPG-induced CRTC1 peak corresponding to Arc, nor is there a peak at the *fgf1b CRE1* locus (Fig. S4), which was identified by ChIP-qPCR to be an important CRTC1 target in the DG of fear-conditioned mice[59].

The list of 113 DHPG-CRTC1 peaks was further analyzed by the *de novo* motif identification software included in Homer, which revealed that 65% of targets within this list harbor CRE sites in their promoter regions (Fig. 12). To further validate CRTC1 ChIP peaks, I searched for CREB and other ChIP datasets generated from material that would be most comparable to the acute hippocampal slices used in my dataset. Literature search yielded many CREB datasets that could be used to compare against my CRTC1 dataset, though unsurprisingly, none were conducted in exactly the model system as my experiments were (Table S3). Unfortunately, the rat and mouse genomes are divergent enough that one cannot load a rat alignment onto a mouse genome build, and using LiftOver to transform genomic coordinates from one genome is messy and undesirable. I thus settled on two other datasets: one from Michael Greenberg's lab targeting CREB, CREB-binding Protein (CBP), SRF from unstimulated and KCl-stimulated cultured neurons[25], and another from Michael Rosenfield's lab targeting CREB from unstimulated and Reelin-stimulated cultured neurons[24]. As I was unable to download CREB ChIP-seq datasets from adult mouse brain, these datasets from mouse cultured neurons were the closest model system to mine from acute mouse hippocampal slices. While the Kim dataset was from KCl-stimulated neurons, which is a closer stimulation to my DHPG stimulation than Reelin, the data quality was somewhat inferior to that of the Telese dataset. Thus, I compared my data to both. Visual inspection of 113 DHPG-CRTC1 peaks

revealed that most overlapped with CREB peaks from both the Telese and Kim datasets. In both of these datasets, there were very few stimulus-induced CREB peaks that were not present in the unstimulated condition, which is consistent with previous observations (Martin lab, unpublished), and in contrast to the multitude of DHPG-induced CRTC1 peaks. DHPG-CRTC1 peaks sometimes overlapped with SRF peaks, and those contained in promoter regions often overlapped with CBP peaks. Interestingly, the two peaks identified in ACSF-CRTC1 ChIP from acute hippocampal slices did not overlap with CREB, SRF, or CBP peaks from either of the datasets from cultured neurons. Using Homer to call peaks on both the Kim and Telese CREB datasets returned thousands of peaks, which were unfeasible to inspect manually as was conducted for CRTC1 peaks. However, CREB peaks from these datasets that were inspected in verifying CRTC1 peak overlap were generally robust to visual inspection.

To further analyze the DHPG-CRTC1 peaks, the list of 113 peaks was analyzed using several software analysis suites. The GREAT software suite[156] showed that peaks in this dataset were not enriched for any particular distance from TSS's. DHPG-CRTC1 peaks are found in promoter and non-promoter regions of the genome (Fig. 13), whether one chooses a stringent (-110 to +5 bp) or looser (-5kb to +500bp) cutoff distance from TTS's to define promoter regions. Homer's integrated gene ontology (GO), molecular function, and cellular component analysis returned several terms related to nuclear proteins, transcriptional regulation. Similar terms were identified using DAVID[157,158] and GREAT (Fig. 14).

Finally, to compare this DHPG-CRTC1 dataset to a broader pool of other ChIP datasets, I utilized the ChEA analysis suite[159]. ChEA analysis revealed that the DHPG-CRTC1 dataset contains peaks that overlap with many other datasets, most notably and strongly with CREB and T-Cell Factor7/Transcription Factor 7 (TCF7) ChIP datasets (Fig. 15). ChEA also compares input datasets to ENCODE histone modification datasets; certain subsets of DHPG-CRTC1 peaks show enrichment for certain histone modifications that bear some indication of chromatin state at these loci. One set of 8 genes clusters with histone 3 lysine 4 monomethylations

(H3K4me1), which generally indicates active promoter regions or TSS, and another set of 9 genes clusters with histone 3 lysine 36 trimethylation (H3K36me3), which generally reflects to exons. These observations, however, are at best suggestive and motivate future studies. Individual transcription factors and histone modifications are each only single components of complex regulatory systems that mediate gene expression; histone modifications and transcription factor binding data from different cells may not completely or accurately reflect information about the comprehensive genomic environment acute hippocampal slices[160–162].

In summary, DHPG-CRTC1 peaks are distributed amongst genomic locations without bias toward any particular categorization of annotation (promoter, enhancer, intergenic, exonic, etc). They nearly entirely overlap with CREB datasets from cultured neurons, partially overlap with SRF peaks, and CRTC1 peaks within promoter regions often overlap with CBP peaks from the same datasets. GO and similar analyses of genes from the DHPG-CRTC1 dataset return terms related to DNA/transcriptional regulation.

Discussion

This initial dataset for CRTC1 peaks from ACSF control and DHPG-stimulated acute hippocampal slices reveals DHPG-induced CRTC1 binding to protein-DNA complexes at 113 loci. The strong overlap with CREB ChIP-seq data from studies in cultured neurons is encouraging, as CRTC1 is known to bind CREB and thus expected to overlap with CREB ChIP. While there is no prior data from neurons to indicate that CRTC1 binds other transcription factor complexes, the overlap with SRF indicates that this may be an avenue of research ripe for exploration. Interpretation of the present CRTC1 data, however, bears careful consideration of the experimental design and technical limitations.

As acquiring large amounts of CA1s for each ChIP experiment is extremely laborious and costly in terms of numbers of animals, it is not feasible to generate similar input quantities as studies that are conducted in cultured cells. Thus, the amount of input tissue used for these

experiments is far less than those from ChIP-seq experiments from cultured neurons (Fig. S2).

In addition, it is not clear how abundant CRTC1-protein-DNA complexes are after any

stimulation in acute hippocampal slices. DHPG was chosen for initial experiments because it

drove the highest amount of translocation in CA1 relative to other treatments and ACSF control,

but as IHC using any antibody must be controlled within-antibody and it is impossible to infer

true protein quantities across different proteins using different antibodies, it is impossible to

know the amount of CRTC1 in the nucleus compared to a highly-expressed protein such as

CREB or histones that bind DNA directly. While IHC shows a strong DHPG-induced increase in

CRTC1 immunostaining in the nuclei of CA1 cells, it is impossible to infer that this results in

abundant CRTC1 interaction with protein-DNA complexes. For this reason, the complete lack of

data for other ChIP targets from acute hippocampal slices prepared in a similar fashion, and the

possibility that stimulation-specific changes in CRTC1 PTM may greatly influence its binding to

proteins in the nucleus, it is impossible to hold any reasonable expectation of how many peaks

this DHPG-CRTC1 dataset should produce. One hundred and thirteen peaks is a very low

number compared to other ChIP-seq datasets including those from Kim and Telese used in the

present analysis, however due to vastly different input amounts and ChIP targets, there is no

reason to expect that peak count would be higher with greater input amount; there are too many

confounding variables. Though one previous study examined specific mRNAs after DHPG

induction in organotypic acute hippocampal slices and observed upregulation of IEGs[154], there

are significant differences between acute and organotypic slice preparations that prohibit true

comparison of these datasets. As there are no ChIP-seq or RNA-seq datasets from acute

hippocampal slices at the present time, technical differences between sample preparation from

culture and brain tissue disallow scientifically-grounded expectations for CREB binding to DNA

or changes in mRNA expression after DHPG-LTD in acute hippocampal slices.

Despite limitations in comparison to other studies or attempts to understand the

completeness of ChIP peak capture in the DHPG-CRTC1 dataset, internal data validation of

sequencing quality and peak identity is consistent; visual verification of peaks strongly suggests that they are robust in shape and believable in identity. There are robust peaks at IEGs and other genes (such as CREM) that are both interesting and known to be regulated by activity, though not all activity-regulated genes. It is important also to note that as there are so many contributing variables to the identity and number of peaks identified in this dataset compared to others, it is impossible to the same CRTC1 or CREB targets identified in other studies conducted in different experimental contexts.

The two ACSF-CRTC1 peaks are tantalizing in identity; both *Crtc1* and *Camk2a* are believable genomic targets of CRTC1-complexes. As CaMK2a is a very important neuronal gene that is expressed at high levels in adult neurons[163–165], it is feasible that CRTC1 drives its transcription in ACSF-unstimulated CA1 cells. The lack of CREB, SRF, or CBP ChIP peaks from either of the other datasets examined at the locus of the ACSF-CRTC1 peak is interesting; it may indicate that this and other loci that bear CRTC1 peaks but lack CREB peaks may reflect CRTC1-containing transcription factor complexes that lack CREB and instead contain other bZIP transcription factors, or it may simply reflect the differences in model system and experimental context between datasets. This is also the case for the *Crtc1* locus that bears many ACSF-CRTC1 peaks within the gene body. In this scenario, CRTC1 may bind protein complexes that localize to the *Crtc1* gene body and silence the gene in a more labile manner than would chromatin modifications. Perhaps most importantly, the nearly undetectable quantity of nuclear CRTC1 in the ACSF condition by IHC indicates that this sample may truly operate at "low-input" unlikely to yield many ChIP peaks. The identification of these two peaks (*Crtc1* and *Camk2a*) was surprising, and may indicate that they are in fact very robust; minimal amounts of nuclear CRTC1 may restrict its binding to only a few high-affinity complexes. However, these peaks could equally be more likely to reflect artifacts of the ChIP-seq protocol, as no peaks were expected from the nuclear-CRTC1-depleted ACSF sample. Further biological replicates will assist in addressing these possibilities.

It is also worth noting that the motif and GO analysis methods employed by Homer and other software suites bear caveats. The Homer *de novo* motif identification software analyzes all entries contained in the input peak file. It then looks for conserved motifs in the promoter regions of genes represented in this list, and calculates frequency; in this analysis of DHPG-CRTC1 peaks, 65% contained the CRE motif but no other motifs were sufficiently enriched to return a low p-value. This software does not, however, subcategorize peaks based on genome annotation by sorting them into promoter, TSS, enhancer, gene body, intergenic, exonic, or other types of genomic features. Thus, it is possible that one or more of these subcategories contains motifs specific to the type of ChIP peak. It is possible that CRTC1 peaks at TSS/promoter regions lie close to motifs that dictate binding of specific transcription factors, and that these results are washed out by the overall percentage calculation across all entries in the peak file. In order to dissect these possibilities, peaks must be carefully subcategorized (by eye, to achieve most careful designation) before submission to Homer or GO analysis.

Finally, a brief discussion of the meaning of CRTC1 nuclear translocation is warranted. While a theoretical complete lack of CRTC1 in the nucleus of CA1 cells would certainly prevent pulldown of any CRTC1-containing protein-DNA complexes in ChIP-seq, the ACSF condition does not appear to reflect such a complete lack of nuclear CRTC1. Upon further consideration, there is no reason to assume that more CRTC1 in the nucleus leads to increased number of genomic targets. Though it still seems most logical that this would be the case, there is a distinct possibility that the PTMs on CRTC1 following DHPG-LTD may cause surprising effects in the nucleus. It is possible, for example, that these PTMs cause CRTC1 translocated to the nucleus by DHPG-LTD stimulation to bind all previously-genomically-targeted CRTC1 molecules and sequester them from the protein complexes they once resided in, rather than further binding such complexes. Furthermore, there are only two copies of any given genomic locus per cell (one per chromosome), and the increase in CRTC1 molecules that flood the nucleus following DHPG-LTD is dramatic. As CRTC complexes form a 2:2:1 stoichiometry with

CREB and DNA, respectively[42], it appears that there would be a saturation effect of increasing

nuclear CRTC1; each CREB-occupied CRE on the genome can only accept 2 molecules of

CRTC1. Such saturation may be mediated by existence of multiple adjacent CRE or CRE-like

sequences within a given genomic region and increasing CREB-binding capacity. While there

are many caveats to this reasoning, such as the lack of correlation between increases in

fluorescence by IHC and the true number of molecules reflected by this signal, there may exist

both lower and upper thresholding to the effects on transcription of increasing nuclear CRTC1.

Thus, the present ChIP-seq dataset reveals many CRTC1 peaks that appear robust to quality

control, though rigorous interpretation of these results requires further experimentation and

analysis

Concluding remarks

As is often the case for datasets that are limited in background literature, the present

ChIP-seq data spawns more questions than it answers. While this dataset is invaluable for

many reasons, including validating a new ChIP protocol for use with low starting material from

adult rodent brain and revealing CRTC1 genomic targets following DHPG-LTD in acute

hippocampal slices, understanding the meaning of these peaks requires further investigation.

Excited by the possibility that different stimulations may lead to differential CRTC1 binding to

transcription factor complexes localized to different genomic loci, I have conducted a large set of

experiments to corroborate the present results and expand upon them for all four conditions

discussed in the introduction to this chapter: ACSF, FSK-LTP, DHPG-LTD, and NMDA-LTD.

Sample preparation and sequencing has been completed for all samples in this larger study, is

currently undergoing analysis, and is discussed in detail in the next chapter.

Materials and Methods

        All experiments were performed with approval from the UCLA Institutional Animal Care and Use Committee.

Hippocampal slice preparation

        400 μm thick hippocampal slices were prepared from wild-type adult male C57/Bl6J mice at 8-12 weeks of age. Slices were recovered for 2 hours at 30°C in a custom 8-well interface chamber system with oxygenated (95% O_2/5% CO_2) ACSF containing 124 mM NaCl, 4 mM KCl, 25 mM $NaHCO_3$, 1 mM NaH_2PO_4, 2 mM $CaCl_2$, 1.2 mM $MgSO_4$, and 10 mM glucose.

Pharmacological induction of plasticity

        After resting, slices were submerged in ACSF/drug solutions to induce plasticity. For DHPG-LTD, slices were submerged for 10 minutes in normal ACSF containing 100μM DHPG (Tocris 0805). For NMDA-LTD, slices were perfused with ACSF containing 4mM (rather than normal 2mM) Ca^{2+} for at least 30 minutes, then submerged in 4mM Ca^{2+} ACSF, containing 20μM NMDA (Tocris 0114) for 3 minutes. After 3-minute NMDA application, slices were washed of NMDA and submerged in 4mM Ca^{2+} ACSF for an additional 7 minutes. ACSF control slices were submerged in unmodified ACSF for 10 minutes. Immediately after the 10-minute mark for each incubation, slices were either snap-frozen to the side of tissue-homogenization microcentrifuge tubes that were pre-chilled on dry ice or fixed overnight (O/N) at 4°C in 4% PFA to be processed for IHC.

IHC

        After fixing in PFA, slices were rinsed 3x in phosphate-buffered saline (PBS), covered in HistoGel (VWR HG-4000-12), then paraffin-embedded. 4 μm thick paraffin sections were

serially rehydrated and deparaffinized. After heat-induced antigen retrieval, cell membranes were permeabilized with 0.1% Triton-X-100 (Tx-100) at RT for 30 minutes, then blocked in 10% goat serum at RT for 1 hour. Slices were then incubated in primary antibodies O/N at 4°C and with secondary antibodies and Hoechst (Thermo Fisher Scientific H3570) for 2 hours at RT.

Confocal images were acquired using a Zeiss LSM 700 with 405, 488, 555, and 639 nm solid-state lasers. Zen 2009 software was used for data acquisition and preliminary image analysis.

Nuclear values of CRTC1 were quantified using ImageJ software. Breifly, raw confocal images of CA1 were taken using a 40x oil objective were imported into ImageJ. For each neuron, masks and regions of interest (ROIs) were manually drawn around the cell nucleus (outlined by Hoechst staining and MAP2 staining). Pixel intensities were quantified to obtain nuclear values. Data was then plotted using Prism Graphpad software. All data sets are presented as mean ± SEM as scatter plots and *p*-values determined using One-Way analysis of variance (ANOVA) with Bonferroni's Correction *post-hoc* test.

Primary antibodies used were: rabbit anti CRTC1 (Bethyl Labs A300), chicken anti MAP2 (Cell Signaling 9106), and rabbit anti p44/42 MAPK (ERK) (Cell Signaling 9102). Secondary antibodies used were: IRDye 800CW goat anti mouse (Li-Cor 926-32210), IRDye 680LT goat anti rabbit (Li-Cor 926-68021).

ChIP protocol and sonication

Please refer to Appendix 1 for a detailed explanation of sonication and ChIP protocols. Briefly, CA1s were thawed from the side of tissue-homogenization tubes in PBS containing protease (Roche cOmplete) and phosphatase (Roche phosSTOP) inhibitors and CA1 was microdissected. 20 CA1s per condition were pooled 4 at a time and fixed for 25 minutes in disuccinimidyl glutarate (Fisher Scientific 20593), then 10 minutes in formaldehyde (Sigma Aldrich 252549), then quenched for >10 minutes with 125mM glycine. CA1s were pooled in

siliconized microcentrifuge tubes (Active Motif) and lysed on ice using a 1% NP-40 buffer as outlined in Appendix 1. Solution was then switched for a 1% sodium dodecyl sulfate (SDS) sonication buffer. Tissue was sonicated using a MiSonix 3000 microtip with the following settings: 3 seconds ON, 15 seconds OFF, power 5.5, 2 minutes 30 seconds total time. Tubes were submerged in wet ice to cool samples during sonication.

ChIP was conducted along the lines of a Low-cell ChIP Seq Kit (Active Motif 53084). Antibodies used were: rabbit anti CRTC1 (Bethyl Labs A300) and purified rabbit IgG (Bethyl Labs P120-101).

ChIP-seq and data analysis

ChIP-seq libraries were prepared using the Next-Gen Library Kit included in the Low-cell ChIP Seq Kit (Active Motif). Library integrities were analyzed using the Agilent 2200 Tapestation machine. 50 base pair single-end sequencing was conducted on an Illumina HiSeq 4000 machine through the Broad Stem Cell Research Center core sequencing facility at UCLA. Raw sequencing reads were filtered for PCR duplicates using the unique molecular identifiers included in the Active Motif kit, and aligned to the mm9 build of the mouse genome.

The Homer analysis suite was used using default settings for peak-calling, motif, and GO analysis to analyze CRTC1-ChIP data from ACSF and DHPG conditions, with corresponding IgG IP as a background BED file. Adjustment of input parameters for peak-calling or motif analysis had little effect on the output peak file. Alignments were loaded into IGV or the UCSC Genome Browser and each peak identified by Homer was visually inspected. For comparison, two previously published datasets were loaded into browsers (Kim et al. *Nature* 2010, GEO: GSE 21161 and Telese et al. *Neuron* 2015, GEO: GSE66710).

To further examine the DHPG-CRTC1 list of visually-confirmed peaks, peak files were run through other analysis suites. Using GREAT, DAVID, and ChEA software suites.

Generation of constructs and cell line experiments for CRTC1$^{1-270}$-De2

Site-directed mutagenesis was used to introduce point mutations into pDendra-CRTC1$^{1-270}$-De2 (Ch'ng et al. 2015) and generate the S3A and CBD mutants. Plasmids were transfected into HEK and N2a cells using lipofectamine, fixed in paraformaldehyde (PFA, Electron Microscopy Sciences 15710) for 10 min at room temperature (RT) and stained using standard immunocytochemical procedures.

HEK and N2a cells were treated with 10 μM FSK (LC Laboratories F-9929) and/or 1 μM A23187 (Sigma-Aldrich, C7522) for 4 hours as in Altarejos et al. *Nat. Med.* 2008.

Western Blotting

Cells were lysed in RIPA buffer (Sigma-Aldrich R0278) and quantitated using BCA assay (Fisher Scientific 23225). SDS/PAGE gels containing 4% and 10% acrylamide for stacking and resolving gels respectively were loaded with ~20μg protein per lane. Protein was transferred to 0.2 μm nitrocellulose membranes using standard apparati (Bio-Rad) at 40mA O/N. Membranes were blocked using tris-buffered saline (TBS) Odyssey blocking buffer (Li-Cor Biosciences 927-50000) for 1 hour, then incubated O/N in blocking buffer + antibody at 4°C. TBS containing 0.05% Tween-20 (TBST) was used to wash membranes 3x 5 minutes, then incubated in blocking buffer + fluorescent secondary antibody for 2-4 hours at RT. Following another 3x 5 minute set of TBST washes, immunoblots were imaged using an Odyssey scanner (Li-Cor) and analyzed using Image Studio and Image Studio Lite (Li-Cor).

Primary antibodies used were: rabbit anti CRTC1 (Bethyl Labs A300), mouse monoclonal anti phospho-p44/42 MAPK (ERK) (Cell Signaling 9106), and rabbit anti p44/42 MAPK (ERK) (Cell Signalin 9102). Secondary antibodes used were: IRDye 800CW goat anti mouse (Li-Cor 926-32210), IRDye 680LT goat anti rabbit (Li-Cor 926-68021).

Figure Legends

Figure 3-1. Activation of c-fos promoter during fear-conditioning (Adapted from Liu et al. Nature 2012). Images of the DG from c-fos-tTA mice injected with AAV-TRE-ChR2-EYFP and stained after the following experimental treatments: *A)* on Dox; *B)* off dox for 2 days in home cage; *C)* off dox for 2 days in home cage, followed by FC; *D)* same as *C*, but without shock; *E)* same as *C*, 5 days after training; *F)* same as *C,* 30 days after training; *G)* same as *B*, followed by kainate-induced seizure. *H)* Quantification of the percentage of ChR2-EYFP-positive DAPI-positive cells after the treatments represented in *A-G* (n = 5 subjects each; *P < 0.05; ***P < 0.001). N.S., not significant.   Error bars shown are mean ± S.E.M. Although not specifically relevant to the data in this chapter, it is worth noting that the *no-shock* and *FC* groups exhibit similar levels of ChR2-EYFP expression, indicating that activation of the *c-fos* promoter in these cells was not dependent on the fear-learning itself but rather on the context and/or tone of the conditioning cage. Regardless, *no-shock* mice did not exhibit freezing upon light-activation of ChR2, indicating that the information required for the fear memory is not simply encoded by activation of the *c-fos* promoter.

Figure 3-2. CRTC expression in the brain. A) Adapted from Watts et al. 2011. qPCR showing relative enrichment of CRTC1, 2, and 3 mRNAs from murine hippocampus. *B)* Adapted from Watts et al. 2011. *In-situ* hybridization (ISH) matching qPCR from *A.* The lack of a control ISH probe renders interpretation of the CRTC2 and 3 ISH difficult, though they are clearly much weaker than that of CRTC1. *C)* ISH from the Allen Brain Atlas, revealing virtually absent CRTC3, barely detectable CRTC2, and robustly expressed CRTC1 in the hippocampus. In this ISH, hippocampal CRTC2 mRNA expression appears even more greatly reduced than CRTC1 and CRTC3 appears below the threshold of detection entirely.

Figure 3-3. Localization of CRTC1 constructs in different cell types A) Constructs were generated for the first 270 amino acids of CRTC1 fused to the fluorescent protein Dendra2 (CRTC1$^{1\text{-}270}$-De2). In addition, parallel constructs containing either S64A-S151A-S245A (S3A) triple mutant or F38A-M42A (CBD) double mutant were created. The F38-M42 mutations reside in the CREB-binding domain of CRTC1 (hence "CBD"). These three constructs were transfected into HEK and N2a cells, and subcellular localization assayed by confocal microscopy. CRTC1$^{1\text{-}270}$-De2 and the two mutant constructs seem not to follow a consistent pattern of localization; their cytoplasmic or nuclear localization appears to be mutation- and cell type-specific. In the rightmost image, the CBD mutant was transfected using standard calcium phosphate methods into rat primary cultured hippocampal neurons and fixed and stained to assay subcellular localization. In neurons, the CBD mutant is constitutively nuclear. *B)* table summarizing subcellular localization of reporter constructs. The amino-terminal 270 aa's of CRTC1 localize to the cytoplasm of N2a, HEK and cultured

neurons, and in cultured neurons undergoes activity-regulated translocation from synapse to nucleus (see Ch'ng et al. 2015 and Ch'ng et al. 2012). The S3A mutant is constitutively nuclear in cultured neurons (see Ch'ng et al. 2015) and N2a cells, but not in HEK cells. *C)* CRTC1 responds differently to 4-hour forskolin (FSK) or forskolin/A23187 calcium ionophore (F/A) stimulation of either HEK or N2a cells, as shown by electrophoretic mobility on WB. Stimulation of HEK with F/A generates low molecular-weight CRTC1 bands that do not appear in lysates from N2a cells stimulated with the same pharmacological agents. In lysates from unstimulated or FSK-stimulated N2a cells, there is also CRTC1 immunoreactivity at molecular weights above 90kDa that is not present in HEK cells. *D)* Lysates from HEK and N2a cells reveal complex regulation of CRTC1 changes in electrophoretic mobility. Lysates from untreated (UT) or DMSO-treated HEK cells reveal that CRTC1 resides mostly at high molecular weights. F/A stimulation leads to a shift in the proportion of CRTC1 immunoreactivity toward lower molecular

weights, though inclusion of dorsomorphin (DM) to block salt-inducible kinase (SIK) activity has little additional effect. This shift is also blocked by cyclosporine A (CsA) to block calcineurin activity. DMSO-control lysates incubated with lambda phosphatase (LP) for 30 minutes show a strong conversion of CRTC1 to low-molecular weight forms, indicating that changes in electrophoretic mobility of CRTC1 are likely due to significant changes in phosphorylation state. In N2a cells, the spread of CRTC1 species is far less broad. F/A has little effect on CRTC1 in N2a cells, though inclusion of DM causes a conversion of a small proportion of high-molecular-weight CRTC1 to low molecular weight. Inclusion of CsA has little effect on F/A stimulation, as F/A stimulation had little effect on CRTC1 in the first place, however incubation of lysates from DMSO-treated N2a cells generates significant low-molecular weight CRTC1, indicating that CRTC1 is significantly phosphorylated in N2a cells.

Figure 3-4. Bethyl antibody recognition of CRTC1 is specific (All data generously provided by Wendy Herbst in the Martin Lab). A) WB showing Bethyl antibody recognition of CRTC1 from brain lysate of wt mice versus CRTC1 constitutive knock-out (KO) mice. The major species recognized after denaturing polyacrylamide gels reside above 70 kDa, and are completely depleted from the KO brain. *B)* Confocal images of CA1 in paraffin sectioned hippocampi from wt and KO brain. CRTC1, in red, is completely absent from KO brain, though it strongly stains the dendrites and cytoplasm of CA1 neurons in wt brain.

Figure 3-5. Optimization of sonication parameters. A) DNA gel comparing sonication of cultured neurons samples (DIV 28) with different lysis buffers. Next to each sample is a small "non-de-x-linked" sample, though phenol-chloroform DNA recovery of these samples was poor. The lysis buffer from Xin, employing sarkosyl rather than SDS, is supposed to reduce bubbling created by the sonication process, though in my hands these were the only samples that created bubbles, and sonication was stopped after 0:31 or 1:21 min for "Xin1" and "Xin2", respectively. Even in

87

these samples, the sonication of cultured neurons was robust. Using my 0.5% SDS buffer

(SLB1 and 2) or the Active Motif 0.1% SDS (AM1 and 2) did not results in bubble formation, and

3' ON-time created very robustly (even slightly over-) sonicated DNA. *B)* Using any of these

three buffers to sonicate CA1s was completely unsuccessful at 1' ON-time. Increasing ON-time

to 4' resulted in much better sonication in my 0.5% SDS buffer, though inclusion of n-octyl-

glucoside to assist in solubilizing myelin basic protein did not improve sonication. As 4' ON-time

is excessive and likely would result in destroyed epitopes and/or oversonicated fragments, I

proceeded to try other sonication methods. *C)* Consultation with Dina Mattheos from the Wood

Lab at UC Irvine yielding a 2-step lysis/sonication method in which brain tissue is first digested

on ice in 1% NP-40, then switched to 1% SDS for sonication. This resulted in a marked

improvement and approached ideal sonication of DNA from brain tissue, even with 2' ON-time.

Figure 3-6. Characterization of FSK-LTP (All images adapted from Chotiner et al. 2003 and

Makhinson et al. 1999). A) FSK-LTP is dependent upon NMDAR signaling, as it is abrogated in

the presence of APV. *B-C)* The maintenance of FSK-LTP is degraded by preincubation with

either cycloheximide (CXM) to inhibit protein synthesis or actinomycin-D (Act-D) to inhibit

transcription. *D)* After treatment with high potassium/calcium, it is impossible to further induce

LTP with HFS that is normally efficacious, indicating that the FSK-LTP chemical protocol and

HFS-LTP rely on overlapping induction pathways. *E)* FSK-LTP induces robust spontaneous

bursting in CA1, which is silenced by TTX. *F)* Quantification of FSK-LTP induction in acute

slices without further modification, in TTX, or in slices where CA3 is removed, indicating that

synaptic output from CA3 is necessary for the induction of LTP in postsynaptic CA1 cells.

Figure 3-7. Characterization of DHPG-LTD. A) Adapted from Huber et al. 2000. 10-minute

application of 50μM DHPG onto acute hippopcampal slices causes robust LTD lasting over 100

minutes. This LTD can be abrogated by 60-minute preincubation of slices with 20μM

anisomycin, but is unaffected by 30-60-minute preincubation of slices with 25μM Act-D (not

shown). *B) Adapted from Delgado & O'Dell 2005.* DHPG depotentiates synapses that have

been potentiated with HFS. Potentiation can then be restored by inhibition of group I mGluRs

with LY341495, indicating that the molecular underpinnings of HFS-LTP are occluded and not

abrogated by DHPG-induced depotentation. DHPG-induced depotentiation can be induced

even hours after HFS stimulation (not shown), lending more evidence to the separation of

molecular mechanisms that underlie HSF-LTP and DHPG-LTD. *C) Adapted from Delgado &*

O'Dell 2005. Though DHPG can induce depotentiation of HFS-induced LTP, further HFS is

incapable of restoring potentiation. This also suggests that DHPG-induced depotentiation relies

on distinct pathways from those that underlie HFS-LTP, as those pathways appear to remain

saturated and cannot be further activated even after depotentiation. *D)* Representative WB from

whole acute hippocampal slices treated with ACSF control or 100μM DHPG for 10 minutes.

DHPG induces robust upregulation of phospho-ERK (pERK).

Figure 3-8. Characterization of NMDA-LTD (A, B, and D adapted from Delgado et al. 2007. C

adapted from Babiec et al. 2014). A) A 3 minute application of 20μM NMDA in ACSF containing

standard 2mM Ca^{2+} depresses synapses transiently, but does not result in LTD (left). When

applied in ACSF containing slightly elevated (4mM) Ca^{2+}, however, NMDA causes LTD for over

one hour (right). *B)* NMDA-LTD is prevented when slices are preincubated in cantharidin to

block protein phosphatases 1 and 2 (PP1 and PP2), showing that NMDA-LTD is dependent on

protein phosphatase activity. *C)* NMDA-LTD causes a robust increase in p38 MAPK

phosphorylation and decrease in AMPA receptor GluA1 phosphorylation at S845 and T840 by

WB, all of which are blocked by MK-801. D) Quantification of WBs; NMDA-LTD (N) mediated

dephosphorylation of GluA1 T840 relative to untreated slices (UT) persists even 40 minutes

after washout (Wash). Preincubation of slices with cantharidin increases basal GluA1 pT840 IR, and abolishes NMDA-mediated dephosphorylation of this site.

Figure 3-9. Translocation of CRTC1 to CA1 nuclei following pharmacological induction of plasticity. The nuclei of ACSF and FSK-LTP stimulated CA1 neurons exhibit undetectable and very low levels of CRTC1 immunoreactivity, respectively, while DHPG-LTD and NMDA-LTD exhibit higher levels.

Figure 3-10. DHPG-CRTC1 ChIP-seq peaks. Analysis of DHPG-CRTC1 ChIP-seq mouse mm9 genome alignments using Homer software revealed 117 computationally-identified ChIP peaks. Manual inspection of all 117 peaks revealed that 4 were false positives, resulting in 113 real peaks. *A)* The top 36 of these peaks (arranged by descending peak score) are displayed, and well-known IEGs are highlighted in red. The full list of manually-curated peaks contains many IEGs including Nr4a1, Nr4a2, Nr4a3, Jun, Fos, and other lesser-known activity-regulated genes. *B)* Visualization of alignment files using the Integrative Genome Viewer reveals DHPG-induced CRTC1 binding at the Fos transcriptional start site (TSS). *C)* DHPG-induced CRTC1 binding at in the Jun promoter region. *D)* DHPG-induced binding of CRTC1 at the Nr4a TSS. Note that this peak is much higher than some others and is cut off in this image; the ACSF-IgG enrichment around this region is smaller and comparable to other identified peaks, if the y-axis scale is adjusted to the DHPG-CRTC1 peak height. *E)* DHPG-induced CRTC1 peaks in the promoter and gene body of CREM.

Figure 3-11. ACSF-CRTC1 ChIP-seq peaks. Analysis of ACSF-CRTC1 ChIP-seq mouse mm9 genome alignments using Homer software revealed 26 computationally-identified ChIP peaks. Manual inspection of all 26 peaks reveals that 24 were uncertain or false positives, resulting in 2 peaks that were robust to visual inspection. *A)* The two real peaks are *Crtc1* and *CamK2a. B)*

CRTC1 peaks within the gene body of *Crtc1*, indicating possible autoregulatory inhibition

transcription. *C)* CRTC1 peak at the TSS of *CamK2a.* As this is a highly-expressed gene

known to play pivotal roles in neuronal activity and the CRTC1 peak is centered on its TSS,

which contains several CRE sites, there is a distinct possibility that CRTC1 may play a role in

CamK2a transcription. Interestingly, other ChIP datasets for SRF, CREB, and CBP from KCl-

stimulated cultured neurons[25] do not show overlapping peaks with this CRTC1 peak from

unstimulated acute hippocampal slices.

Figure 3-12. CRTC1 peaks reside in regions that are predicted and observed to be bound by

CREB and other chromatin-associated proteins. A) Homer software conducts *de novo* search

for conserved motifs in the promoter regions of genes in the DHPG-CRTC1 ChIP dataset.

Identifying one motif with high confidence, and searching this sequence through databases of

transcription-factor recognition sites, it reveals that most genes in the DHPG-CRTC1 dataset

contain CRE motifs in their promoter regions. *B)* Comparison of the present CRTC1 ChIP

datasets to ChIP data from KCl-stimulated cultured mouse cortical neurons for CREB, SRF, and

CREB-Binding Protein (CBP)[25], reveals that many DHPG-CRTC1 peaks overlap with these,

lending credence to their location as true genomic targets of CRTC1. In the IGV image shown,

the DHPG-CRTC1 peak at the TSS of Fos overlaps with CREB, SRF, and CBP peaks, which

also cover several CRE sites.

Figure 3-13. Analysis of DHPG-CRTC1 peak locations. GREAT software suite analysis of peaks

from the DHPG-CRTC1 dataset shows that they are located in promoter and non-promoter

regions, whether one chooses a stringent (-110 to +5 bp) or looser (-5kb to +500bp) cutoff

distance from TTS's to define promoter regions, without a clear bias toward any group over the

other.

Figure 3-14. Gene Ontology and similar analyses of genes identified in the DHPG-CRTC1 dataset. A) Homer molecular function analysis returns terms related to DNA/transcriptional regulation. *B)* Homer cellular function analysis returns terms related to nuclear function and transcription factor complex regulation. *C)* DAVID gene ontology (GO) analysis returns similar terms for regulation of nuclear functions, phosphoproteins (phosphorylated proteins are abundant in the nucleus), and transcription. *D)* GREAT GO molecular function also returns terms related to DNA/transcription factor regulation.

Figure 3-15. ChEA analysis of DHPG-CRTC1 peaks. A) Comparison of DHPG-CRTC1 peaks to a broad pool of other ChIP datasets shows the strongest overlap with two CREB datasets and one TCF7 dataset. Some of the genes, such as Hook2, Fos, and Jun, have overlap with the datasets from the zinc-finger transcription factor KLF2, which may simply reflect the importance of these genes and their transcription in many circumstances. *B)* Comparison of DHPG-CRTC1 peaks to ENCODE histone modifications reveals enrichment of some peaks for H3K4me1 or H3K4me3 (indicating active promoter/TSS regions), H3K36me3 (indicating exon regions), or H3K27ac (indicating active enhancers). It is important to note that all ChEA comparisons must be interpreted with caution; histone modifications and transcription factors are known to exhibit cell-type and stimulus-specificity, and the datasets to which DHPG-CRTC1 peaks are compared are from a wide range of experimental contexts.

Supplementary Figure Legends

Figure 3-S1. Further optimization of sonication. A) The initial sonication pilot yielded mostly unsonicated DNA and some fragments of very small size. *B)* increasing the number of slices did not result in more uniform sonication, and in this experiment DSG was allowed to proceed for up to 60' for some slices (as slices were allowed to accumulate in DSG as they were dissected and pooled). Fearing that over-fixation may have contributed to failure of sonication, number of slices per pilot experiment was reduced to 5 for subsequent experiments. *C)* increasing sonication time to 7' was successful in creating some more sonicated DNA, though the majority of DNA remained unsonicated. *D)* A second round of sonication (after freezing and thawing the next day) on the same material from *C* resulted in further sonication of the previously-sheared DNA, but still left much of the DNA completely unsonicated. *E)* As the freeze-thaw can destroy epitopes and DNA, it was unsuitable for a real experiment. Thus, in the next pilot, ON-time was increased to 10 minutes without including freeze-thaw. This was virtually completely unsuccessful in sonicating DNA. Notably, this pilot was similar to (and in fact included 3 more minutes of sonication than) that in *C*, yet resulted in less DNA shearing. This suggests there may be other parameters that contribute to sonication efficiency. *F)* The sonicator amplitude was doubled to 50% and ON-time kept at 10 minutes. This created a marginal improvement in sonication, but again resulted in mostly un-sheared DNA. *G)* As 50% amplitude is high (may destroy epitopes), and did not make a great improvement in sonication, in this pilot amplitude was returned to 25% and ON-time increased to 17'. This again resulted in some sonicated DNA, but most remained un-sheared. As both 50% amplitude and 17 min ON-time are parameters that are too high and will likely damage DNA that is sonicated, while leaving most of the DNA untouched, this sonicator proved unsuitable for my experiments.

Figure 3-S2. Comparative input amounts for ChIP from cultured neurons and acute hippocampal slices. Pictures showing the relative cellular material between twenty-eight CA1s

dissected from acute hippocampal slices and seven 10-cm dishes, pooled in 1.5ml

microcentrifuge and 50ml conical tubes, respectively. The red line on the 50ml conical tube

delineates the top of the cell pellet.   Typically, many of these falcon tubes are pooled and

sonicated to conduct ChIP-seq from cultured neurons. This is clearly a great difference in input

amount to the 20 CA1s used per IP from acute hippocampal tissue, and the experimenter must

expect lower yield from ChIP process.

Figure 3-S3. Screentape analysis of ChIP-seq libraries. A) Agilent Technologies Screentape

D1000 analysis of ACSF-IgG, ACSF-CRTC1, DHPG-IgG, and DHPG-CRTC1 ChIP-seq libraries

shows a reasonable spread of fragment sizes centered around ~400bp for all samples. This is

ideal for sequencing on Illumina HiSeq platforms with 50bp SE. *B)* Average fragment size and

DNA concentration for each sample; all are within the ideal range for sequencing. *C)*

Quantification of reads for each sample. Raw reads are well above the 40-50 million per

sample target for ChIP-seq, and collapsing duplicates does not deplete them below this target,

indicating that this dataset passes sufficient checkmarks to be aligned to the genome and

analyzed using ChIP-seq analysis software.

Figure 3-S4. The DHPG-CRTC1 ChIP dataset does not contain peaks at fgf1b or Arc as have

been observed in other studies. A) IGV browser track showing no CRTC1 peaks in the

promoter region of *fgf1b*. *B) Adapted from Uchida et al. 2017*. ChIP-qPCR reveals that fear

conditioning induces binding of CREB and CRTC1 to complexes at the fgf1b CRE1 locus, but

not the CRE2 locus (two different CRE sites in the promoter region of *fgf1b*). HC, home cage

control; Trained, milder fear conditioning using a single shock or stronger fear conditioning using

a triple shock. *C)* A previous ChIP-seq dataset from Martina DeSalvo in the Martin Lab utilizing

virally-overexpressed FLAG-tagged CRTC1 in rat cultured neurons shows a clear peak

upstream of the *Arc* gene body. The top ChIP track was conducted on TTX-silenced neurons

and the bottom track on BIC-stimulated neurons, using FLAG IP of exogenous CRTC1. *D)* The

DHPG-CRTC1 ChIP-seq dataset does not contain a peak upstream of the *Arc* gene body. Note

that the two studies cannot be visualized on the same browser session, as *C* is aligned to the

rat genome, while *D* is aligned to the mouse genome. The discrepancy of this peak between

the two studies is uninterpretable due to confounding factors; overexpression could have

caused aberrant CRTC1 binding in the cultured neuron expeiments, and the presence of the

peak in TTX-silenced neurons indicates this may be the case. Alternatively, there could be

minimal quantities of CRTC1 in the nucleus of TTX-silenced neurons that truly bind to

complexes upstream of *Arc.* DHPG-induced changes in CRTC1 could prevent its binding to

particular transcription factor complexes including those upstream of *Arc*, and the discrepancy

could reflect the different CRTC1 PTMs between protein isolated from DHPG-stimulated mouse

acute hippocampal slices and culture rat neurons. Finally, the low peak-count in the DHPG-

CRTC1 dataset may indicate that only the strongest peaks are visualizable, and there may be a

true peak at a comparable location in the vicinity of *Arc* that is undetectable in this dataset due

to technical limitations and low starting material.

Table 3-S2. Summary of ChIP-seq kits considered for my experiments. Several ChIP scientists

dis-recommended Diagenode's sonicators (personal communication – Vondriska Lab), which

made me uneasy about their other products. The kit from Millipore seemed a decent choice, as

it was validated for some tissue types, though the kit was not commonly cited in literature. The

Takara (Clontech) kit was designed especially for low-input ChIP-seq, but accomplished

increased DNA yield by using Chelex to retrieve ssDNA from IP. This made me uncomfortable,

as it may introduce confounding effects to the sequencing data produced. Finally, the Active

Motif Low Cell ChIP-seq kit had just come on the market, and seemed the best choice for my

experiments. Active Motif is a highly reputed company whose reagents are used by many ChIP

scientists at UCLA whose products are used commonly by ChIP publications. This kit also

bears several clever optimizations to the ChIP process that do not compromise the quality of the
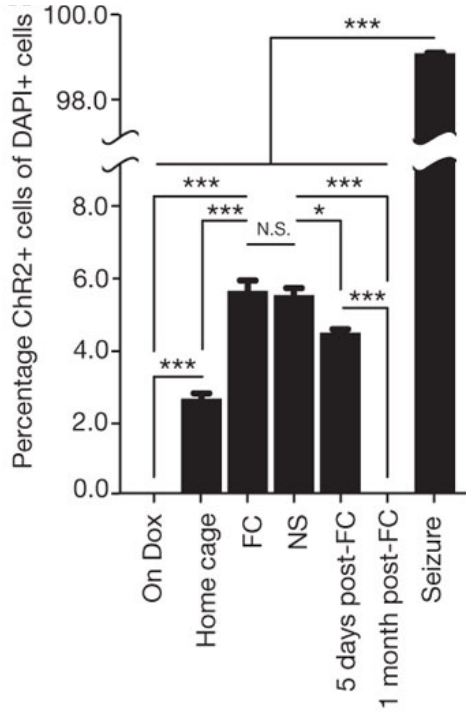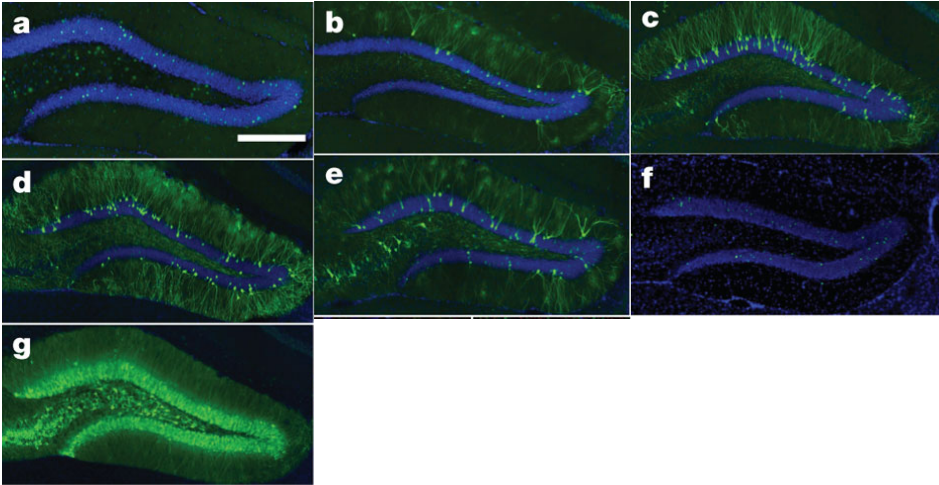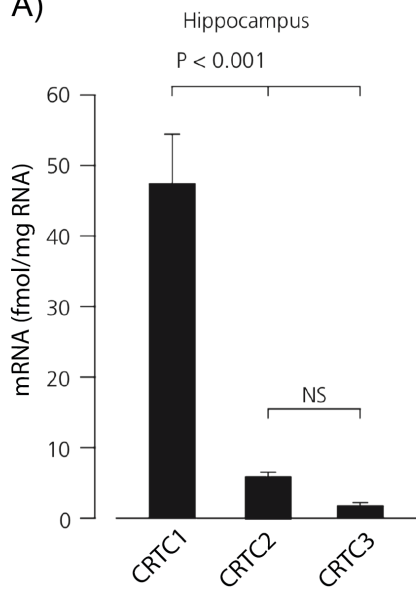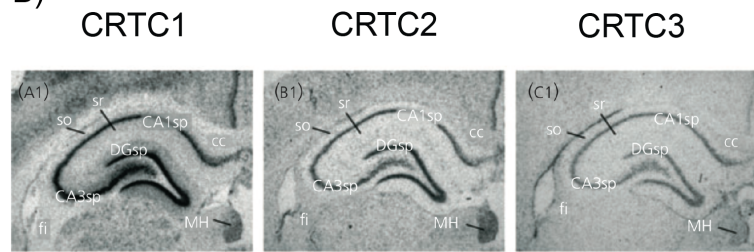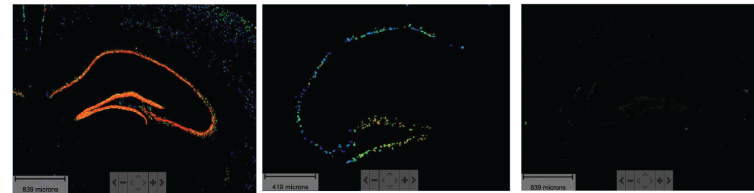
DNA returned.

Figure 3-1

Figure 3-2

A) Hippocampus

B) CRTC1 CRTC2 CRTC3

C)

Figure 3-3

A)

B)

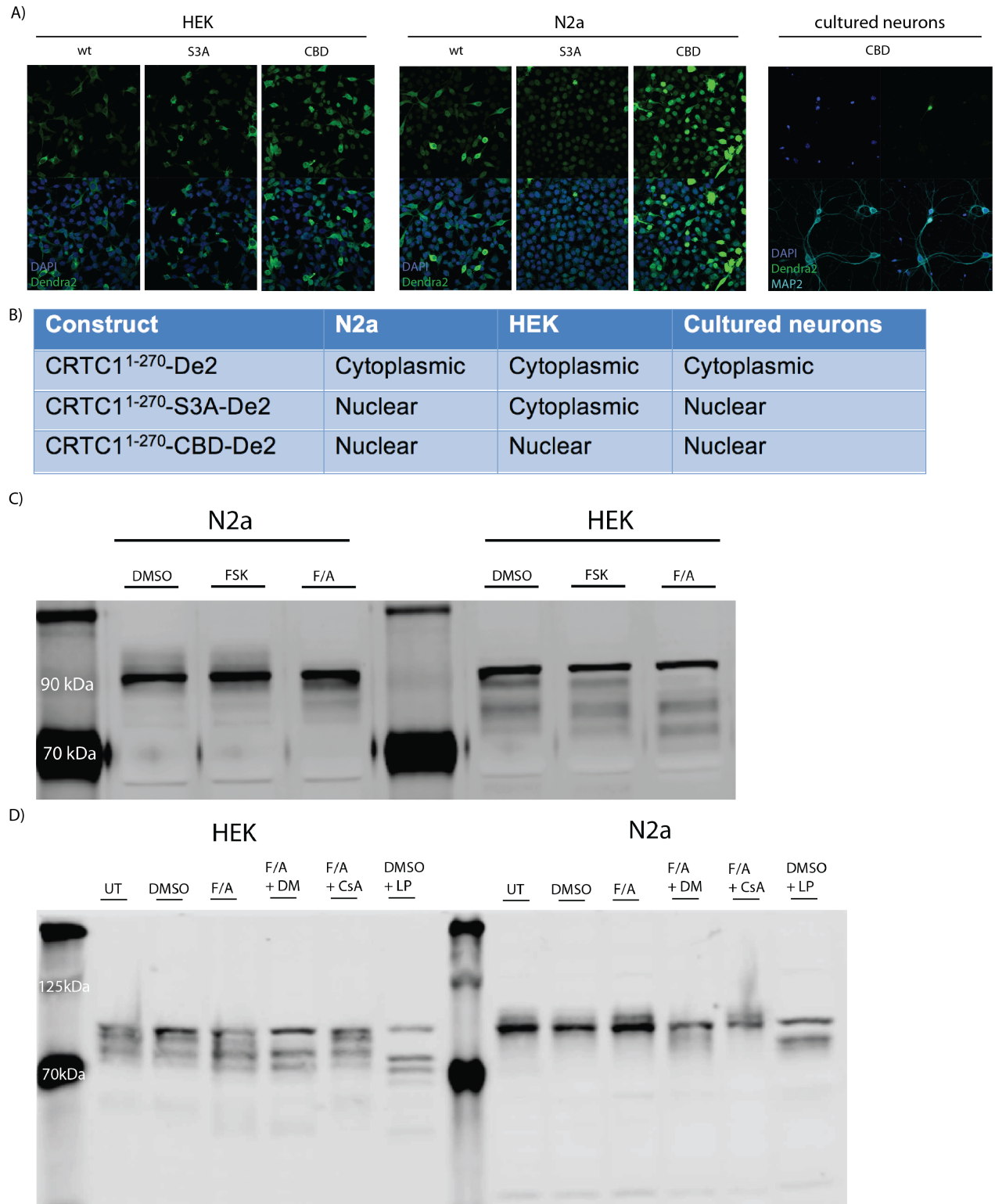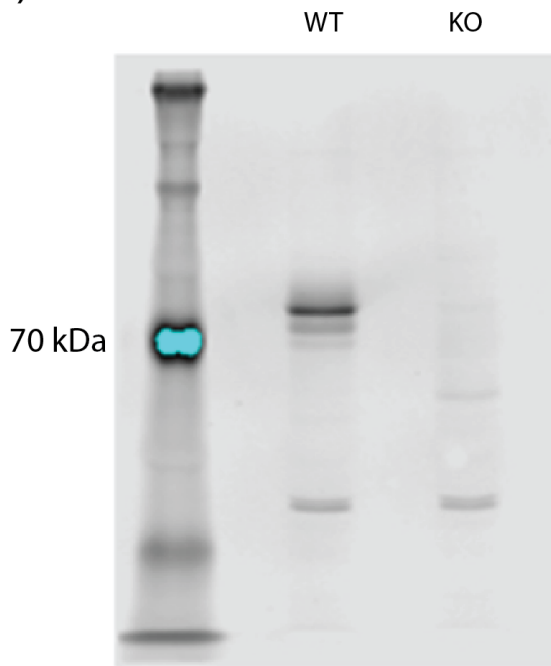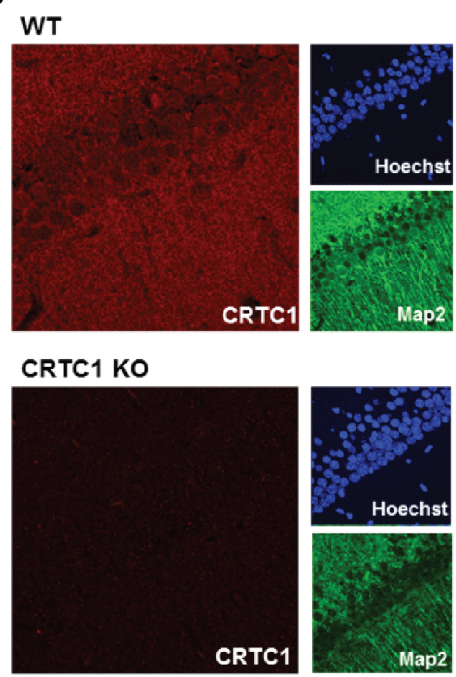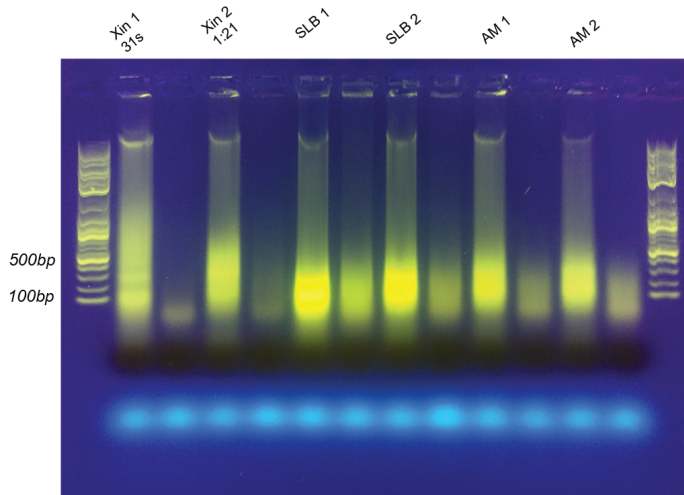| Construct	N2a	HEK	Cultured neurons
CRTC1$^{1-270}$-De2	Cytoplasmic	Cytoplasmic	Cytoplasmic
CRTC1$^{1-270}$-S3A-De2	Nuclear	Cytoplasmic	Nuclear
CRTC1$^{1-270}$-CBD-De2	Nuclear	Nuclear	Nuclear

C)

D)

Figure 3-4

A)

B)

Figure 3-5

A) Cultured neurons - 3s ON, 15s OFF, 1'
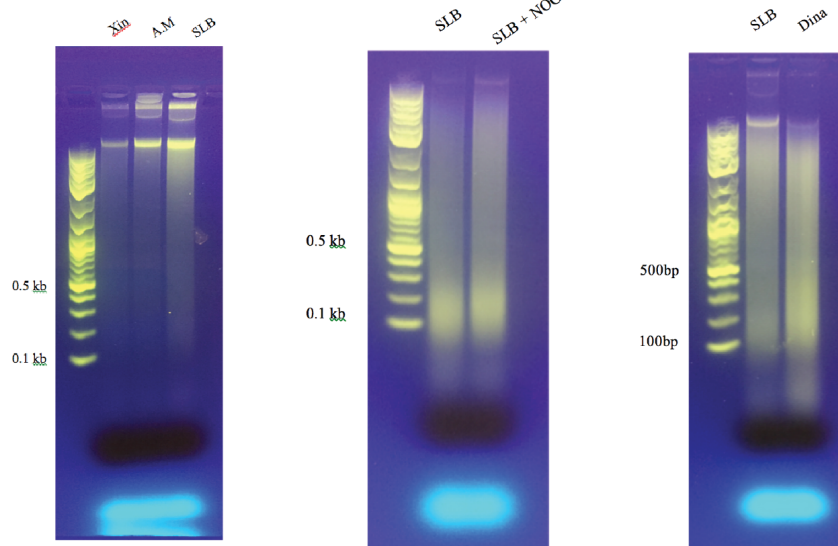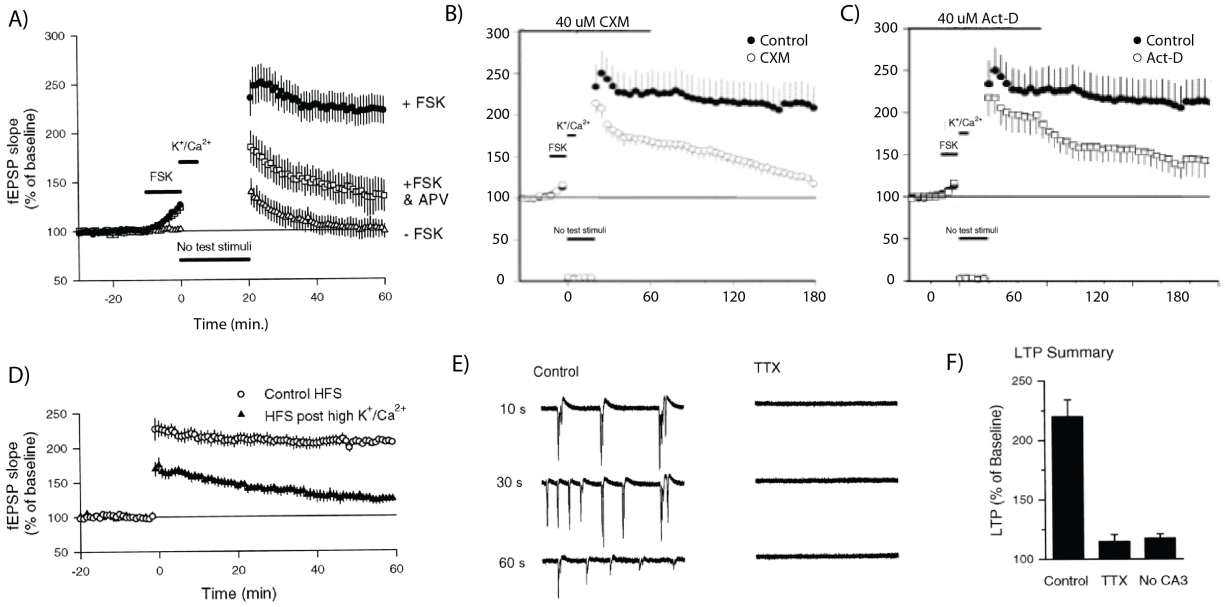
B) CA1s - 3s ON, 15s OFF, 1'   3s ON, 15s OFF, 4'   3s ON, 15s OFF, 2'
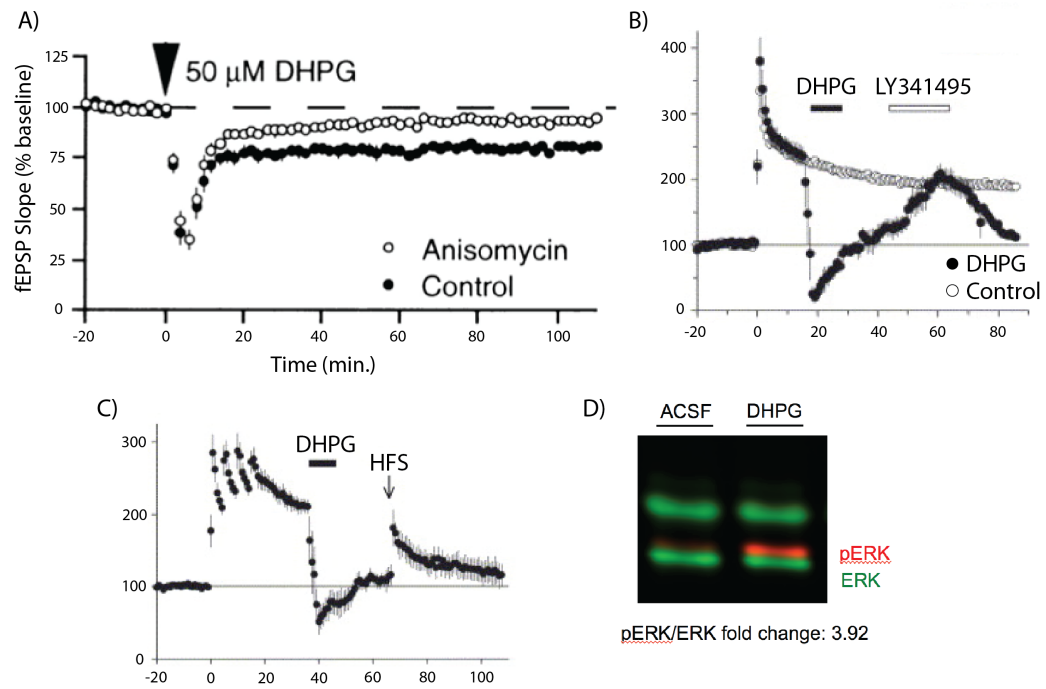
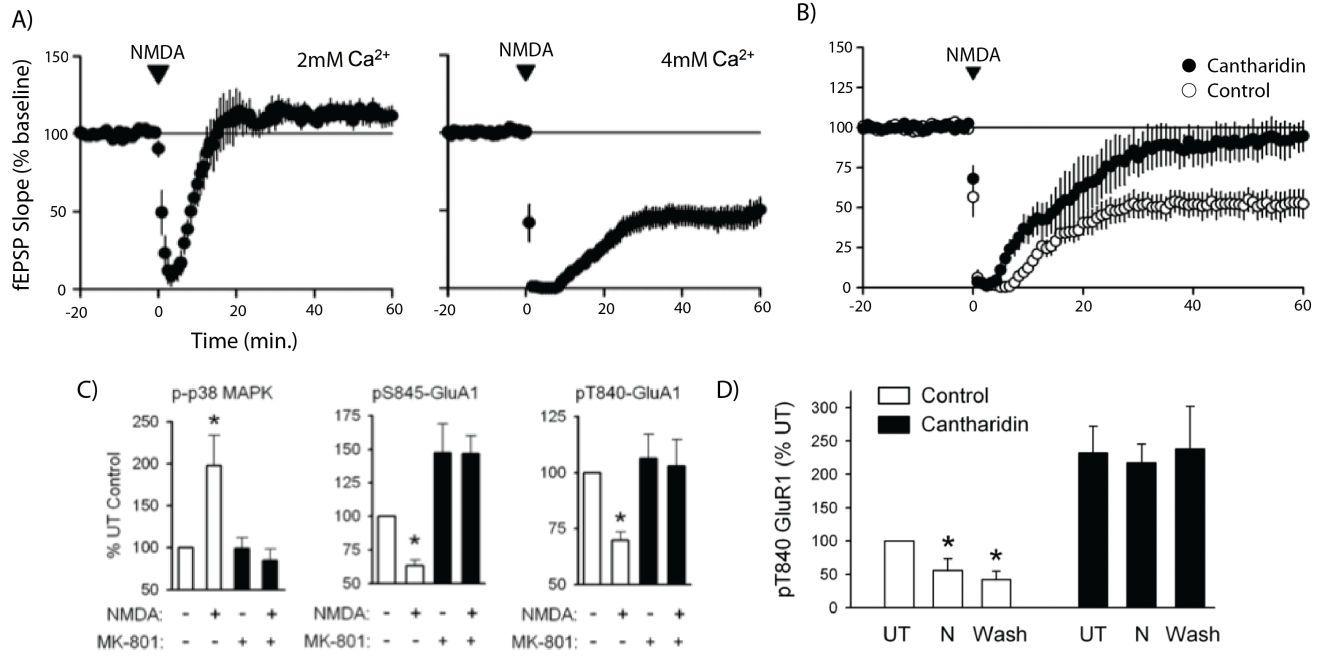*Figure 3-6*

Figure 3-7

Figure 3-8

Figure 3-9

ACSF   FSK-LTP   DHPG-LTD   NMDA-LTD

CRTC1

CRTC1
MAP2
Hoechst
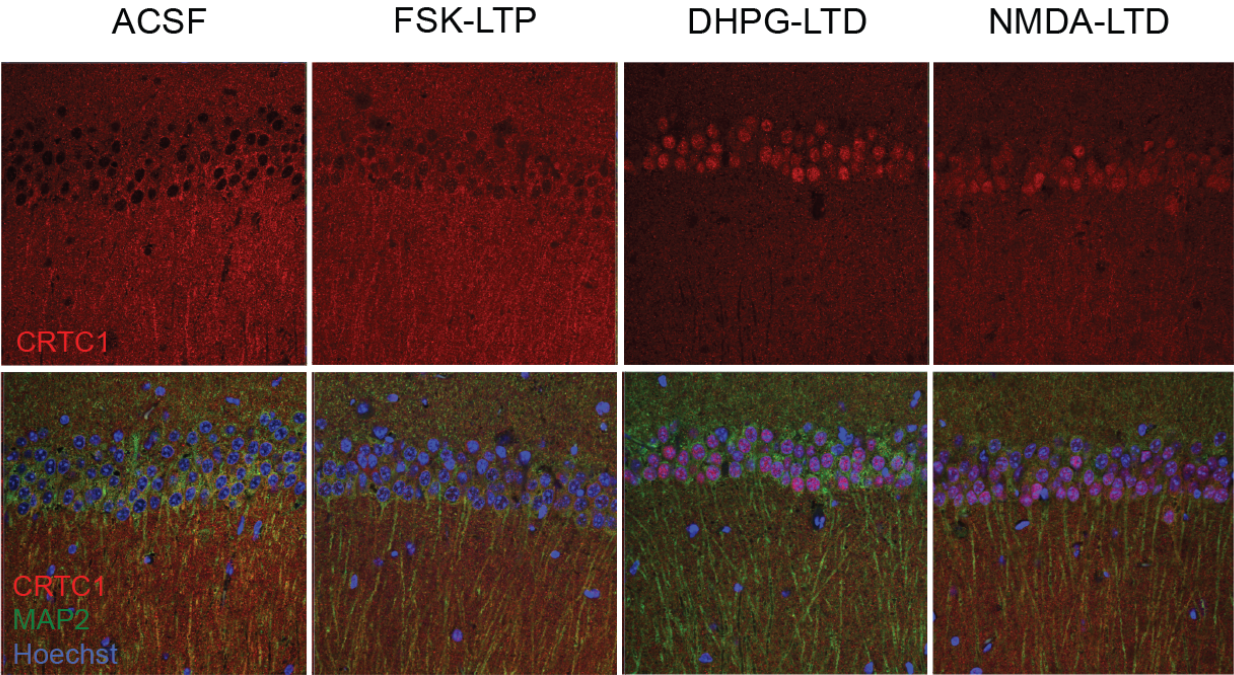
Figure 3-10

A)

Peak Score	Annotation	Gene Name	Gene Description	Gene Type
8.76	promoter-TSS (NM_010444)	Nr4a1	nuclear receptor subfamily 4, group A, member 1	protein-coding
7.13	promoter-TSS (NM_133934)	Isy1	ISY1 splicing factor homolog	protein-coding
6.83	intron (NM_001161620, intron 1 of 12)	Mpp7	membrane protein, palmitoylated 7 (MAGUK p55 subfamily member 7)	protein-coding
5.81	Intergenic	Ccdc63	coiled-coil domain containing 63	protein-coding
5.2	promoter-TSS (NM_153196)	Bre	brain and reproductive organ-expressed protein	protein-coding
4.99	promoter-TSS (NM_001311066)	Crem	cAMP responsive element modulator	protein-coding
4.79	promoter-TSS (NM_001039710)	Coq10b	coenzyme Q10B	protein-coding
4.69	Intergenic	Hook2	hook microtubule tethering protein 2	protein-coding
4.69	Intergenic	Pde10a	phosphodiesterase 10A	protein-coding
4.58	Intergenic	Mef2d	myocyte enhancer factor 2D	protein-coding
4.48	Intergenic	Pde10a	phosphodiesterase 10A	protein-coding
4.48	intron (NM_175314, intron 17 of 29)	Adamts9	a disintegrin-like and metallopeptidase (reprolysin type) with thrombospondin type 1 motif, 9	protein-coding
4.48	Intergenic	Zfp219	zinc finger protein 219	protein-coding
4.48	Intergenic	Borg	BMP/OP-responsive gene	ncRNA
4.48	promoter-TSS (NM_001290811)	Adal	adenosine deaminase-like	protein-coding
4.38	intron (NM_018779, intron 15 of 15)	Slco1c1	solute carrier organic anion transporter family, member 1c1	protein-coding
4.38	Intergenic	Hlx	H2.0-like homeobox	protein-coding
4.28	Intergenic	BC030867	cDNA sequence BC030867	protein-coding
4.18	intron (NM_019980, intron 1 of 3)	Litaf	LPS-induced TN factor	protein-coding
4.18	intron (NM_134133, intron 1 of 1)	Smim3	small integral membrane protein 3	protein-coding
4.07	promoter-TSS (NM_029735)	Eprs	glutamyl-prolyl-tRNA synthetase	protein-coding
4.07	Intergenic	Mir3089	microRNA 3089	ncRNA
4.07	intron (NM_001139509, intron 1 of 7)	Nr4a2	nuclear receptor subfamily 4, group A, member 2	protein-coding
3.97	intron (NM_007395, intron 1 of 8)	Mir6962	microRNA 6962	ncRNA
3.87	promoter-TSS (NR_002688)	Ptp4a1	protein tyrosine phosphatase 4a1	protein-coding
3.87	intron (NM_001083967, intron 3 of 19)	Tcf4	transcription factor 4	protein-coding
3.77	exon (NM_001289582, exon 4 of 10)	Liph	lipase, member H	protein-coding
3.77	promoter-TSS (NM_198092)	Usp2	ubiquitin specific peptidase 2	protein-coding
3.67	Intergenic	Hnrnpl	heterogeneous nuclear ribonucleoprotein L	protein-coding
3.67	intron (NM_026775, intron 1 of 4)	Tmed10	transmembrane p24 trafficking protein 10	protein-coding
3.67	Intergenic	Rorb	RAR-related orphan receptor beta	protein-coding
3.57	promoter-TSS (NM_010234)	Fos	FBJ osteosarcoma oncogene	protein-coding
3.46	intron (NM_001170847, intron 5 of 13)	Pdcd4	programmed cell death 4	protein-coding
3.46	Intergenic	Nr4a3	nuclear receptor subfamily 4, group A, member 3	protein-coding
3.46	Intergenic	Trappc9	trafficking protein particle complex 9	protein-coding
3.46	intron (NM_172117, intron 1 of 13)	Entpd6	ectonucleoside triphosphate diphosphohydrolase 6	protein-coding

B)
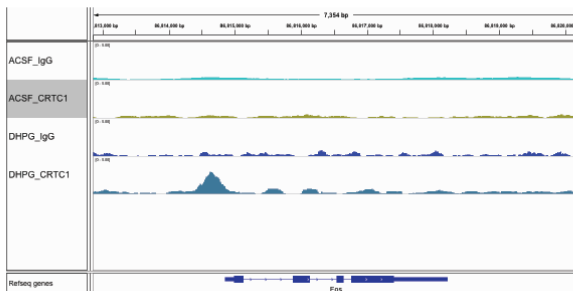
C)
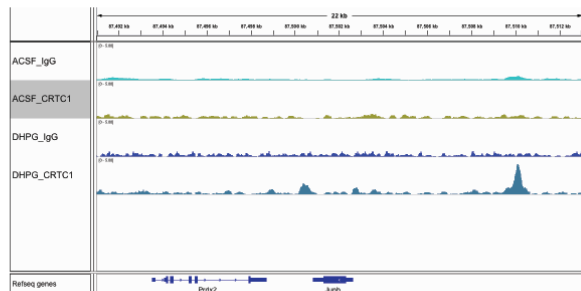
D)
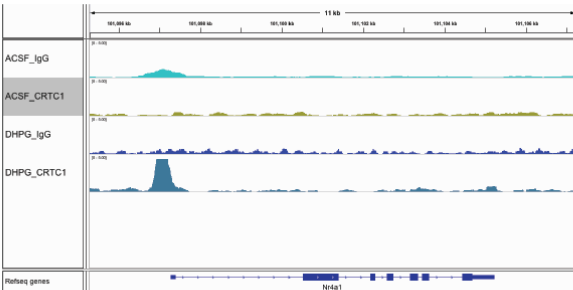
E)
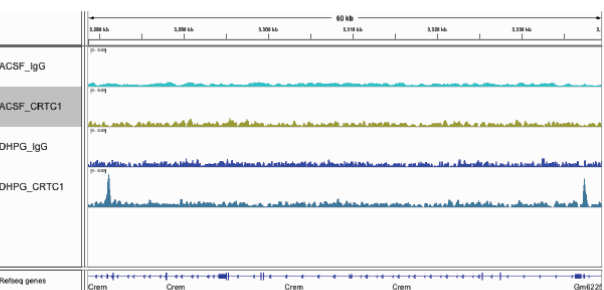
Figure 3-11

A)

Peak Score	Annotation	Gene Name	Gene Description	Gene Type
6.93	promoter-TSS (NM_177407)	Camk2a	calcium/calmodulin-dependent protein kinase II alpha	protein-coding
2.94	promoter-TSS (NM_001004062)	Crtc1	CREB regulated transcription coactivator 1	protein-coding

B)

C)

107
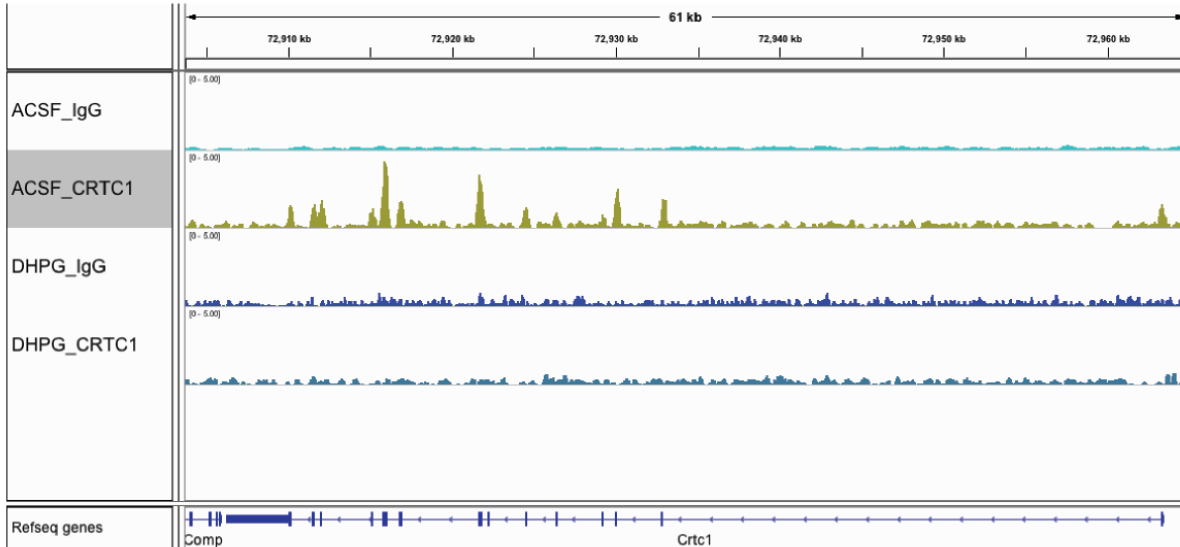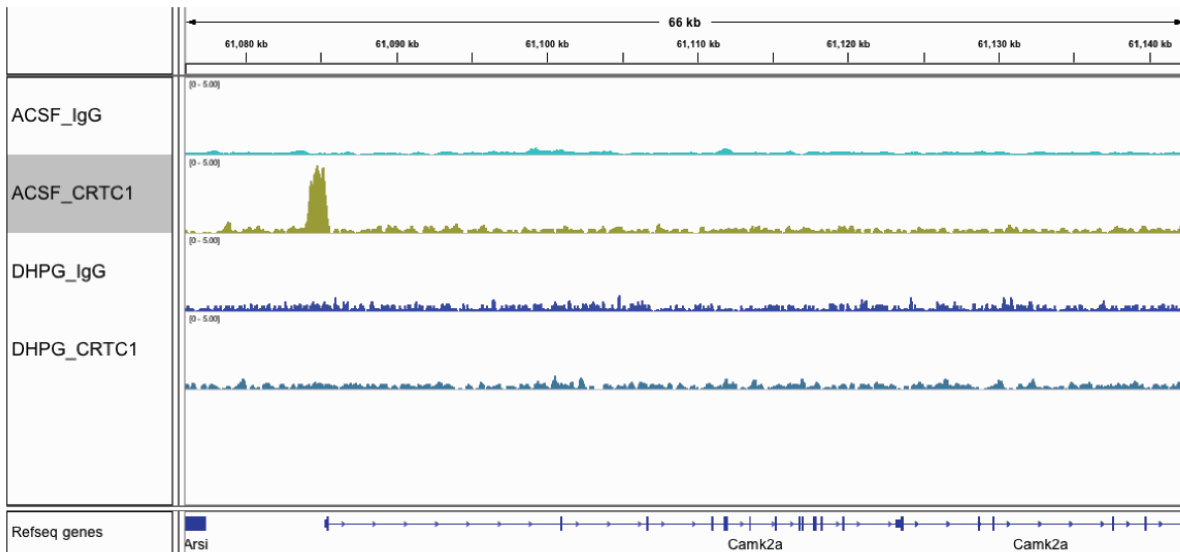
Figure 3-12

A)

Rank	Motif	P-value	log P-pvalue	% of Targets	% of Background	STD(Bg STD)	Best Match/Details
1		1e-33	-7.766e+01	65.81%	15.49%	170.0bp (325.1bp)	MF0002.1_bZIP_CREB/G-box-like_subclass/Jaspar(0.970) More Information | Similar Motifs Found

B)

Figure 3-13

Figure 3-14

A) Homer - Molecular Function

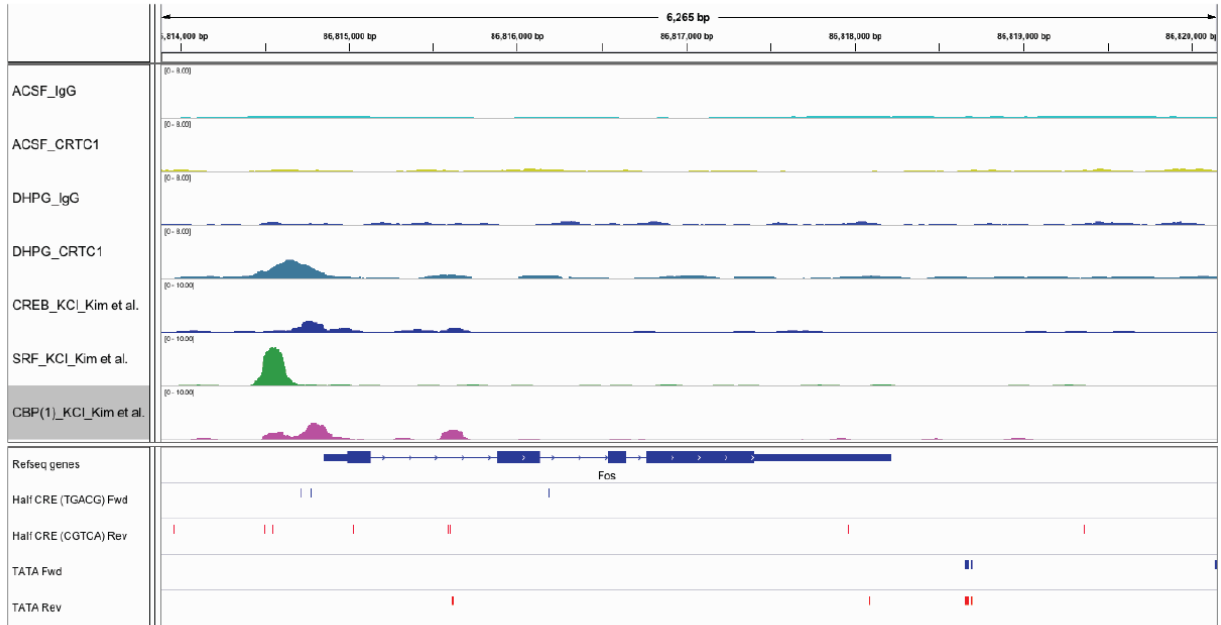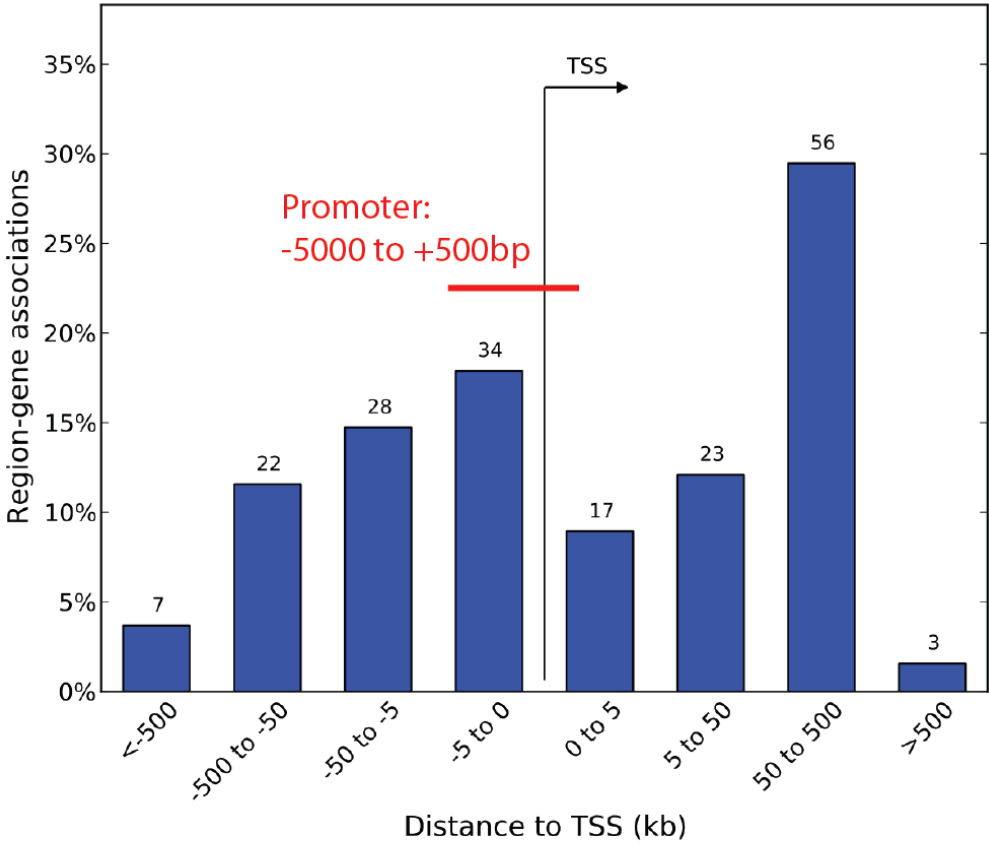| Term	Enrichment	logP	Genes in Term	Target Genes in Term	Gene Symbols
transcription regulatory region DNA binding	1.07E-07	-16.05	834	17	Junb,Bhlhe40,Hnrnpl,Per1,Tcf4,Fosl2,Nr4a3,Mnt,Arid5a,Mef2d,Bcor,Hdac4,Fos,Zfp219,Nr4a2,Atf3,C
regulatory region DNA binding	1.11E-07	-16.01	836	17	Junb,Bhlhe40,Hnrnpl,Per1,Tcf4,Fosl2,Nr4a3,Mnt,Arid5a,Mef2d,Bcor,Hdac4,Fos,Zfp219,Nr4a2,Atf3,C
regulatory region nucleic acid binding	1.17E-07	-15.96	839	17	Junb,Bhlhe40,Hnrnpl,Per1,Tcf4,Fosl2,Nr4a3,Mnt,Arid5a,Mef2d,Bcor,Hdac4,Fos,Zfp219,Nr4a2,Atf3,C
transcription factor activity, RNA polymerase II core promoter proximal region sequence-specific binding	7.96E-07	-14.04	378	11	Junb,Bhlhe40,Mef2d,Fos,Nr4a1,Fosl2,Tcf4,Nr4a3,Zfp219,Atf3,Nr4a2
RNA polymerase II transcription factor activity, sequence-specific DNA binding	1.24E-06	-13.6	671	14	Junb,Rorb,Bhlhe40,Mef2d,Fos,Zkscan6,Nr4a1,Nr4a3,Fosl2,Tcf4,Zfp219,Atf3,Nr4a2,Mnt
sequence-specific DNA binding	1.66E-06	-13.31	1015	17	Junb,Per1,Nr4a1,Tcf4,Fosl2,Nr4a3,Mnt,Rorb,Hlx,Mef2d,Bcor,Hdac4,Fos,Zfp219,Nr4a2,Atf3,Crem
RNA polymerase II core promoter proximal region sequence-specific DNA binding	3.40E-06	-12.59	354	10	Junb,Mef2d,Per1,Fos,Tcf4,Fosl2,Nr4a3,Zfp219,Nr4a2,Atf3
core promoter proximal region sequence-specific DNA binding	5.53E-06	-12.11	374	10	Junb,Mef2d,Per1,Fos,Tcf4,Fosl2,Nr4a3,Zfp219,Nr4a2,Atf3
core promoter proximal region DNA binding	5.79E-06	-12.06	376	10	Junb,Mef2d,Per1,Fos,Tcf4,Fosl2,Nr4a3,Zfp219,Nr4a2,Atf3
transcription factor binding	6.31E-06	-11.97	564	12	Junb,Rorb,Bhlhe40,Mef2d,Bcor,Per1,Hdac4,Fos,Nr4a1,Tcf4,Nr4a3,Arid5a
transcription regulatory region sequence-specific DNA binding	7.03E-06	-11.86	672	13	Junb,Mef2d,Bcor,Per1,Fos,Tcf4,Fosl2,Nr4a3,Zfp219,Atf3,Mnt,Nr4a2,Crem
double-stranded DNA binding	7.10E-06	-11.86	780	14	Mterf4,Junb,Mef2d,Bcor,Per1,Fos,Tcf4,Fosl2,Nr4a3,Zfp219,Atf3,Mnt,Nr4a2,Crem
RNA polymerase II regulatory region sequence-specific DNA binding	9.94E-06	-11.52	590	12	Junb,Mef2d,Bcor,Per1,Fos,Tcf4,Fosl2,Nr4a3,Zfp219,Atf3,Mnt,Nr4a2
RNA polymerase II regulatory region DNA binding	1.10E-05	-11.42	596	12	Junb,Mef2d,Bcor,Per1,Fos,Tcf4,Fosl2,Nr4a3,Zfp219,Atf3,Mnt,Nr4a2
sequence-specific double-stranded DNA binding	1.10E-05	-11.41	701	13	Junb,Mef2d,Bcor,Per1,Fos,Tcf4,Fosl2,Nr4a3,Zfp219,Atf3,Mnt,Nr4a2,Crem
DNA binding	4.48E-05	-10.01	2021	22	Junb,Bhlhe40,Hnrnpl,Per1,Nr4a1,Tcf4,Fosl2,Nr4a3,Mnt,Arid5a,Mterf4,Rorb,Hlx,Mef2d,Bcor,Hdac4,F
transcription factor activity, direct ligand regulated sequence-specific DNA binding	4.87E-05	-9.93	46	4	Rorb,Nr4a1,Nr4a3,Nr4a2
RNA polymerase II transcription factor activity, ligand-activated sequence-specific DNA binding	4.87E-05	-9.93	46	4	Rorb,Nr4a1,Nr4a3,Nr4a2

B) Homer - Cellular Component

Term	Enrichment	logP	Genes in Term	Target Genes in Term	Gene Symbols
nucleus	8.84E-06	-11.64	6419	50	Slc25a3,Magi1,Rpl21,Per1,Bdh1,Nr4a1,Fosl2,Mnt,Arid5a,Ptp4a1,Med13l,Hlx,Nuf2,Pdcd4,Bcor,Litaf,Srrm2,Hdac4,Fos,Zkscan6,Dnajb2,M
nuclear part	0.00031	-8.092	3329	29	Junb,Bre,Bhlhe40,Slc25a3,Magi1,Rpl21,Hnrnpl,Bdh1,Nr4a1,Tcf4,Fosl2,Kctd10,Arid5a,Dyrk1a,Med13l,Mef2d,Pdcd4,Bcor,Litaf,Srrm2,Cd
protein complex	0.00077	-7.17	3003	26	Junb,Bre,Dctn4,Hook2,Nr4a1,Nr4a3,Tcf4,Kctd10,Mpp7,Arid5a,Med13l,Nuf2,Bcor,Tmed10,Eprs,Cdkn1a,Arpc3,Hdac4,Fos,Pex5,Ccnl1,D
intracellular membrane-bounded organelle	0.00086	-7.051	9669	60	Slc25a3,Magi1,Coq10b,Rpl21,Per1,Bdh1,Nr4a1,Fosl2,Mnt,Arid5a,Ptp4a1,Med13l,Mlc1,Hlx,Nuf2,Pdcd4,Bcor,Litaf,Srrm2,Txndc11,Trapp
intracellular organelle part	0.00119	-6.731	6229	43	Ccdc63,Slc25a3,Magi1,Coq10b,Dctn4,Rpl21,Bdh1,Nr4a1,Fosl2,Arid5a,Med13l,Nuf2,Pdcd4,Bcor,Litaf,Srrm2,Arpc3,Hdac4,Fos,Pex5,Dna
organelle part	0.00124	-6.692	6438	44	Ccdc63,Slc25a3,Magi1,Coq10b,Dctn4,Rpl21,Bdh1,Nr4a1,Fosl2,Arid5a,Med13l,Zswim6,Nuf2,Pdcd4,Bcor,Litaf,Srrm2,Arpc3,Hdac4,Fos,F
transcription factor complex	0.00146	-6.529	366	7	Junb,Fos,Nr4a1,Nr4a3,Tcf4,Crem,Arid5a

C) DAVID - Gene Ontology

Sublist	Category	Term	RT	Genes	Count	%	P-Value	Benjamini
☐	UP_SEQ_FEATURE	domain:Leucine-zipper	RT		8	7.2	7.1E-7	2.1E-4
☐	UP_KEYWORDS	Phosphoprotein	RT		54	48.6	1.9E-6	2.7E-4
☐	UP_KEYWORDS	Transcription regulation	RT		23	20.7	2.2E-6	1.5E-4
☐	UP_KEYWORDS	Alternative splicing	RT		40	36.0	3.1E-6	1.5E-4
☐	UP_KEYWORDS	Transcription	RT		23	20.7	3.8E-6	1.3E-4
☐	UP_KEYWORDS	Nucleus	RT		38	34.2	6.7E-6	1.9E-4
☐	UP_SEQ_FEATURE	DNA-binding region:Basic motif	RT		8	7.2	8.3E-6	1.2E-3
☐	GOTERM_BP_DIRECT	negative regulation of transcription from RNA polymerase II promoter	RT		15	13.5	1.1E-5	6.7E-3
☐	GOTERM_CC_DIRECT	nucleus	RT		47	42.3	1.2E-5	1.6E-3
☐	GOTERM_BP_DIRECT	positive regulation of transcription from RNA polymerase II promoter	RT		17	15.3	2.2E-5	6.7E-3
☐	GOTERM_BP_DIRECT	transcription, DNA-templated	RT		24	21.6	2.4E-5	5.0E-3
☐	GOTERM_MF_DIRECT	RNA polymerase II core promoter proximal region sequence-specific DNA binding	RT		10	9.0	2.8E-5	5.6E-3
☐	INTERPRO	Orphan nuclear receptor	RT		3	2.7	5.2E-5	1.1E-2
☐	GOTERM_BP_DIRECT	regulation of transcription, DNA-templated	RT		26	23.4	5.9E-5	9.1E-3
☐	GOTERM_MF_DIRECT	transcription regulatory region DNA binding	RT		8	7.2	7.5E-5	7.5E-3
☐	INTERPRO	Basic-leucine zipper domain	RT		5	4.5	7.6E-5	8.0E-3
☐	GOTERM_MF_DIRECT	sequence-specific DNA binding	RT		12	10.8	1.0E-4	6.7E-3
☐	UP_SEQ_FEATURE	splice variant	RT		39	35.1	1.1E-4	1.0E-2
☐	GOTERM_MF_DIRECT	transcription factor activity, sequence-specific DNA binding	RT		14	12.6	1.2E-4	5.9E-3

D) GREAT - GO Molecular Function

Term Name	Binom Rank	Binom Raw P-Value	Binom FDR Q-Val	Binom Fold Enrichment	Binom Observed Region Hits	Binom Region Set Coverage	Hyper Rank	Hyper FDR Q-Val	Hyper Fold Enrichment	Hyper Observed Gene Hits	Hyper Total Genes	Hyper Gene Set Coverage
activating transcription factor binding	1	2.0900e-9	7.2794e-6	14.8013	10	8.62%	4	3.3934e-2	13.0781	5	46	2.84%
transcription regulatory region DNA binding	2	1.1174e-6	1.9459e-3	3.6377	19	16.38%	2	1.2319e-2	4.5076	13	347	7.39%
regulatory region DNA binding	3	1.2910e-6	1.4989e-3	3.6021	19	16.38%	3	1.0483e-2	4.4060	13	355	7.39%
sequence-specific DNA binding	5	9.2763e-6	6.4618e-3	2.5812	25	21.55%	1	2.3082e-2	3.2518	19	703	10.80%
sequence-specific DNA binding RNA polymerase II transcription factor activity	18	1.5873e-4	3.0715e-2	3.1334	14	12.07%	7	3.5341e-2	4.5923	10	262	5.68%
sequence-specific DNA binding transcription factor activity	21	2.0926e-4	3.4707e-2	2.1331	25	21.55%	5	3.5949e-2	2.7099	20	888	11.36%
nucleic acid binding transcription factor activity	23	2.2868e-4	3.4630e-2	2.1209	25	21.55%	6	3.0428e-2	2.7068	20	889	11.36%

The test set of 116 genomic regions picked 176 (1%) of all 21,176 genes.
GO Molecular Function has 3,483 terms covering 15,735 (74%) of all 21,176 genes, and 181,165 term - gene associations.
3,483 ontology terms (100%) were tested using an annotation count range of [1, Inf].

110

Figure 3-15

Figure 3-S1

A)

4 CA1s
25% amp
5' ON

B)

28 CA1s
60' DSG
25% amp
5' ON

C)

5 CA1s
25% amp
7' ON

D)

5 CA1s
25% amp
7' ON
f/t
7' ON

0.1kb

3 kb

1 kb

3 kb

1 kb

0.5 kb

0.5 kb

0.1 kb

E)

5 CA1s
25% amp
10' ON

F)

5 CA1s
50% amp
10' ON

G)

5 CA1s
25% amp
17' ON

0.5 kb

0.1 kb

1 kb

0.5kb

0.1kb

1 kb

0.5kb

0.1kb
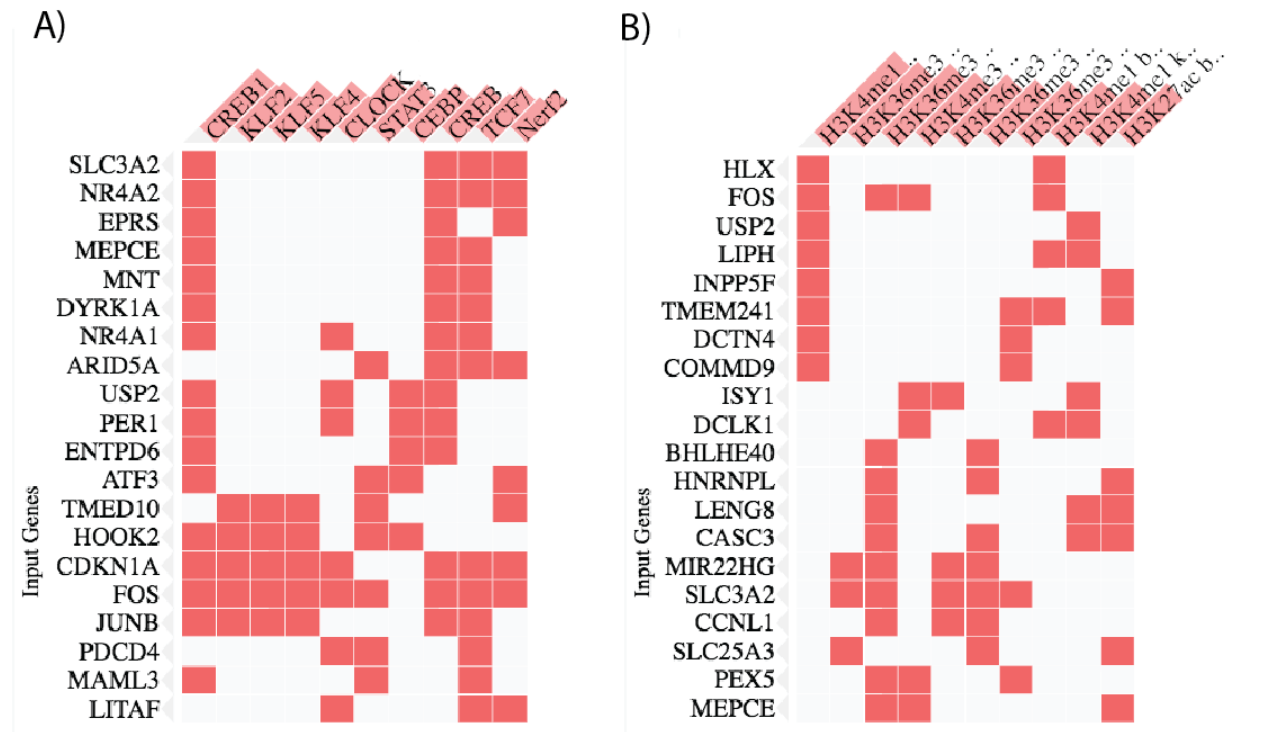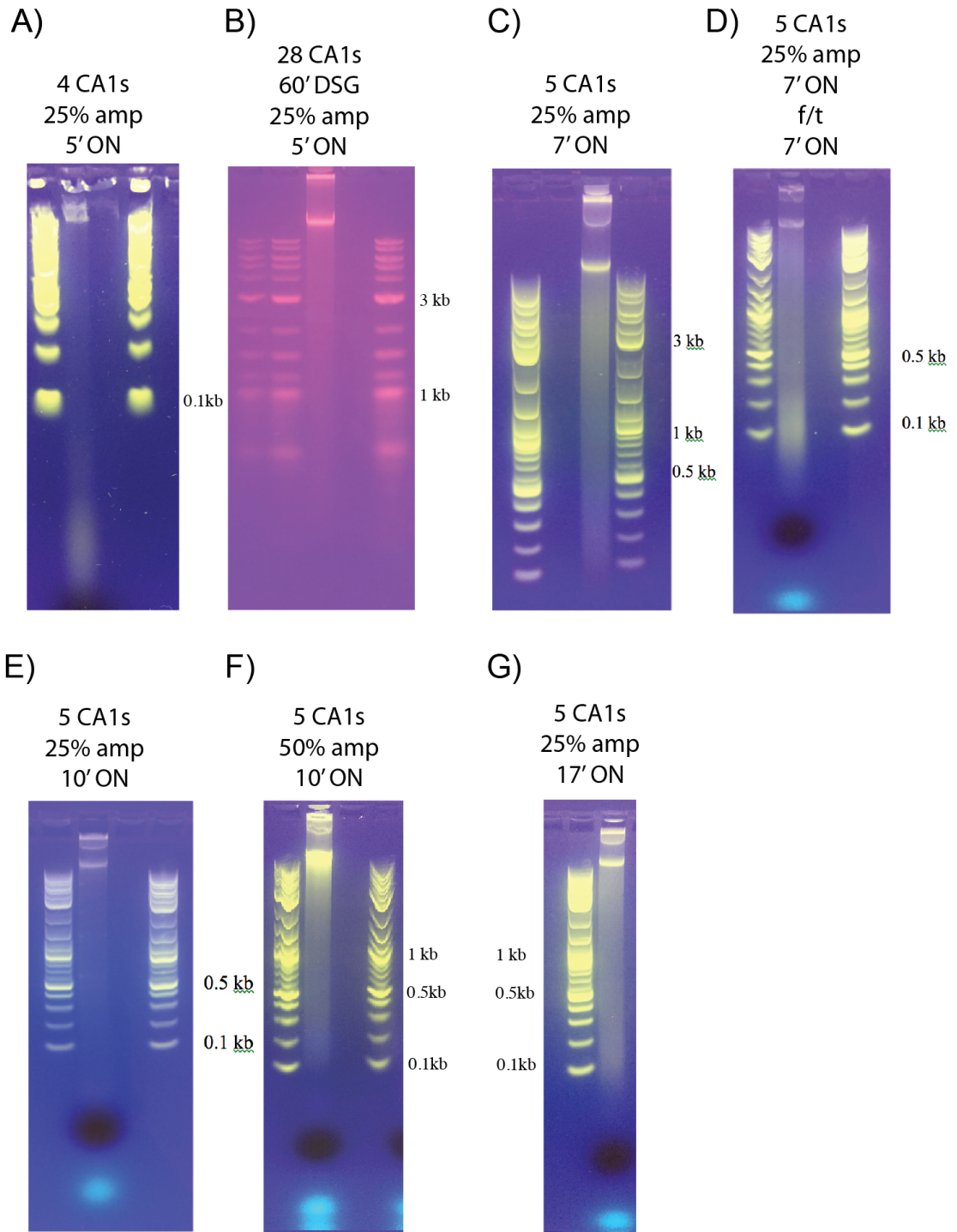
Figure 3-S2

28 x CA1s
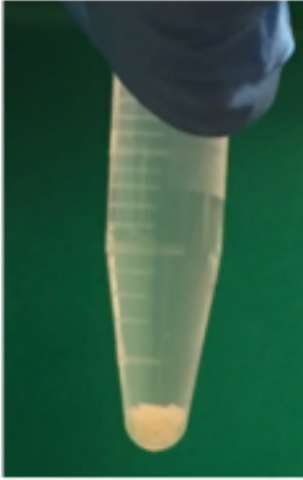
7 x 10-cm dishes

Figure 3-S3

A)
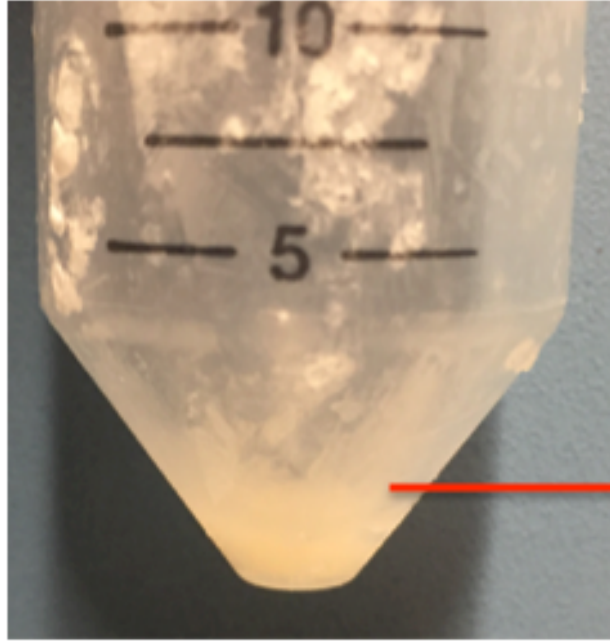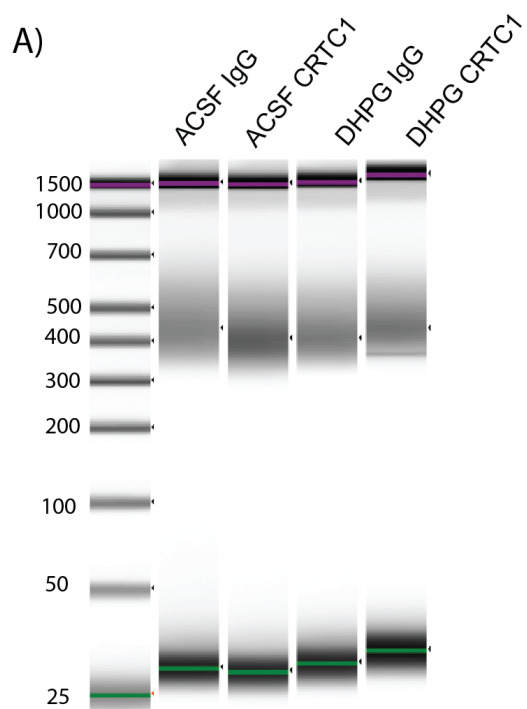
B)

Sample	Size	Calibrated conc. [ng/ul]
ACSF IgG	393	15.5
ACSF CRTC1	401	13.6
DHPG IgG	380	11.2
DHPG CRTC1	377	15.0

C)

Sample	Raw Reads	Unique Reads
ACSF IgG	71m	54m
ACSF CRTC1	110m	83m
DHPG IgG	90m	76m
DHPG CRTC1	68m	51m

Figure 3-S4

A)

B)

ChIP: CREB

ChIP: CRTC1

☐ HC
■ Trained (1-shock)
■ Trained (3-shock)

C)

D)

115

Table 3-S1

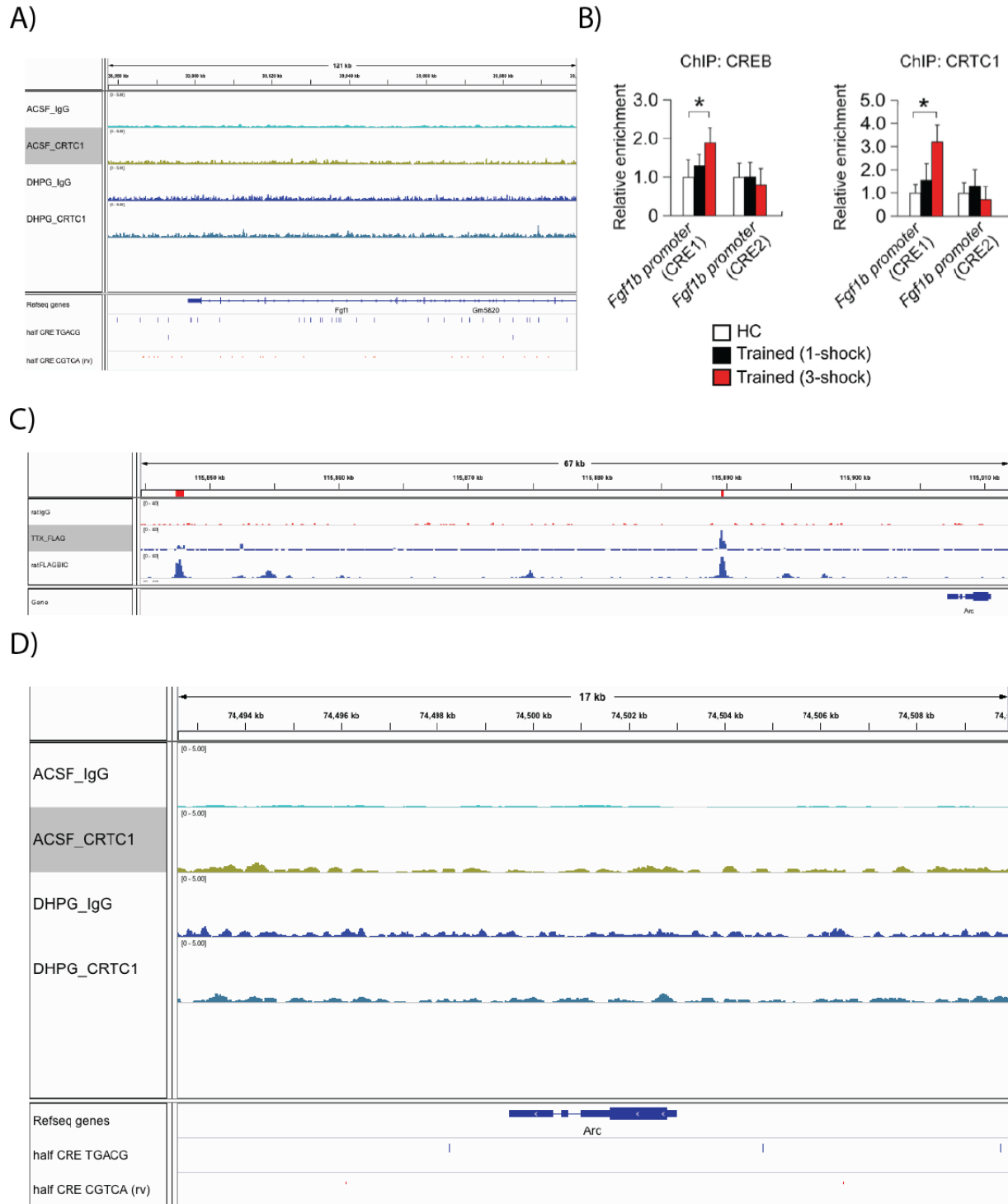|	Shumyatsky 2016	Boergesen et al (Mandrup) 2012. RXR, LXR, PPARa in liver	From Mandrup lab (sent from Brandon in Smale Lab)	Kostas cell culture protocol	Marcelo Wood Lab	Shivan's combination
input material	take 3-4 mice, dissect out HIP, then CA subregion, mince into 1mm pieces. This constitutes "1 ChIP sample".	snap frozen livers (#?). Homogenize in PBS.	2-3 mice at a time. Cut tissue into "small pieces". Transfer to 15ml tube and resuspend 5ml PBS	number of cells for each ChIP is empirically determined. How many dishes did MD use?	brains flash frozen by submesion into dry, ice-cold isopentane and stored @ -80. 2 x 500 um3 punches from one hemisphere for PCR and the other for ChIP in a counterbalanced fashion. From coronal sections	start with 4 mouse brains. Seized, dissect out brain 30' post-SE. (CRTC1 should be potently translocated in most neurons in CTX and HIP). Dissect out HIP. Chop into 1mm (even smaller?) pieces. Resuspend in 5ml PBS
Freeze samples?	yes	yes	no	no		no
fixing	place tissue in 1% Form, 15' RT. Quench w/ 125mM Gly.	1 % Form, 10', RT	add 5ml 2xDSG, rotate RT, 30'. Spin 1', 700 g, RT. Use syringe to remove supe. Add 10ml PBS. Add 270ul 37% Form, rotate RT, 10'. Spin 700 g, RT. Use syringe to remove supe, add 5-10ml PBS and store on ice	10' 1% From (with or without methanol. 20' without) --> 2ml 2.5M Gly.		add 5ml 2xDSG, rotate RT, 30'. Spin 1', 700 g, RT. Carefully remove supe. Add 10ml PBS. Add 270ul add 5ml 2xDSG, rotate RT, 30'. Spin 1', 700 g, RT. Use syringe to remove supe. Add 10ml PBS. Add 270ul 37% Form, rotate RT, 10'. Add 125mM Gly and incubate 2-5'. Spin 700 g, RT. Use syringe to remove supe, add 5-10ml PBS and store on ice
washes	3x w cold PBS++	centrifuge 400g, 2', 4°C. Wash 2x in cold PBS.	see fixing section. Basically PBS wash (spin) after DSG and Form.	Spin down cells 1000 g, 5'. Wash 2x w/ PBS. Can store pellet at -80		centrifuge 700g, 2', 4°C. wash 2-3x w/ ice-cold PBS++.
purify nuclei	?	resuspend in 200ul Lysis buffer/10mg chromatin (how to know amt chromatin?)	spin for 700 g, 1', RT. Remove PBS Q (?). Wash tissue "quickly" once in 10ml cold cell lysis buffer. Manually dounce 5x to get single cell suspension. Sit on ice 20'. Dounce 20x to lyse cells. Transfer to a 15ml tube (reduce loss in nuc.) Pellet nuc at 1000 g for 5', 4°C. transfer supe back to douncer on ice, keep nuc pellet. repeat 5x dounce, 20x dounce etc until no more nuclei can be spun down (3-4 times for adipose tissue). resuspend and pool nuclei in 5ml cell lysis buffer. run through mesh filter. rinse with 5 ml cell lysis buffer. pellet nuc at 1000 g for 5', 4°C. Resuspend in 1ml cell lysis buffer, transfer to a 1.5 ml tube. Pellet at 1000 g for 5', 4°C. Discard supe.	resuspend in 2ml ice-cold buffer I, add 2ml cold buffer II (hypotonic w sucrose that leads to swelling and preserves nuclei structure), mix and inc. on ice 10'. Fill 2 14x89mm beckman tubes w/ 8ml Buffer III (sucrose cushion). Layer on 2 ml cell suspension. spin 10k g 20', 4°C. remove supe, do not disturb white nuc pellet at bottom. wash pellet 2x w PBS w/o Ca or Mg (prevent nuc pellet from "clamping")		spin for 700 g, 1', RT. Remove PBS Q (?). Wash tissue "quickly" once in 10ml cold cell lysis buffer. Manually dounce 5x to get single cell suspension. Sit on ice 20'. Dounce 20x to lyse cells. Transfer to a 15ml tube (reduce loss in nuc.) Pellet nuc at 1000 g for 5', 4°C. transfer supe back to douncer on ice, keep nuc pellet. repeat 5x dounce, 20x dounce etc until no more nuclei can be spun down (3-4 times for adipose tissue). resuspend and pool nuclei in 5ml cell lysis buffer. run through mesh filter. rinse with 5 ml cell lysis buffer. pellet nuc at 1000 g for 5', 4°C. Resuspend in 1ml cell lysis buffer, transfer to a 1.5 ml tube. Pellet at 1000 g for 5', 4°C. Discard supe.
shear chromatin	treat nuclear samples w Mnase (150-900bp). Sonicate to "disrupt nuc. Membrane)	sonicate using Diagenode Bioruptor twin. Centrifuge 2', 10k g. supe = input for IP	Resuspend nuc in 5x volume of ChIP lysis buffer, aliquot 200ul into eppie (for sonication consistency). Sonicate with Biorupter (see details). Spin at max speed, 5', 4°C. Transfer supe to new tubes	resuspend ~ 40e6 x-linked nuc in 400ul sonication buffer (0.1-2% SDS w deoxycholate. Do not use deoxychol. For monoclonal Abs) Sonicate in Diagenode Bioruptor water bath sonicator (?). Start with 3 rounds of 30s ON, 1 min OFF for 10 min. Make sure viscosity decreases substantially! Reverse x-link (?) run some sample on gel to see that most DNA is below 500bp. if not, keep sonicating.		Resuspend nuc in 5x volume of 400ul sonication buffer (0.1-2% SDS w deoxycholate. Do not use deoxychol. For monoclonal Abs) , aliquot 200ul into eppie (for sonication consistency). Sonicate with Biorupter (see details). Spin at max speed, 5', 4°C. Transfer supe to new tubes. Start with 3 rounds of 30s ON, 1 min OFF for 10 min. Make sure viscosity decreases substantially! Reverse x-link (?) run some sample on gel to see that most DNA is below 500bp. if not, keep sonicating.

116

Step						
bind to Ab	O/N 4°C. IgG control.	for each IP dilute 200ul chromatin "one time" in IP wash buffer 1. incubate w/ Ab for 3h rotating at 4°C. (how to quantitate chromatin?)	?	from Mnase section: conjugate 5ug (empirical) Ab to beads. Do 4 replicates and pool to ensure 5-10ng "IP material". Wash 10ul "active motif" magnetic protein G beads 2x in PBS. Resuspend them in 10ul PBS. Add Ab to beads on ice. Adjust volume to 100ul (never dilute beads more than 1:10). Incubate 4h, 4°C on rotor. place Ab-beads on magnet, wash 1x w PBS, 1x w RIPA. Resuspend in 20ul RIPA.		conjugate 5ug (empirical) Ab to beads. (remember IgG control) Do 4 replicates and pool to ensure 5-10ng "IP material". Wash 10ul "active motif" magnetic protein G beads 2x in PBS. Resuspend them in 10ul PBS. Add Ab to beads on ice. Adjust volume to 100ul (never dilute beads more than 1:10). Incubate 4h, 4°C on rotor. place Ab-beads on magnet, wash 1x w PBS, 1x w RIPA. Resuspend in 20ul RIPA. quantitate chromatin
IP Ab-chromatin	Cell Sig. ChIP Grade Protein G magnetic beads	add protein A beads while still rotating at 4°C O/N	?	Mix 10ug S1 and 10ug S2 in 1.5 ml tube. For x-linked material use 20ug chrom. Complete the volume to 500ul w RIPA (Tx100 in RIPA sequesters SDS from sonication buffer --> better IP.) add 5-10ug pre-conjugated proteinG-Ab. Rotate 4°C, O/N		Mix 10ug S1 and 10ug S2 in 1.5 ml tube. For x-linked material use 20ug chrom. Complete the volume to 500ul w RIPA (Tx100 in RIPA sequesters SDS from sonication buffer --> better IP.) add 5-10ug pre-conjuugated proteinG-Ab. Rotate 4°C, O/N
wash	5x w/ RIPA	wash beads 2x w/ IP wash buffer 1, 4°C. Wash beads 2x w/ IP wash buffer 2, 4°C. Wash beads 1x w/ IP wash buffer 3, 4°C. Wash 2x w/ Tris-EDTA buffer.	?	place beads on magnet, wait 3'. Aspirate supe and resuspend in 600ul wash buffer I. Rotate 4°C, 3-5'. Repeat. Resuspend beads in wash buffer II, rotate at 4°C, 3-5'. Repeat. Resuspend in wash buffer II (no rotation). Repeat.wash once with 1x TE (can also wash first with TE + TX100)		place beads on magnet, wait 3'. Aspirate supe and resuspend in 600ul wash buffer I. Rotate 4°C, 3-5'. Repeat. Resuspend beads in wash buffer II, rotate at 4°C, 3-5'. Repeat. Resuspend in wash buffer II (no rotation). Repeat.wash once with 1x TE (can also wash first with TE + TX100)
elution	1x Cell Sig. ChIP elution buffer	400ul EB (1% SDS, 0.1M NaHCO3)	?	resuspend beads in 150ul TE. Add 2ul of RNaseA (2ug/ul), inc. 37°C, 5'. Add 3ul 10%SDS and 5ul 20ug/ul proteinase K.		resuspend beads in 150ul TE. Add 2ul of RNaseA (2ug/ul), inc. 37°C, 5'. Add 3ul 10%SDS and 5ul 20ug/ul proteinase K.
reverse x-link, proteinase K	?	add NaCl to 0.2M, shake O/N 65°C	?	reverse x-link O/N 60°C		add NaCl to 0.2M, shake O/N 65°C (to reverse x-link?)
purify DNA	ChIP kit columns	phenol-chloroform	?	given low yield, recommend using EtOH precipitation instead of column. Transfer samples on magnet, wait 3'. Transfer supe to new tube. Wash with 100ul TE + 0.5M NaCl. Retain wash and combine with supe1. extract with 250ul phenol:chlor. Spin 5' max speed.s transfer aqueous layer in a new tube. Add 2ul 20ug/ul glycogen, 25ul #M NaOAc (pH 5.2) and 700 ul 100% EtOH. place in -20°C O/N or 4h. Spin 1h 4°C to precipitate DNA. Wash pellet 1x w 70% EtOH. Resuspend each pellet in 15ul TE.		given low yield, recommend using EtOH precipitation instead of column. Transfer samples on magnet, wait 3'. Transfer supe to new tube. Wash with 100ul TE + 0.5M NaCl. Retain wash and combine with supe1. extract with 250ul phenol:chlor. Spin 5' max speed.s transfer aqueous layer in a new tube. Add 2ul 20ug/ul glycogen, 25ul #M NaOAc (pH 5.2) and 700 ul 100% EtOH. place in -20°C O/N or 4h. Spin 1h 4°C to precipitate DNA. Wash pellet 1x w 70% EtOH. Resuspend each pellet in 15ul TE.
sequencing	no. qPCR only. FGF1 is a good control.	either qPCR or seq.				qPCR or seq. FGF1 is a good +-ctrl (Shumyatsky)
Notes		different lysis and wash buffers for each step. They seem to quantitate chromatin before adding lysis buffer (after x-linking). Published seq for a set of "no gene" qPCR neg-ctrl primers	For adipose tissue. After fixation, add 5ml PBS for eWAT and 10ml PBS for BAT	KC notes that buffers containing spermine and sperimidine can stabilize nuclei. Lower SDS in sonication steps allows for better chromatin recovery, as SDS is an anionic denaturing agent. Make sure that deoxycholate is not too high - @ 2mM forms micelles which lead to chrom loss.		

Table 3-S2

Company	Brief descriptions	Input requirement
Diagenode True MicroChIP Kit C01010130	Not validated by mfr. For tissue. Illumina seq reagents not included or in protocol	10k cells
Millipore Magna-ChIP HiSens 17-10460	Validated for tissue Protocol calls for nuclear prep Not specialized for low input	10k cells
Takara (Clontech) DNA SMART ChIP-IT kit	Validated for tissue Adapted for low input Streamlined with Illumina seq Utilizes Chelex retrieval of ssDNA to increase DNA yield SMART adapter introduction	1k cells
Active Motif Low Cell ChIP-seq kit	Highly reputed company Column purification of DNA/protein complexes Streamlined with illumina seq Transparent protocol Personal communication with Active Motif reps	1-50k cells

Table 3-S3

Citation	Sample/source	Interesting findings
Martina/Kostas/Sylvia	• Rat FB cultures • 2 CREB commercial Abs • TTX, Basal, BIC	• Much less BIC-induced CREB binding than other TFs examined → it is poised on chromatin at rest
Hartzell et al. *BMC Genomics* 2009	• HeLa cells transfected with CREB-HaloTag	• CREB has strong pref. for binding at bidirectional proms and unlike unidirectional proms, binding often occurs downstream of TSS • Transcriptional data from promoter-luc arrays show unprecedented high level of activation of CREB-bound proms in the presence of CRTC1
Choi et al. *Neuroscience* 2016	• A549 cells treated with dexamethasone • Murine CREB ChIP from Lesiak et al. 2013	• CREB ChIP tracks provided by Encode Consotrium and uploaded under ENCODE Regulation 'Super-track' setting • UCSC accession: wgEncodeEH001662 • [163–165]
Lesiak et al. *PLoS ONE* 2013	• CREB ChIP from P1/2 rat HIP cultures • 25bp reads and mm9	• Data should be downloadable at: http://sacoserver.ohsu.edu/LesiaketalPlosOne2013 but link is broken
Kim et al. (Greenberg) *Nature* 2009	• E16.5 C57/Bl6 mouse embryo CTX seeded ~4x10^7 cells on 15cm dishes • Used @ DIV7 • KCL (pre-treat w TTX O/N)	• Although both SRF and CREB bind enhancers before depol, sometimes this increases their binding (Fig. 2, Supp F1d, 2, 4a, 5) • Seq data is on GEO: GSE21161 – ChIP and RNA-seq, HM047267 – circ. Arc enh. RNA • GO using DAVID
Tanis et al. *Biol. Psych.* 2008	• ChIP-chip for CREB • Adult male rats, ECT	
Malik et al. (Greenberg) *Nat. Neuro.* 2014	• 40 million ms CTX/ChIP library • DIV 7, KCl-depol • ChIP-seq for H3K4me1, H3K4me3, H3K27ac, H3K27me3, CBP, Pol II, pCREB, DHS, FOS, FOSB, JUNB	• Activity-dependent changes in enhancer activity
Hong et al. (Greenberg) *Neuron* 2008	• A-CREB, CBP, hypophos. Pol II (monoclonal 8WG16), MEF2D ChIP from adult FB of CREmKI and loxP ctrl littermates	• CREmKI ms harbors mut. in BDNF proim that disrupt CRE site • (-) ctrls are: CREB or MEF2D Ab with antigen used to raise Ab or irrelevant antigen for experimental ChIP • Cannot access through NCBI's GEO as of Spring 2018
MacIsaac et al. *PLoS Comp. Biol.* 2010	• Liver and cerebellar tissue	• https://www.ncbi.nlm.nih.gov/geo/query/acc.cgi?acc=GSE17067
Qi Ma 2015	• Ms CTX neurons +/- Reelin treatment • CREB ChIP	• Also ref. HIP tissue from adult mice 3mo. • https://www.ncbi.nlm.nih.gov/geo/query/acc.cgi?acc=GSM1629376

Chapter 4

Ongoing Experiments

Introduction

The initial chromatin immunoprecipitation sequencing (ChIP-seq) experiment reported in Chapter 2 was an important step in establishing the feasibility of the experimental workflow from input material to sequencing data. This experiment showed that using 20 dihydroxyphenylglycine (DHPG)-stimulated CA1s per CREB-regulated transcriptional coactivator (CRTC1) immunoprecipitation (IP) was sufficient to yield ChIP-seq peaks that pass many checkmarks of validation. However, as there is little precedent for ChIP-seq experiments of exactly this nature – from acute brain tissue, using low input amounts, on a synaptonuclear translocating transcriptional cofactor that exhibits dynamic magnitude of nuclear occupancy and possibly post-translational modifications (PTMs) in a stimulus-specific manner – there are many considerations to qualify interpretation of this data. Nevertheless, the sequencing data quality, identity of the peaks from the initial DHPG-CRTC1 ChIP-seq dataset, overlap with CREB datasets from cultured neurons, and results of analysis using various software suites are highly encouraging.

This initial dataset inspired a new set of experiments. As the intent of my work was to study the binding of CRTC1 to protein-DNA complexes during the induction of bidirectional synaptic plasticity, I designed a set of further experiments to investigate other stimulations of acute hippocampal slices in addition to DHPG-LTD, and compare them.

Suggestive evidence that CRTC1 binds protein-DNA complexes at different genomic loci in response to different stimulations

It has long been a tantalizing hypothesis that different stimulations mediate differential binding of CRTC1 to protein-DNA complexes, resulting in different programs of gene expression. This would provide an elegant method by which different synaptic stimulations could by encoded in the PTM-state of CRTC1 such that it could mount appropriate

transcriptional responses across many different contexts. Acquiring direct evidence for this has been challenging, as robust analysis of CRTC1 PTMs has been moored by lack of phospho-specific antibodies and technical challenges of conducting mass spectrometric analyses of PTM (see Chapter 1). Moreover, our research group and others have thus far been unsuccessful in purifying nuclear CRTC1 for analysis without contamination from cytoplasmic species; this is particularly important for CRTC1 whose PTM-state can be highly complex and regulate its subcellular localization[51,109,125]. As discussed briefly in Chapter 2, CRTC1 ChIP-seq data from DHPG-stimulated acute hippocampal slices lacks peaks at *Arc* (Martin Lab unpublished) and *fgf1b*[59], as have been identified in other studies, suggesting that DHPG may generate forms of CRTC1 that are unable to bind protein-DNA complexes at these loci, and instead bind other loci. The possibility that these peaks are missed simply due to low starting input cannot be ruled out without replicates or positive controls, however.

To conduct analysis of several known CRTC1 targets within a more tractable model system for exploratory research, I conducted ChIP-qPCR on CRTC1 from NMDA- and DHPG-stimulated cultured neurons (Fig. 1). The strong fold change between CRTC1 and IgG IPs and difference in enrichment between DHPG and NMDA-stimulated cultured neurons suggests that different stimulations may indeed induce differential CRTC1 binding and unbinding to transcription factor complexes.

To examine this possibility further in more careful experiments, I conducted ChIP-seq on acute hippocampal slices stimulated with a panel of different pharmacological plasticity-induction protocols. In parallel, I conducted RNAseq experiments with the aim of correlating changes in ChIP-seq with changes in the transcriptome of CA1 neurons. An additional benefit of these experiments is that they are the first, to my knowledge, to use RNAseq to systematically compare the changes in gene expression induced by these specific and distinct forms of synaptic plasticity.

Strategies for the validation of ChIP-seq results have undergone revision within the ChIP scientific community in recent years, and there are several methods left to employ to continue validating my results. While it was once commonplace to conduct an immunoglobulin protein G (IgG) IP in parallel to target-protein IPs for each sample and this strategy was useful in guiding my analysis of the initial ACSF vs. DHPG ChIP-seq experiments in Chapter 2, IgG controls have their own caveats. Most IgG antibodies are not obtained from true preimmune serum from the same animal in which the specific antibody was raised (as is the case for the Bethyl antibodies used in Chapter 2). In addition, IgG antibodies usually IP much less DNA than specific antibodies do, and thus limited, rather than equally distributed genomic fragments, from the control may be overamplified during library preparation[123]. For this reason, the ChIP community shifted toward using 10% of the input sonicate rather than a parallel IP to create control libraries for sequencing. This has many advantages and although ideally the input sonicate would accurately represent an unbiased sampling of the entire genome, bias in fragment capture still exists. Certain areas of the genome may be more susceptible than others to sonication-induced fragmentation due to lack of stabilizing factors, especially after cross-linking DNA to protein, and library prep and sequencing introduces some inherent bias toward fragments of certain sizes. Moreover, recent ChIP-seq studies usually target many different proteins within a given experimental context and attempt to triangulate the binding of different factors to chromatin, to extract a system of genetic regulation. Sequencing data from multiple ChIP target proteins control for each other and dispense with the utility of sequencing "input", as each ChIP bears peaks in different locations, with different shapes, depending on the nature of the targeted protein. In this way, sequencing conducted on ChIP DNA IP'd by each individual antibody reveals its specificity for DNA fragments surrounding certain genomic loci; if these are unoccupied by other antibodies, the peak is unlikely due to background that would have

123

appeared in all samples. Importantly, though this logic lends considerable comfort to acquired data, it does not completely verify the specificity of any antibody for its intended target. It is possible that nonspecific antibody binding to other protein-DNA complexes would yield a ChIP peak that appears robust in shape and enrichment over baseline, but reflects capture of the wrong protein; this is an especially important tale of caution for proteins within the same family as the target protein. In order to address this concern for antibodies that have not yet been validated for ChIP, experimenters often target the same protein with different antibodies that recognize different epitopes. These controls are robust and have been employed in many typical ChIP studies, however the design of my ChIP experiments differs significantly from such studies and appropriate controls are best designed with the entire experiment in mind.

As CRTC1 is virtually absent from the nuclei of unstimulated CA1 cells by immunohistochemistry (IHC, see Chapter 2), the ACSF condition serves as an elegant control unavailable in studies that focus on proteins that do not undergo dramatic changes in nuclear occupancy. DHPG-LTD and N-methyl-D-aspartate (NMDA)-LTD cause robust translocation of CRTC1 into CA1 nuclei, and it is logical to assume that these samples would yield many more ChIP peaks than ACSF, though this was determined empirically by the ChIP-seq experiments described in Chapter 2. The appearance of two robust peaks in the ACSF-CRTC1 sequencing indicates that levels of CRTC1 that are undetectable by IHC may still bind DNA at key locations. This said, the strong peak enrichment at 113 locations in the DHPG-CRTC1 condition over ACSF-CRTC1 control indicates that ACSF serves as a powerful control in future experiments and largely dispenses with the utility of an "input" or IgG control.

In addition, the tantalizing possibility that different stimuli create different patterns of CRTC1 PTM may influence its binding to transcription factors at different genomic loci and yield different ChIP peaks in response to different stimuli. The diversity of CRTC1 PTMs in response to different stimulations has been observed many times (see Chapters 1 and 2), and it has been observed that another synaptonuclear translocating protein, Jacob, induces transcription of

124

different targets depending on its phosphorylation state[60]. Thus, the ACSF control, forskolin-LTP (FSK-LTP), DHPG-LTD, and NMDA-LTD conditions may contribute control validation to each other; peaks that are clearly observable in one or some conditions but not others are likely stimulus-specific CRTC1 targets. As all IPs were conducted from the same input material, using the same antibody, differences in peak identification are far less likely due to nonspecific activity of the antibody. This cannot be declared without any qualification, however. Though unlikely, it is still conceivable that different stimulations cause changes in other proteins that change their ability to bind the CRTC1 antibody nonspecifically, and yield nonspecific ChIP peaks in one sample but not others.

Validation of ChIP peaks in regions that do not predict transcriptional activation such as gene bodies, intergenic regions, or in regions that are less-obviously associated with a single gene is challenging without prior data. Though validation of promoter and TSS-bound peaks would seem more approachable through the prediction that such genes would be transcriptionally upregulated, this is also an inaccurate assumption. Binding of factors to promoter regions can cause repression of transcription, as in the case of transactive DNA response protein 43 (TDP43)[166], protein inhibitor of activated stat4 (PIAS4)[167], or activating transcription factor 6 (ATF6)[168,169]. Though CRTC1 has been shown to drastically potentiate CREB-mediated expression[41], it is a distinct possibility that this does not hold true for every CRTC1 target. First, CRTC1 may interact with different proteins in the nucleus, which may mediate transcriptional repression or activation. Second, differential CRTC1 PTM may mediate its ability to activate or repress transcription; one PTM form may promote recruitment transcriptional machinery, while another may prevent recruitment and instead recruit other factors or simply act as a steric block.

These caveats and possible others that have yet to be explored render data validation challenging, though not insurmountable. As with any scientific exploration, the most parsimonious interpretation is to describe experiments in detail and allow them to stand for

themselves, inspire refinement of successive experiments, and integrate with other studies that slowly converge upon an understanding of CRTC1-mediated gene expression associated with the expression of bidirectional synaptic plasticity.

Exploration of LTP-induction protocols in acute hippocampal slices

As FSK-LTP drives little CRTC1 to the nucleus of CA1 cells in acute hippocampal slices (see Chapter 2), I explored whether altering chemical LTP-induction protocols would result in greater CRTC1 translocation. The rationale for these experiments is that the absence of test-pulses in the FSK-LTP conducted in the custom chamber system may have prevented the induction of LTP. Reducing the KCl concentration in part two of the FSK-LTP protocol from 30mM to 15 in an attempt to reach a concentration that would increase the excitation of CA1 cells rather than overwhelm the neurons' ability to fire was insufficient to drive significantly greater translocation than the unmodified FSK-LTP protocol. Modification of a chemical LTP protocol from Tom Lisman using ACSF with slightly elevated (15mM) KCl and 0 Mg^{2+} was also unsuccessful in driving robust CRTC1 nuclear translocation in CA1 or inducing LTP (Fig. S1).

These experiments were attempts to find a pharmacological LTP protocol that drove greater CRTC1 translocation in CA1, to increase the chances of obtaining robust CRTC1 ChIP-seq results. However, neither of the protocols caused a significant improvement in translocation. As it may be possible to identify real ChIP peaks from samples with low nuclear CRTC1 as in the case of the ACSF sample discussed in Chapter 2, I decided to proceed with the previously published unmodified FSK-LTP protocol for ChIP and RNA samples.

Experimental Design

Acute hippocampal slices were stimulated with FSK-LTP, DHPG-LTD, NMDA-LTD, or ACSF (control) and snap-frozen directly after stimulation. When enough slices were

accumulated for each condition, the CA1 regions were dissected and subjected to the ChIP protocol described in Chapter 2 and Appendix 1.

For RNA samples, acute hippocampal slices were stimulated as for ChIP samples, then pharmacological stimulations were aspirated off and slices allowed rest for 30 minutes with ACSF perfusion in order to allow sufficient time for synthesis of new RNA transcripts. Slices were then snap-frozen and accumulated until sufficient material was acquired to purify RNA.

Libraries were prepared for ChIP-seq as described in Chapter 2 and Appendix 1. Libraries for RNA-seq were prepared in collaboration with Marco Morselli from the Pellegrini Lab and Institute for Quantitative and Computational Biology (QCB) at UCLA (see Materials and Methods).

Preliminary Results

Acute hippocampal slices were treated with ACSF (control), FSK-LTP, DHPG-LTD, or NMDA-LTD and accumulated at -80°C. Slices were then pooled and processed using the ChIP protocol in Appendix 1. Libraries with high integrity were obtained for two replicates of each condition (Fig. 2) and sequenced using 50 base pair single-end (50bp SE) reads on an Illumina HiSeq 4000. Work is in progress unzipping, demultiplexing, concatenating reads, and converting this data.

For RNA samples, slices were allowed to recover for 30 minutes post-stimulus to allow induced transcript synthesis to accumulate. For 3 replicates of the 4 conditions, slices were pooled, RNA extracted, DNAseI-treated, and depleted of ribosomal RNA (rRNA) before sequencing libraries were prepared, pooled, and size-selected (Fig. 3). Libraries were sequenced using 100 base pair paired-end (100bp PE) reads from an Illumina HiSeq 4000. Work is in progress unzipping, demultiplexing, concatenating reads, and converting this data.

Planned Analysis

Obtaining datasets for biological replicates will allow validation and stringent methods of analysis that were not available before. Peaks will be called on BED files as in Chapter 2, and peak files will be curated in a number of ways. If the data returns a similar number of peaks as the first round (~100), it will be feasible to load all into a single browser window and visually inspect all peaks. At the same time, they will be manually categorized into promoter, TSS, gene body, and intergenic categories. These designations will then be compared to similar categorizations conducted computationally by Homer and GREAT analysis. Using manually-curated peak files, peaks will be sorted by type of genetic region (TSS, promoter, etc.). These peaks can then be compared to CREB ChIP datasets, and Homer's *de novo* motif analysis software can be run on each categorization separately.

The promoter/TSS group of ChIP peaks will be analyzed through gene ontology (GO) and visually inspected. It is possible that these peaks activate transcription of the IEGs identified, such as *c-fos*, *nr4a1*, *nr4a2*, and *nr4a3*, and *junb*.

RNA differential expression (DE) will be conducted on all RNA-seq conditions against ACSF control and sorted by up/down regulation. GO analysis will be conducted on each sample to assess whether the different plasticity stimulations induce different programs of gene expression.

Discussion

ChIP-seq

While it is impossible to hold reasonable expectations about the difference between CRTC1 ChIP-seq from DHPG-LTD and NMDA-LTD stimulated slices, there is an exciting possibility that there are robust peaks in one sample but not the other. The same is true for the ACSF and FSK-LTP samples, though it is likely that these conditions will produce fewer peaks, as there is significantly less nuclear CRTC1 assayed by IHC. With these methods, it will be impossible to say whether differential peaks arise from different CRTC1 PTM forms, different

amounts in the nucleus, or indirect effects such as stimulus-induced changes in DNA binding by transcription factors bound by CRTC1. Though the latter is unlikely to be true for CREB, which is usually pre-bound on chromatin awaiting activation, it may be true for other CRTC1 binding partners.

By comparing CRTC1 ChIP-seq to CREB and SRF datasets, it is possible to categorize CRTC1 peaks as overlapping with CREB, SRF, or neither. As it has been shown that SRF and CREB regulate some distinct and some overlapping sets of genes[170], it may be interesting to compare CRTC1, SRF, and CREB peaks. Subsequent Homer *de novo* motif analysis of the CRTC1 peaks in non-CREB groups may reveal possible alternative transcription factors that interact with CRTC1 besides CREB and SRF. Of course, the CREB datasets are from a different model system, and all comparisons are suggestive.

RNA-seq

The present set of RNA-seq experiments was conducted with many analyses in mind that exceed the boundaries of this work. They were sequenced with 100bp SE reads to enable deeper analysis such as alternative splicing, though this would require further sequencing runs and substantial data processing. In this study, RNA-seq data will be assessed simply by gene count and comparison of each condition to ACSF. CRTC1 ChIP peaks found at promoters, TSSs, or enhancers will be correlated to mRNA DE for the gene in question, with the expectation that these peaks correlate with increases in transcription.   This correlation, however, is complicated by the fact that assessing total RNAs at 30 minutes post-induction does not take into account the half-lives of different RNAs, that changes in RNA concentration result not only from transcription, but also from regulation of RNA stability, and that the 30 minute time point will likely not capture the "second wave" of transcription enacted by newly synthesized activity-induced IEGs such as Jun and Fos. Thus, we are not looking for complete overlap

between the ChIPseq and RNAseq datasets, but rather for information about how the ChIPseq data correlates with changes in the transcriptome of CA1 neurons at this specific point in time.

To begin to explore differences in stimulus-induced RNA expression between the different protocols, differentially expressed genes will be submitted to GO analysis. It is a distinct possibility that each stimulation involves induction of different programs of gene expression. Subtractive comparison of DE between groups, to isolate genes that are particular to each protocol may hint at interesting biological differences between the stimulations. Analysis of the list of DE genes that are shared between experimental groups may be equally interesting and hint at general programs of gene expression that support general synaptic plasticity.

Concluding Remarks

These experiments represent the culmination of many years of work to understand the function of CRTC1 during the induction of bidirectional plasticity. Material was pooled over many months to acquire sufficient input material in a dedicated collaboration with Jenny McGrady-Achiro in the Martin Lab. Given the painstaking effort, animal sacrifice, and cost of these datasets, it is well worth their thorough and methodical analysis. To this end, I will analyze the data to the best of my ability and ingenuity in collaboration with the Pellegrini Lab and QCB, using conventional and exploratory methods made possible by the tractable (100s) number of ChIP peaks likely to be identified. This will yield some insight into CRTC1 genomic targets during plasticity, though publishing and uploading this data to the GEO server is key to the completion of this project. Without making files such as these publicly available, it would have been impossible for me to conduct crucial comparisons of my datasets to others that have been previously published. The gratitude I feel for the possibilities this opened up in my own research drives me to desire nothing more than to return this favor.

Finally, these experiments were carefully designed to yield results that would illuminate the genomic targets of CRTC1 while remaining interpretable due to careful control of variables. This said, no experimental system is without caveats and complications, and these datasets speak only within their experimental confines; further research is warranted to explore the details and meaning of the genes identified in this study.

Materials and Methods

All experiments were performed with approval from the UCLA Institutional Animal Care and Use Committee.

Acute hippocampal slice stimulation

Acute hippocampal slices were prepared as described in Chapter 2 and recovered for 2 hours at 30°C in a custom 8-well interface chamber system with oxygenated (95% O_2/5% CO_2) ACSF containing 124 mM NaCl, 4 mM KCl, 25 mM $NaHCO_3$, 1 mM NaH_2PO_4, 2 mM $CaCl_2$, 1.2 mM $MgSO_4$, and 10 mM glucose. They were then stimulated with FSK-LTP, DHPG-LTD, NMDA-LTD, or ACSF (control) as described in Chapter 2, and immediately snap-frozen. When enough slices were accumulated for each condition, CA1s were dissected and processed through the ChIP-seq protocol described in Chapter 2 and Appendix 1.

For RNA samples, acute hippocampal slices were stimulated as for ChIP samples, then pharmacological stimulations were aspirated off and slices allowed rest for 30 minutes with regular ACSF perfusion in order to allow sufficient time for synthesis of new RNA transcripts. Slices were then snap-frozen and accumulated until sufficient material was acquired to purify RNA.

For the altered chemical LTP protocol experiments, ACSF was altered as follows. For the Lisman protocol, ACSF contained 124 mM NaCl, 15 mM KCl, 25 mM $NaHCO_3$, 1 mM NaH_2PO_4, 2 mM $CaCl_2$, 0 mM $MgSO_4$, and 10 mM glucose. For the modified FSK-LTP protocol,

the ACSF used in the second application of FSK contained 124 mM NaCl, 15 mM KCl, 25 mM NaHCO$_3$, 10 mM CaCl$_2$, 0 mM MgSO$_4$, and 10 mM glucose.

Data Analysis of ChIP-seq

Raw reads were demultiplexed and concatenated with barcodes. Reads will be converted into fastq format, and analyzed for data quality using FastQC. Adapters will be trimmed using CutAdapt or Trimmomatic, then verified for adapter excision using FastQC. Mapping indices will be created and alignment of data will be conducted using STAR. Peak calling will be conducted using Homer. Peaks will be visually verified for each condition and manually categorized by the type of DNA element upon which they reside. GO analysis will be conducted using Homer, DAVID, and GREAT. ChEA analysis will be conducted to correlate each ChIP sample with a broad pool of other ChIP datasets. Peak overlap with CREB and SRF datasets will be conducted manually, and sorting of peaks by type followed by GO analysis and visual inspection will be conducted in search of gene programs mediated by peak subcategories.

RNA-sequencing

10 CA1s per condition were pooled and homogenized in Trizol (Thermo Fisher 15596026), then RNA precipitated by phenol:chloroform extraction. The aqueous phase was passed over an RNA-binding column (Qiagen RNeasy kit 74104). DNaseI (Qiagen 79254) digestion was performed on-column for 15 minutes followed by washes and RNA elution. RNA yield was quantified using the Qubit RNA BR kit.

Libraries were prepared using the NEBNext Ultra II Directional RNA Library Prep (NEB E7765), rRNA depletion (NEB E6350S), and Multiplex Oligo set 4 (E7730S) kits. They were sequenced using 100 base pair paired-end reads on two lanes of an Illumina HiSeq 4000.

Data Analysis of RNA-seq

Raw reads were demultiplexed, and will be concatenated with barcodes. Reads will be converted into fastq format, and analyzed for data quality using FastQC. Adapters will be trimmed using CutAdapt or Trimmomatic, then verified for adapter excision using FastQC. Mapping indices will be created and alignment of data will be conducted using STAR. Differentially expression analysis will be conducted using the DESeq2 package in R.

Preparation mouse forebrain cultures

Mouse forebrain tissue was dissected from P0 or P1 pups, dissociated, and plated on Poly-DL-lysine (0.5 mg/ml) coated 10-cm dishes containing several coverslips (Carolina Biologicals, Burlington, NC). Cells were cultured in a defined serum-free media: Neurobasal A medium (Invitrogen, Carlsbad, CA); β-mercaptoethanol (Sigma, St. Louis, MO); monosodium glutamate (Sigma); B27 (Invitrogen); GlutaMAX (Invitrogen).

Pharmacological treatments

Neurons were incubated with pharmacological agents in conditioned medium, in a 37°C, 5% CO_2 incubator for the specified amount of time before cells were scraped in sonication buffer for ChIP. 100 μM DHPG (Tocris) was applied to cultures for 10 minutes. 20 μM NMDA/glycine (Tocris) was applied to cultures for for 3 minutes. Unmodified, conditioned media was applied to basal cultures for control samples.

ChIP DNA preparation from cultured neurons

After pharmacological stimulation, plates were scraped in Active Motif ChIP buffer (0.1% SDS) and sonicated using a Misonix 3000 probe microtip sonicator with the following settings: 3 seconds ON, 15 seconds OFF, 3 minutes total time. Sonicates were then divided in two and subjected to ChIP following the Low-cell ChIP Seq Kit (Active Motif 53084) unmodified protocol.

Antibodies used were: rabbit anti CRTC1 (Bethyl Labs A300) and purified rabbit IgG (Bethyl Labs P120-101).

qPCR

qPCR primers were designed by hand using genomic regions exported from the Integrative Genome Viewer (IGV) displaying CRTC1 ChIP peaks from the DHPG-LTD dataset from acute hippocampal slices and the previous CRTC1-FLAG ChIP dataset from rat cultured neurons in the Martin Lab. Primers were validated by running qPCR on gDNA (or no template) and confirming one-product amplification. A set of primers previously used for mouse CRTC1 ChIP-qPCR (Uchida et al. 2017) was used to analyze the *fgf1b CRE1* locus.

qPCR using primers for *CREM*, *Nr4a1*, *Junb*, *Arc*, and *fgf1b* were used on equal amounts of ChIP DNA from DHPG and NMDA samples, for IgG control and CRTC1 IPs. Ct values for CRTC1 IP samples were converted to fold-change over corresponding IgG samples, then plotted using Graphpad software (Prism).

Figure Legends

Figure 4-1. ChIP-qPCR. Primers used for qPCR were designed by hand to anneal within regions covered by CRTC1 ChIP peaks in previous datasets, and validated by qPCR off of total genomic DNA (gDNA) for single amplification product and reasonable Ct values before use in these experiments. *A)* Immunocytochemistry reveals that both DHPG and NMDA application drive CRTC1 nuclear accumulation. *B)* Sonication of cultured neurons is efficient and generated fragments suitable for ChIP. C) qPCR on CRTC1 ChIP DNA for candidate genes. The *CREM*, *Nr4a1*, and *Junb* loci tested by qPCR show strong enrichment over IgG for DHPG-stimulated neurons, but much lower enrichment for NMDA-stimulated neurons. The *Arc* locus tested appears de-enriched compared to IgG in both samples, and the difference between stimulations is not significant. Surprisingly, the *fgf1b CRE1* locus that showed enrichment in dentate gyrus of fear-conditioned mice (Uchida et al. 2017) shows de-enrichment in NMDA-stimulated neurons.

Figure 4-2. ChIP libraries for 2 replicates of 4 conditions. A) After sonication, most of the genomic DNA resides in the ~200-1200 bp range with a bias toward ~300 bp. The gel on the right contains contaminant DNA fragments at very low molecular weight, though this does not reflect sonicated gDNA. For this gel, samples were mistakenly incubated in pre-clearing immunoprecipitation beads before light centrifugation and pipetting of 10% for de-cross-linking and analysis by gel electrophoresis. The small-fragment DNA contamination likely comes from salmon sperm DNA used in equilibrating pre-clearing beads used in the ChIP process. B) Screentape analysis of 8 libraries exhibit high integrity and target fragment size.

Figure 4-3. ChIP-seq and RNA-seq library analysis. A) Agarose gel showing the spread of DNA from the combined RNA libraries (comb.) and the combined libraries after size-selection (size-sel.) to optimize them for 100bp SE sequencing. *B)* Screentape analysis of all 12 libraries (3

replicates, 4 conditions) shows that DNA resides within the target fragment size range. *C)*

Graph of fragment distributions reflects adequate concentration of appropriately-sized

fragments.

Figure 4-S1. Modified chemical LTP protocols – all data acquired by Jenny McGrady Achiro in the Martin Lab. A) Neither of the two 15mM KCl chemical-LTP protocols successfully drove

significant CRTC1 translocation in CA1 cells, though they both drove strong translocation in

CA3, compared to 0.005% DMSO controls. *B)* The 15mM KCl Lisman protocol failed to elicit

LTP measured by electrophysiology.   For comparison, a trace from a successful chemical-LTP

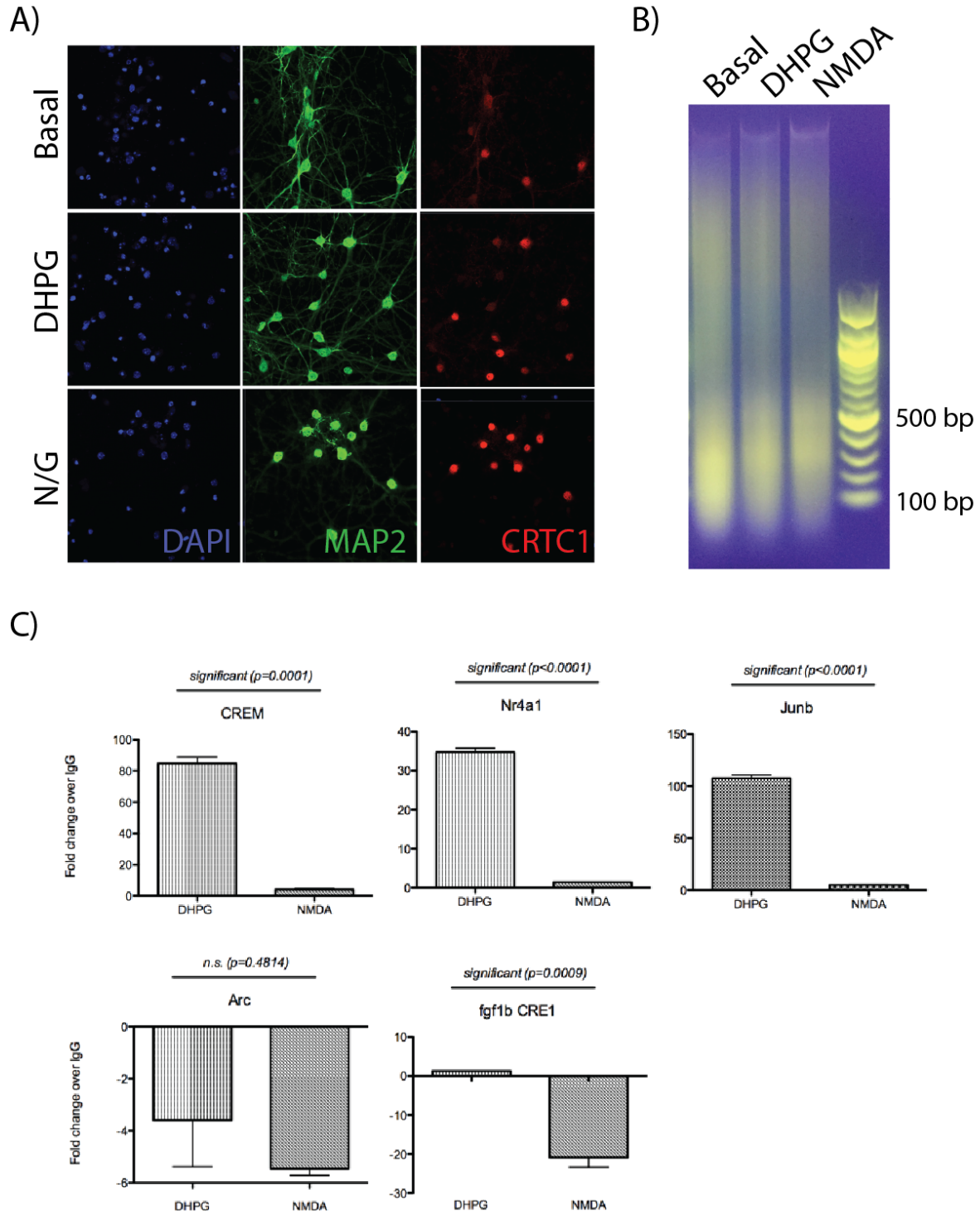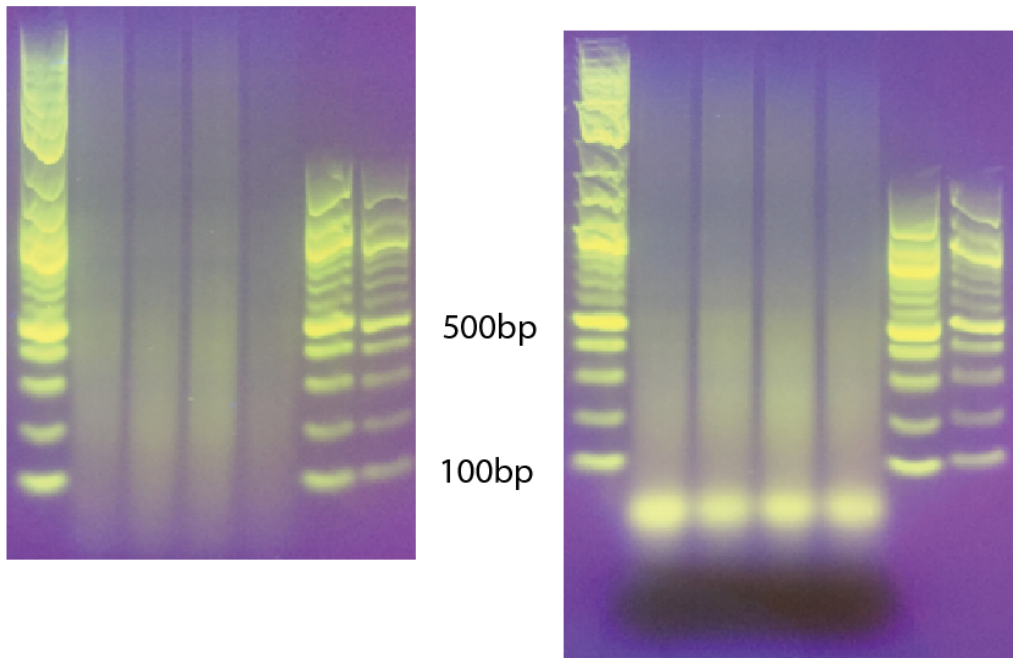induction (cLTP) using the FSK-LTP protocol is overlaid.
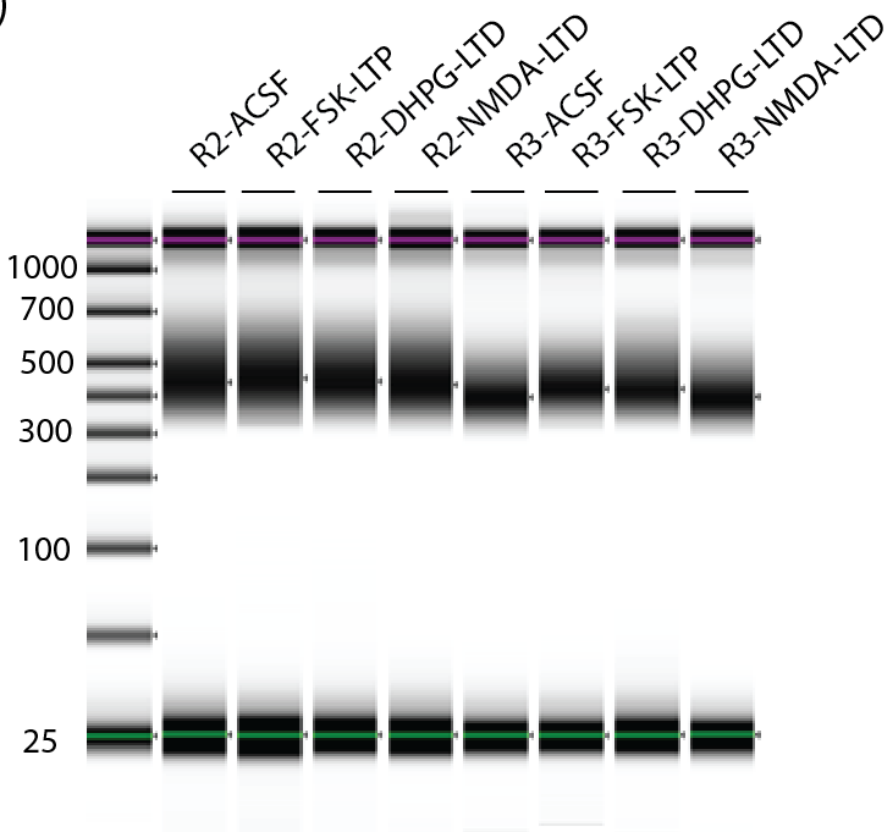
Figure 4-1

Figure 4-2

A)

B)

138

Figure 4-3

139

Figure 4-S1

A)
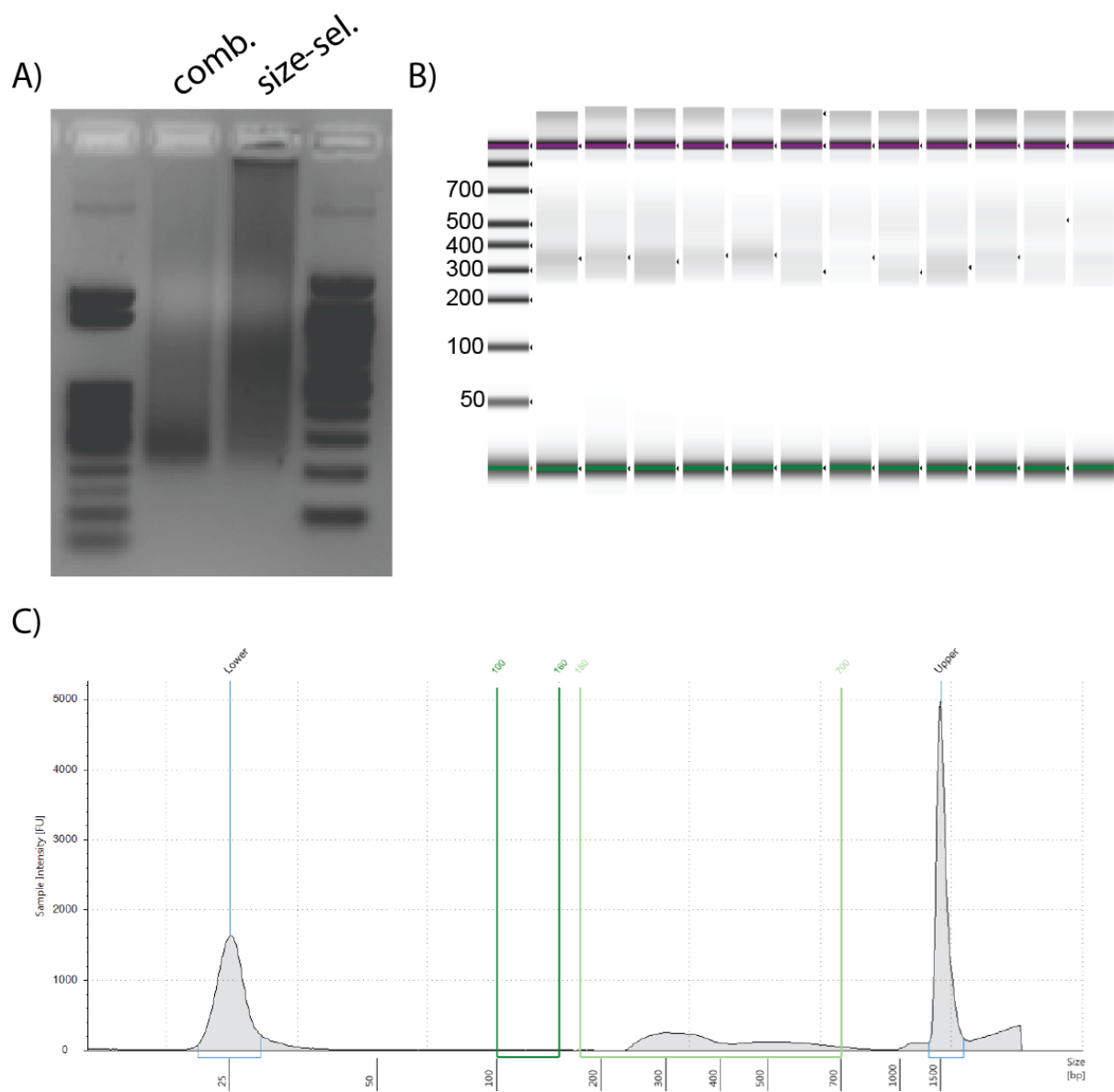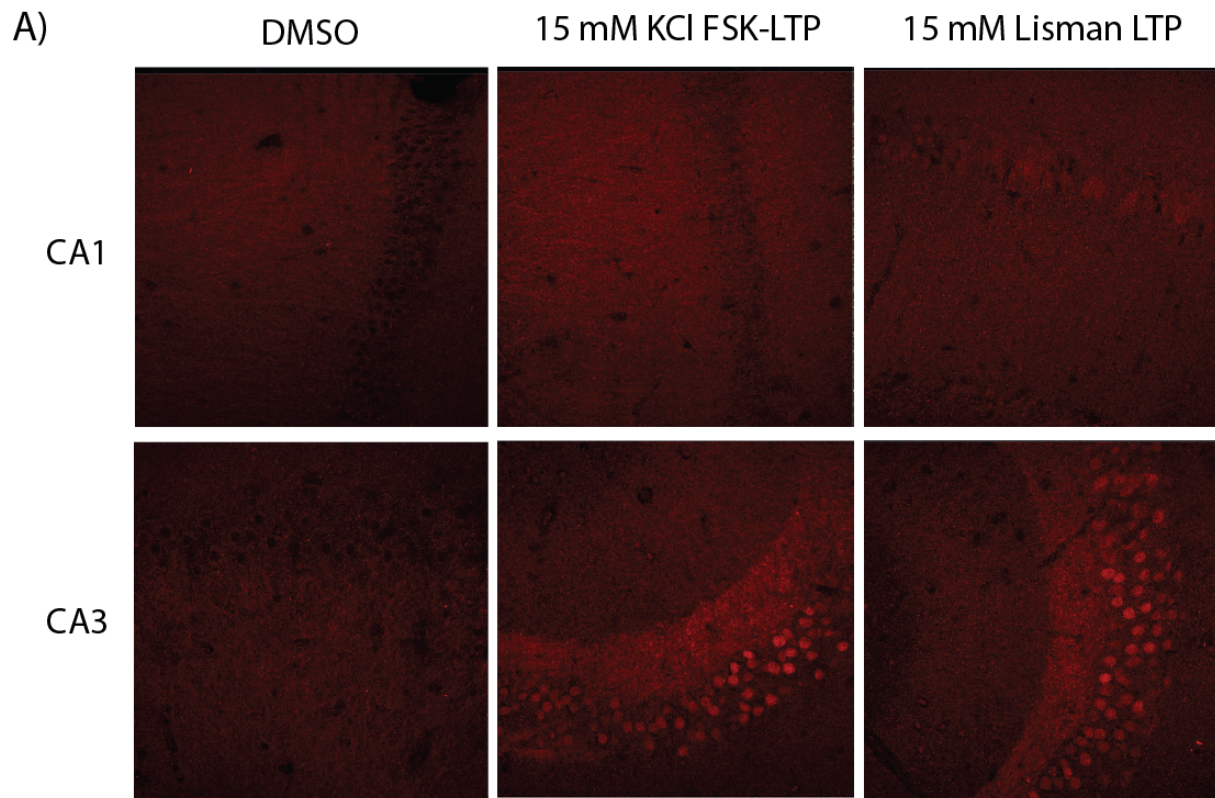
B)
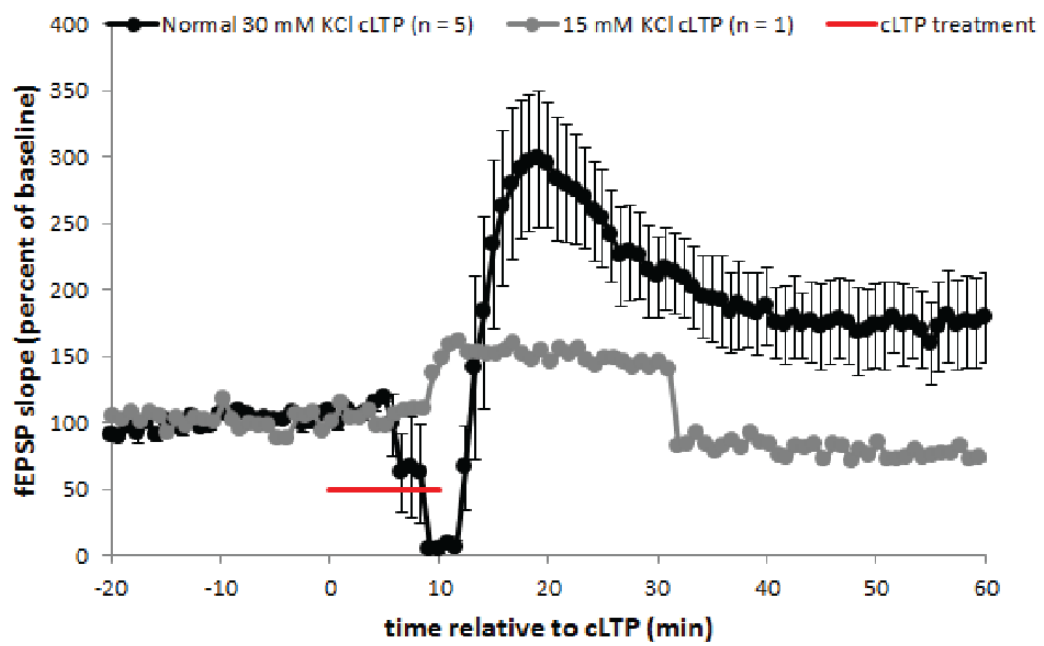
Appendix I

ChIP protocol for CRTC1 from acute hippocampal slices

<u>Preparation and stimulation of hippocampal slices</u>

This protocol is written to aid the reader in designing his or her own experiments for ChIP-seq from acute brain tissue. The experiments for which it was developed involved dissection of acute hippocampal slices and pharmacological treatment, which are delineated here

Mouse hippocampal dissection was conducted as previously described. Please refer to a more comprehensive delineation of these methods, but briefly:

400 mm thick hippocampal slices were prepared from hippocampi dissected from C57/Bl6J mice. Slices were allowed to recover for 2 hours at 30°C in interface-type chambers with oxygenated (95% O_2 / 5% CO_2) artificial cerebrospinal fluid (ACSF) containing the following components:

ACSF:

	[mM]
NaCl	124
$NaHCO_3$	25
KCl	4.4
NaH_2PO_4	1.0
$MgSO_4\ 7H_2O$	1.2
$CaCl_2\ 2H_2O$	2.0
Glucose	10

After resting, slices were treated with pharmacological stimulations, one well at a time. Perfusion inlet lines to the appropriate well were clamped and flow halted. 10ml of ACSF containing the appropriate pharmacological agents was droppered onto the slices using a transfer pipet, submerging them (using the vacuum line to prevent the well from overflowing) for

the appropriate amount of time. Please refer to Chapter 2 of my thesis for a detailed explanation of drug treatments.

After completion of the stimulation protocol, slices were lifted from the solution with a paint brush and snap-frozen to the side of an blue tissue-homogenization tube (part no) that was pre-chilled on dry ice. Tubes were stored at -80°C until enough were collected to proceed with ChIP sample prep.

ChIP

Make all reagents

1. DSG and formaldehyde solutions in filtered PBS

    a. 20x tubes of DSG (6 ul in 1500 ul PBS, each) – 4 CA1s/tube, x5 tubes/condition (20 CA1s) = 20 tubes total.

    b. 656 ul 37% Form into 24 ml PBS (1ml needed/tube)

    bring all timers to dissection scope

2. NP40 lysis buffer 1 (filtered) FRESH, w/ Prot and Phos inhibitors

3. 1% SDS lysis buffer 2 (filtered) FRESH, w/ Prot and Phos inhibitors

4. dilution buffer 3 (filtered) FRESH, w/ Prot and Phos inhibitors

5. 80 ml TBS + Prot/Phos inhibitors (for doing CA1 dissections)

6. *all other reagents are specified and supplied by A.M. kit.*

7. **Set up all bead equilibration reactions in the morning! You will equilibrate the pre-clearing beads throughout the day (~4 hours) while you prepare your samples, sonicate, etc. Then pre-clear. Then you will do the IP with the antibody O/N (no beads yet) but the IP beads will equilibrate O/N so they are ready to bind IP when you come back next day.**

It is OK to use stock solutions and then filter the final buffers through a 0.22 PES Millipore filter (same as Nalgene, just smaller scale). Fine to include detergent before filtering, if it is already in solution (in stock).
Put the prot. And phos. Inhibitor tablets directly into tube that you will filter into (no need to filter them) don't touch them as you pop them out of foil – they will dissolve fairly easily especially with detergent in the buffers.

CROSS-LINKING

1. Cool down centrifuge to 4°C so it is ready for later steps

2. Clean working area with 10% bleach
    a. This is particularly important for an actual experiment where you will prepare a library.

3. Dissect CA1s in TBS + prot./phos. Inhibitors (Roche cOmplete and PhosStop). Used 20 slices per condition (ACSF, cLTP, DHPG, NMDA).

    Put them directly in 1X DSG solution (2mM) in low-binding eppie. 4 per tube, so there is not too much variability in incubation time. (10 slices total, 3 tubes)

Incubate 25' at RT, occasionally inverting tubes to mix. Start timer after 2 CA1s have

entered solution, such that one of these slices will undergo 1 extra minute of DSG-cross-

linking, and the next 2 will have 1 or 2 fewer minutes of cross-linking.

For DSG: dissolve whole tube in 306ul DMSO to make 0.5M stock. Dilute 250x

(6ul in 1500 ul PBS) to get 2mM. (Or 144ul DSG in 36ml PBS)

Make sure to mix/vortex quickly as soon as you add DMSO-DSG to PBS to

prevent polymerization! Note that DSG can go bad rather quickly (weeks-months,

and probably also affected by number of freeze-thaw cycles) and polymerize for

this reason as well (even if it looks clear without precipitate in DMSO stock) -

make sure you have a backup, undissolved powder stock at all times. If you add

DMSO-DSG to PBS and it polymerizes, don't use it for your experiment – make a

fresh batch.

DSG dissolving in PBS is also sensitive to pH. Make fresh PBS from the 10x

stock supplied by Active Motif.

4. Exchange solution in tube 1 with <u>1ml</u> 1X Formaldehyde (1%) and incubate 10' at RT,

occasionally inverting tubes to mix.

Add 41 ul 37% Form to 1.5ml PBS. Dina says no problem using 37% Form with

some methanol. Add this at the last minute, before going to dissect.

Note that it takes ~1min/CA1 dissection.

NOTE: Make sure slices have been frozen at -80 for a while, or they don't come

off the wall of the tube easily!

5. Add 100ul 1.25M Glycine (for 125mM final concentration in 1ml), leave at RT for >10'.

    After that, put on ice until all samples have been fixed.

    Note that quenching time has been increased to 10', to ensure thorough

    quenching of Form and prohibit over-fixation – it would likely take a little longer

    for glycine to fully penetrate tissue than in monolayered cultured cells.

6. Let the slices settle to the bottom of the tube. If they don't, you may want to spin 2',

    100g, 4°C (or maybe 400g). Wash 2x w/ ice-cold PBS.

7. spin 800g, 1', 4°C

DINA MATTHEOS (WOOD LAB – UC IRVINE) LYSIS METHOD

NP40 Lysis (Buffer 1)

50mM Hepes pH7.4	500 ul of 1M stock
150 mM NaCl	300 ul of 5M stock
1% NP40	1 ml of 10% stock
10mM EDTA	200 ul of 0.5M stock
Prot/phos inh.	1 tablet each
	For 10ml

SDS Nuclear (Lysis Buffer 2)

50mM Tris-HCl pH8.0	500 ul of 1M stock
1% SDS	500 ul of 20% stock
10mM EDTA	200 ul of 0.5M stock
Prot/phos inh.	1 tablet each
	For 10ml

Dilution (Buffer 3)

0.01% SDS	10 ul of 20% stock
1.1% Triton-X-100	2.2 ml of 10% stock
1.2mM EDTA	48 ul of 0.5M stock
16.7mM Tris-HCl (pH 8.1)	334ul of 1M stock
167mM NaCl	668 ul of 5M stock
Prot/phos inh.	2 tablet each
	For 20ml

Note that you need 20ml of Dilution Buffer 3 (need ~4 ml for each sample – ACSF, cLTP,

DHPG, NMDA), but only 10ml (or less) of Lysis Buffers 1 and 2.

8. Cut the tip off a 1ml pipette tip and combine all slices into one tube (the siliconized

   sonication tubes provided in the kit).

9. Remove PBS and resuspend pellet in 500ul of NP40 Lysis Buffer 1

10. Vortex, incubate on ice 5' (repeat this 3x until it has been 15' on ice). Do a final vortex.

11. spin 800g, 5', 4°C

12. remove supe and resuspend in 500ul SDS Nuclear Lysis Buffer 2/Sonication buffer.

SONICATION

13. Take sample over to sonicator on ice.

    Fill a 250ml glass beaker with wet ice to keep tubes cold.

    Clean probe tip with Nanopure H_2O and EtOH before sonication.

    Clearn probe tip with Nanopure H_2O between samples.

Sonicate: Misonix 3000 microtip (Stephen Smale Lab, UCLA)

1. turn on sonicator, press "program"

2. enter total time, on time, off time, output

3. press enter

4. temperature monitoring? → NO

3s on, 15s off, Power 5.5. 2:30 min total time.

This amount of time worked for the pilot (3 CA1s) done on 6/14.

Remember to clean the probe tip w/ water and ethanol

Notes:

- *AM protocol says to start with 30s ON, 30s OFF, 10' for cultured cells and does not have recommendations for tissue. These parameters are for use with their sonicator, and need to be re-determined for every sonicator.*

14. If the sonicate is clear, this is a good sign the sonication has been efficacious (if you see tissue chunks, you almost certainly have not sonicated sufficiently).

15. Spin 14,000 x g for 10', 4°C. Transfer supe to a new tube

---

DE-X-LINK A SMALL SAMPLE AND CHECK FOR FRAG SIZE

RNase A treatment, SDS/ProteinaseK de-X-linking and digestion

16. De-X-link 20ul of total sonicate (~450ul). Save the remaining ~400ul on ice. Aliquot out

1/10th of remaining volume (40ul) and save as "input".

The whole sonicate from 3 CA1s is more than enough DNA to see with SYBR gold.

In experiment 9/20/17, 10ul sonicate was enough to see on gel. But in this expt we have

half the chromatin concentration, so doubled to 20ul.

For this diagnostic gel, you can use standard reagents for NaCl and proteinase-K (don't

use the kit-supplied reagents – the kit does not supply extra reagents for doing a

diagnostic gel step)

add 10ul proteinase K

add 15ul 5M NaCl

add 45ul sonication buffer (1% SDS)

incubate 1-2hr, 65°C on Thermomixer (600rpm) to de-x-link

Then 10' at 90°C

Then purify by Phenol Chloroform (see below)

17. Purify DNA:

    a. Phenol-chloroform

        i. Take a yellow Heavy Phase-lock gel column and spin for 30s, 14000xg,

            RT, before use.

        ii. Add 1 volume phenol-chloroform-isoamylalcohol mixture to your input

            sample (90 ul), and pipette the mixture onto the pre-spinned column.

iii. Shake for 1' to mix. Spin 5', 14000xg, RT

iv. Remove the top layer into a fresh tube (pay close attention to layers)

   Phenol-chloroform waste is in the DNA gel room. In hood, a

   "trash can" for solid waste; on the opposite bench there are liquid

   waste containers.

v. Add 2.8 volumes of 100% EtOH (252 ul) + 1/10th volume 3M NaOAc

   pH5.2 (9 ul) + 1 ul Glycoblue.

   Glycoblue helps by coloring the DNA – will help to visualize it if the

   pellet is very small. NaOAc and EtOH help precipitate the DNA

   with the cold

   On 4/24/18 – was doing this at 9pm and couldn't find Glycoblue,

   so did not include it.

vi. Mix and incubate @ -80°C for >1hr (O/N is best)

vii. Spin 30', max speed, 4°C.

viii. Remove supe. Wash with 70% EtOH (just add ontop). Spin 10', max

   speed, 4°C.

ix. Remove all EtOH and let dry for a few min before resuspending in half

   volume of your original input (20ul) H_2O

You cannot run this sample directly on the agarose DNA gel because the SDS will cause EtBr or other dye to migrate abnormally.

Note that this protocol does not include RNAse treatment.

Example gel:

8 ul NEB 2-log ladder	ACSF de-x-linked	cLTP de-x-linked	DHPG de-x-linked	NMDA de-x-linked	8 ul NEB 100-bp ladder	4 ul NEB 100-bp ladder

500 bp

100 bp
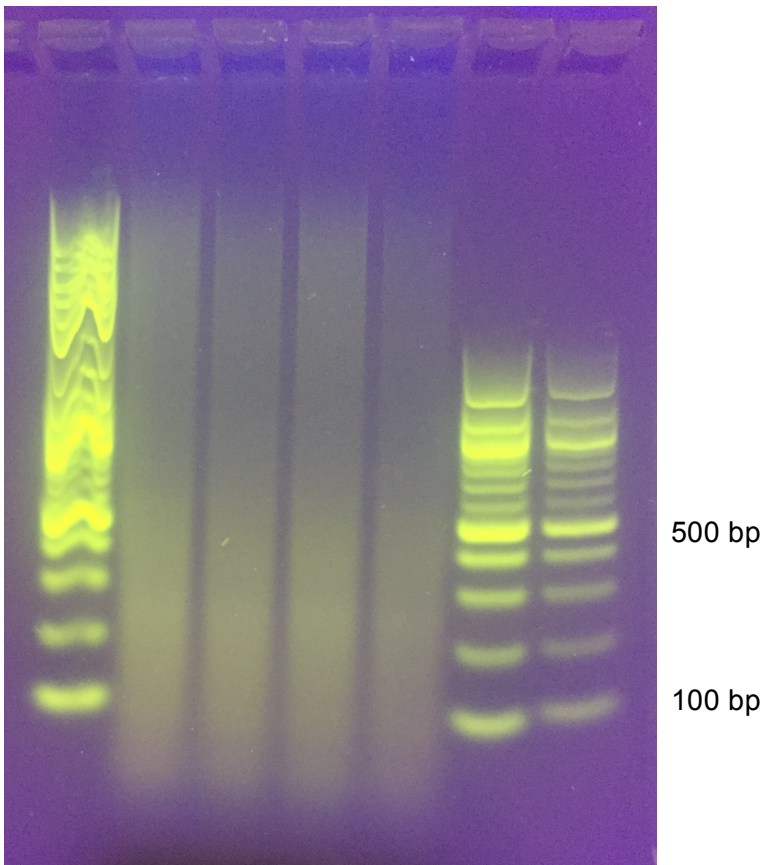
PREPARE BEADS FOR IP AND PRE-CLEARING OF CHROMATIN

In these steps, we prepare beads by equilibrating, blocking, then use some for pre-clearing, then use some for actual IP.

1. Remember that you will dilute your sonicate 1:10, so it will be 5ml. Then you will split this into 4 parallel IPs. So you will need to split each sonicate aliquot of 1.25ml into 4 x 1.5ml low-binding eppies for all reactions below.

2. For each IP, set up a low-binding (Phenix) tube for preparing IP and pre-clearing beads separately. Cut the end off pipet tips before using, to prevent clogging with beads. See the A.M. manual for volumes etc. to use for these rxns.

    In these steps, the beads will rotate end-over-end in the cold room to equilibrate. If you do each bead volume separately, there may not be a lot of total volume per eppie, which may mean the volume doesn't really agitate at all with end-over-end (stays stuck at bottom of tube due to surface tension). I find it better to do >2 equilibration's worth of beads, per tube (here, 4 equilibration reactions per tube)

3. Add 360 ul of Protein G Agarose to each IP tube and 220 ul to each Pre-Clearing tube. Remember to store agarose beads at 4°C now that it has been thawed.

    this is for 4x 85ul beads for IP and 4x 50ul beads for PC.

4. Centrifuge the tubes at 1250 x g, 3', RT. Carefully discard supe.

5. Add 1128ul TE, pH 8.0 to IP beads, 664 ul to pre-clear beads.

You'll need 5.28 ml TE total – make sure you have enough buffer for this and

subsequent steps that need TE

this is for 4x 85ul beads for IP and 4x 50ul beads for PC

6. Centrifuge the tubes at 1250 x g, 3', RT. Carefully discard supe.

7. Set up tubes for blocking (different for IP and pre-clearing bead sets!)

	85 ul beads/rxn	*50 ul beads/rxn*
	IP	**Pre-clearing**
TE, pH 8	360 ul	360
Blocking Reagent AM1	40	40
BSA	40	40
Blocker	40	-

this is for 4x 85ul beads for IP and 4x 50ul beads for PC

"Blocker" is probably salmon sperm (or equivalent) DNA

Incubate IP beads O/N, 4°C on rotator.

Incubate pre-clearing beads for 3-6 hrs, 4°C

PRE-CLEAR CHROMATIN

In these steps, use the beads you equilibrated and blocked, to pre-clear your sonicated

chromatin, before using it for IP.

1. Centrifuge the tubes containing equilibrated beads (pre-clearing only; leave the IP beads
   to continue rotating) at 1250 x g, 3', RT. Carefully discard supe.

2. Add the proper volume (see manual, but here 332ul) of ChIP Buffer to the pre-clearing rxn and invert to mix.

> *In the future, it might be more correct to us Dilution Buffer 3 (1.1% triton, 0.1% SDS) that is used to dilute the sonicate. This is the buffer that the sonicate is in, that will go onto the beads. This step of washing the beads is essentially equilibrating them to the sonicate buffer, so would be more correct to use our dilution buffer than A.M. supplied ChIP buffer, which we don't actually use for lysis. However, I don't think it would make any real difference – I know from personal communication with A.M. that ChIP buffer is 0.1% SDS. They wouldn't give rest of ingredients, but it is probably similar to 1% triton (pretty standard for IPs).*

3. Centrifuge at 1250 x g, 3', RT. Carefully discard supe.

4. Do a second wash with ChIP Buffer using *different volume* (see manual) – 232 ul

> *this is for 2x 50ul beads for PC*

5. Dilute your sonicate 1:10 with dilution buffer

> *Here, aliquot 110ul sonicate to 4 low-binding tubes (per sample). Then add 990 ul dilution buffer on top.*

6. Cut off 2mm from a pipet tip and transfer equilibrated bead slurry to your low-binding eppie that contains sonicated material. Here use 50ul beads.

7. Add 5 ul supplied PIC and 5 ul PMSF to teach tube.

   Cap tubes and rotate 2-3hr 4°C

IMMUNOPRECIPITATION

In these steps, use the beads you equilibrated and blocked for the IP. Using sonicated material, that has been pre-cleared in previous steps.

Be aware that these instructions (mostly volumes) are optimized for 200ul sonicate (undiluted) mixing with 2-4ug antibody in 30ul total volume of PBS/antibody. Due to the need to dilute sonicate 1:10 before IP, the volumes written here are adapted and not optimized by Active Motif.

Here we are forced to use a high volume of beads to promote efficient IP, since sonicate is in large volume. Antibody binding happens O/N, so the Ab should find its target, even though volumes are high. Increasing incubation time after adding beads may also help increase efficiency of IP.

1. Prepare separate low-binding eppies (Phenix) for each IP – 4 parallel IPs per condition. Here, we are doing

2. Add 2.5ug Bethyl antibody (12.5ul) to each of the 4 IP tubes (total 10ug/condition) and using 1x PBS (remember 10x is supplied) with ph. And prot. Inhibitors, and bring each eppie up to 30ul final volume.

   Bethyl Ab is supplied as 100ul of 0.2mg/ml.

156

3. Centrifuge the tube of pre-cleared chromatin at 1250 x g, 3', RT. Carefully remove supe, leaving behind the beads (keep supe this time!!) and transfer to the tube with the antibody.

4. Rotate O/N, 4°C (this is the IP!)

Next Day

5. Quick spin to collect contents to bottom of tube.

6. Cut tip off p200 pipete, resuspend beads gently. Add 100ul of the equilibrated IP bead slurry to each IP rxn. Remember to cut the pipette tip to help with pipetting beads. Resuspend the beads as you are pipetting them out (they may settle to the bottom)

7. Rotate for 3-4hr, 4°C

WASHING AND ELUTION OF IP RXNS

This is where the A.M. column comes into play and allows you to wash beads very efficiently without losing any to pipetting, etc. All washes happen on the column, and then you elute the ChIP DNA. These steps are followed by de-x-linking, so the DNA off the column is still x-linked to protein.

Some of these washes (probably all) will take a bit longer for these experiments than the protocol thinks they will – because we use so many more beads than intended. So leave some extra time for flow through, if needed.

Sarah says it's important to have fresh phenol (<~6mo). Not sure about chloroform, and my experiments have worked using one that's years old. But could be worth just buying new of both

1. Label a ChIP filtration column for each IP rxn. Break off the tab from the bottom of the column right before you use it! Place it in an empty 1ml pipette rack to hold it.

2. Add 600 ul ChIP Buffer to each IP rxn to wash any remaining beads off the sides of the IP tube and transfer the entire volume (including beads) to the column. Let it flow through by gravity

   Since we will have to do IPs in large volume, first transfer all IP volume to column (may take a few rounds to pass all through), then add the 600ul buffer to the IP tube to wash off residual, and pass that through column as well.

3. Transfer 105 ul Elution Buffer AM4 per IP to a new regular 1.5ml eppie. Pre-warm at 37°C

   You will do 2x 50ul elutions from each IP column. So need 100ul, but include a little extra for pipetting error (and pipette super carefully!)
   This buffer is probably 1% SDS (will elute protein from antibody, and high-SDS required for de-x-linking)

4. Wash each column with 900 ul ChIP Buffer. Allow a minute for it to flow through the column.

5. Wash again with 900ul ChIP Buffer.

6. Wash columns with 900ul Wash Buffer AM1. Incubate for 3' on the column and allow the buffer to flow through the column.

7. Wash again with 900ul Wash Buffer AM1. Incubate 3' on the column.

8. Wash each column with 900ul LiCl Buffer.   Incubate 3' on the column.

   LiCl dissolves better than NaCl in SDS (bc SDS is sodium dodecyl sulfate). The use of different types of salts also improves effective removal of non-specific chromatin interactions with beads.

9. Wash again with 900ul LiCl Buffer. Incubate 3' on the column.

10. Wash each column with 900 ul TE Buffer pH 8.0. Allow a minute for it to flow through.

11. Wash again with 900ul TE Buffer pH 8.0. Incubate 1' on the column.

12. Transfer columns to a new 1.5ml regular eppie. Centrifuge 1250 x g for 3', RT to remove residual wash buffer.

13. Label new 1.5ml low-binding (Phenix) eppies. Transfer columns to these tubes. Add 50ul pre-warmed Elution Buffer AM4 to each column and incubate at RT for 5'. Centrifuge 1250 x g for 3', RT to elute DNA

Put AM4 back at 37°C in between elutions.

14. Add another 50ul pre-warmed Elution Buffer AM4 to the column and incubate RT, 5', then spin 1250 x g for 3' *in the same tube.* You should now have 100ul of ChIP DNA eluate per eppie. Throw away the columns.

REVERSE X-LINKS AND PURIFY DNA

The eluate from the column contains ChIP DNA x-linked to protein. In these steps you will de-x-link and get DNA that can be used for qPCR or library prep. The first step here is O/N de-x-linking, so you can do it right after you elute DNA from the columns in previous steps.

15. Select "SLB_DE_X_LINK" program and start it on the thermocycler, to pre-warm it to 65°C.

16. Label a PCR tube for each ChIP rxn.

    Use dedicated, clean PCR tubes. I have some in the ChIP Active Motif box.

17. Transfer each 100ul of ChIP DNA to PCR tubes, and add 2ul ProteinaseK + 5ul 5M NaCl. Vortex, then place in thermocycler at 65°C O/N.

---

18. Transfer DNA to a new low-binding (Phenix) tube. Add 125ul phenol and 64ul chloroform/isoamyl alcohol (24:1). Shake vigorously to mix (don't vortex) for 15 seconds. Incubate at RT, 5'.

    You can't use chloroform w/o isoamyl, here. Talked to Kostas and Robin, they say isoamyl is important for extraction. Read online, didn't find much about this, but some say it prevents chloroform foaming, which can interfere w DNA purification

19. Centrifuge at max speed, RT, 2'. Transfer aqueous (top) layer to a new 1.5 ml low-binding (Phenix) tube.

    A hazy white layer at interface may still be present.

20. Add 125ul chloroform/isoamyl alcohol (24:1) to the aqueous layer in the new tube. Shake vigorously for 15 seconds to mix (no vortex). Incubate at RT, 5'.

21. During the incubation, set up a 1.5 ml low-binding (Phenix) tube for each rxn, and add 2ul Carrier to each tube.

    "Carrier" is probably glycogen.

22. Centrifuge the DNA purifications (with phenol:chloroform) max speed (> 18k x g) for 2', RT. Transfer the top (aqueous) layer to the tube with the carrier.

23. Add 300ul 100% EtOH to the DNA solution and briefly vortex to mix.

24. Put samples at -80°C for 30' to precipitate.

25. Centrifuge max speed (>18k x g), 15', 4°C.

26. Carefully remove supe with a pipet to avoid disturbing or moving the DNA pellet

27. Add 500ul 70% EtOH to each tube and invert to mix

28. Centrifuge max speed (>18k x g), 5', 4°C.

> *You can do 10' instead, if you are worried about not spinning down DNA*
>
> *sufficiently.*

29. Remove 400ul supe, then Centrifuge remainder at max speed (>18k x g), 2', 4°C

30. Remove supe with a p200 pipet and make sure not to disturb the pellet! You can move
    to a p10 pipet to get the last remaining EtOH if necessary.

31. Air-dry the pellet for 10-15' until residual EtOH has evaporated. Resuspend the pellet in
    40ul Low-EDTA TE Buffer.

> *Really try to remove all EtOH before air drying. It is easy for a tiny ball of EtOH*
>
> *to remain at bottom, right on top of pellet. This can take forever to dry, while the*
>
> *outer edges of the pellet overdry (which can be bad for DNA recovery).*

At this point you have 40ul of ChIP DNA! You can store at -20°C or move directly to qPCR or library prep.

Library prep

Notes:
- Many of the rxns are performed in the presence of SPRI beads, but it shouldn't inhibit them
- The A.M. Next Gen Library Kit manual actually lists different ratios/volumes for all these steps, depending on whether you have <10ng input or more. On this doc are listed the amounts for <10ng, because that is what we have in these samples (based on pilots from spring 2017)
- The PEG/NaCl solution referenced in the library prep is provided ready to use as "PEG solution"
- The library prep protocol is oddly specific about the type of tube (PCR, eppie) used to make each reaction master mix. I'm not sure how important this could be, but there is no sense jeopardizing precious samples for no reason. So some of the rxns that are to

163

be done in PCR tubes are split into multiple master mixes, to prevent exceeding max PCR tube volume.

- Master mixes used for my 12 library preps are included here, to provide a template, though they should be adjusted by the experimenter to reflect the number of libraries he or she is making.

- Link to A.M. protocol: [168,169]

QUBIT:

- Did not do Qubit for these experiments, because it only tells you if you have enough material to skip PCR amplification. We are certainly going to need to do at least some PCR library amplification, so better not to waste the 1ul ChIP DNA needed for Qubit.

<u>MAKE ALL REAGENTS</u>

8. Get magnetic PCR tube holder

9. Get well-calibrated pipettes

10. Remove enzymes from -20°C storage and place on <u>ice</u> for >10' to allow reagents to reach 4°C before pipetting.

11. Invert reagents to mix (do not vortex enzymes) and quick tabletop spin to collect contents before opening tube.

12. Prepare fresh 80% EtOH fresh every time! Use clean gold-shield EtOH and nuclease-free water. You will need ~2ml per sample. Discard after use. (here 25 ml = 20.8 ml EtOH + 5.2 ml ultrapure nuclease-free H_2O)

13. Assemble reagent master mixes on ice and scale volumes as needed, using 5% excess volume.

14. Always add reagents in the specified order!

15. Invert reagent stocks to mix (don't vortex enzymes)

16. Use special 8-tube strips with flat attached (individual caps) to prevent splashing from sample-to-sample with all the pipetting to and from PCR tubes in this protocol. Good ones are Thermo Fisher Part No. AB200

LIBRARY PREP

18. Transfer each ChIP DNA sample to a **new PCR tube**. For these samples, do each set (replicate) of 4 stimulations in a separate **8-tube PCR strip**.

19. Place 2 new **PCR tubes** on ice and prepair Repair I reaction:

    Master mixes are for 6 volumes, each (see notes above). Here we have 12 samples total.

Low EDTA TE	13 ul	84.5	84.5
Buffer W1	6 ul	39	39
Enzyme W2	1 ul	6.5	6.5
Total Volume	**20 ul**	**130 ul (6.5x)**	**130 ul (6.5x)**

20. Add the full 20ul Repair I mixture to the 40ul ChIP DNA and mix by pipetting.

21. Place in thermal cycler and run this program:

| 37°C | 10min | |

    Lid heating OFF (not 37) *

22. Post-Repair I SPRI:

a) Ensure the beads are at RT and briefly vortex to homogenize suspension.

b) Add 84ul beads (1.4:1 ratio) to each 60ul Repair I rxn. No PEG NaCl. Vortex to mix and quick-spin down on tabletop fuge.

c) Incubate at RT for 5'

   o In this time, set up the next rxn mixture: Repair II (see next numbered step)

d) Place the sample on magnetic rack until solution clears and pellet is formed (~5')

e) Remove and discard the supe without disturbing the pellet (<5ul may be left behind)

f) Add 180ul fresh 80% EtOH to pellet while it is still on the magnet. Pipet carefully so you don't disturb the pellet. Incubate for 30s, then carefully pipet off the EtOH (all without removing tube from magnetic rack).

g) Repeat step f) for one more wash with 80% EtOH

h) Remove tubes from rack, quick-spin on tabletop fug and place back onto magnet. Remove residual EtOH.

i) Air dry the pellet for **no more than 5'**. *Watch the pellet to avoid over-drying or cracking! (can reduce DNA recovery)*

23. Repair II rxn:

    a. Place a new **Phenix eppie** on ice and prepare the Repair II rxn mix in order.

        Here I have substituted Phenix 1.5ml eppies for 0.65 eppie called for in protocol. They are not specific about the type of 0.65 ml tube.

Low EDTA TE	30 ul	416
Buffer G1	5 ul	65
Reagent G2	13 ul	169
Enzyme G3	1 ul	13
Enzyme G4	1 ul	13
Total Volume	**50 ul**	**650 ul (13x)**

    b. Add this 50ul to the beads from the post-repair I SPRI, and resuspend by pipetting, mixing thoroughly.

    c. Place this tube (still with beads in it) in the thermocycler and run Repair II pgm:

20°C	20min	

lid heating OFF (or leave lid open)

24. Post-Repair II: PEG NaCl, EtOH, but no new beads for this step.

    a. Add 60ul PEG/NaCl (1.2:1 ratio) to 50ul Repair II rxn volume. Mix by vortexing, and quick spin the samples down.

    b. Incubate samples for 5' RT

o In this time, set up Ligation I rxn (see numbered step below)

c. Place the samples on magnetic rack until solution clears and pellet is formed (~5')

d. Remove and discard the supe without disrurbing the pellet (~5ul may be left behind)

e. Add 180ul fresh 80% EtOH. Pipet slowly so as not to disturb pellet. Incubate 30s, then carefully pipet off EtOH.

f. Repeat step e) for a second wash with 80% EtOH

g. Quick spin the samples in a tabletop fuge and place back onto magnet. Remove any residual EtOH from the bottom of the tube.

h. Air dry the pellet for no more than 5'. *Watch the pellet to avoid cracking or over-drying, which could result in reduced DNA recovery.*

25. Ligation I rxn:

a. Place 3 new **PCR tubes** on ice and add reagents in this order:

Low EDTA TE	20 ul	84	84	84
Buffer Y1	3 ul	12.6	12.6	12.6
Enzyme Y3	2 ul	8.4	8.4	8.4
Total Volume	**25 ul**	**105 ul (4.2x)**	**105 ul (4.2x)**	**105 ul (4.2x)**

b. Add 25ul of the pre-mixed Ligation I rxn to beads for each sample. Pipet to mix and resuspend thoroughly.

c. Add 5ul of the desired Y2 Index to each sample (library). And make a note of each one used. Pipet up and down to mix thoroughly.

Sample	Index	
ACSF R1	Y2-5	ACAGTG(A)
cLTP R1	Y2-6	GCCAAT(A)
DHPG R1	Y2-7	GACATC(A)
NMDA R1	Y2-8	ACTTGA(A)
ACSF R2	Y2-9	GATCAG(A)
cLTP R2	Y2-12	CTTGTA(A)
DHPG R2	Y2-13	AGTCAA(C)
NMDA R2	Y2-14	AGTTCC(G)
ACSF R3	Y2-15	ATGTCA(G)
cLTP R3	Y2-16	CCGTCC(C)
DHPG R3	Y2-18	GTCCGC(A)
NMDA R3	Y2-19	GTGAAA(C)

Note that the Y2's supplied are 1-9, 12-16, 18-19.

The bp in parentheses is read during a 7th cycle, but is not considered part of the index sequence

i. See section U in the protocol for an explanation for this, but essentially if you are doing multiplexed sequencing, you need each library to be ligated with a unique Y2 Index. Here we are supplied with many Y2's, so figure out the experiment beforehand and plan accordingly.

      ii.   Multiplexing is essentially a way to save money and time by sequencing several samples in the same lane of a flow cell. "Indexing" here is essentially barcoding.

d. Place in thermal cycler and run pgm Ligation I:

25°C	15min	

lid heating OFF (or leave lid open)

26. Post-ligation I SPRI:

a. Add 25.5ul (0.85:1 ratio) PEG NaCl to the 30ul Ligation I rxn, to clean rxn. Mix by vortexing, and quick spin the samples down.

b. Incubate samples for 5' RT

    o   In this time, set up Ligation II rxn (see numbered step below)

c. Place the samples on magnetic rack until solution clears and pellet is formed (~5')

d. Remove and discard the supe without disrurbing the pellet (~5ul may be left behind)

e. Add 180ul fresh 80% EtOH. Pipet slowly so as not to disturb pellet. Incubate 30s, then carefully pipet off EtOH.

f. Repeat step e) for a second wash with 80% EtOH

g. Quick spin the samples in a tabletop fuge and place back onto magnet. Remove any residual EtOH from the bottom of the tube.

h. Air dry the pellet for **no more than 5'**. *Watch the pellet to avoid cracking or over-drying, which could result in reduced DNA recovery.*

27. Ligation II: place a new **Phenix eppie** on ice and add reagents in order below

Low EDTA TE	30 ul	390
Buffer B1	5 ul	65
Reagent B2-MID	2 ul	26
Reagent B3	9 ul	117
Enzyme B4	1 ul	13
Enzyme B5	2 ul	26
Enzyme B6	1 ul	13
Total Volume	**50 ul**	**650 ul (13x)**

a. Add 50ul of Ligation II rxn to beads for each sample and resuspend by pipetting.

b. Place in thermocycler with Ligation II pgm:

40°C	10min	
25°C	HOLD	

lid heating OFF (or leave lid open)

28. Post-Ligation II SPRI: PEG/NaCl, no beads.

a. Add 42.5ul (0.85:1 ratio) PEG NaCl to the 50ul Ligation II rxn and mix by vortexing, then quick spin the samples down.

b. Incubate samples for 5' RT

    o   No need to setup "elution rxn" this time, you will just elute from beads in Low EDTA TE buffer.

c. Place the samples on magnetic rack until solution clears and pellet is formed (~5')

d. Remove and discard the supe without disrurbing the pellet (~5ul may be left behind)

e. Add 180ul fresh 80% EtOH. Pipet slowly so as not to disturb pellet. Incubate 30s, then carefully pipet off EtOH.

f. Repeat step e) for a second wash with 80% EtOH

g. Quick spin the samples in a tabletop fuge and place back onto magnet. Remove any residual EtOH from the bottom of the tube.

h. Air dry the pellet for no more than 5'. *Watch the pellet to avoid cracking or over-drying, which could result in reduced DNA recovery.*

i. Resuspend beads in 20ul Low EDTA TE buffer, mix well by pipetting up and
    down until homogeneous.

j. Place beads on magnetic rack until solution clears and pellet is formed. Transfer
    supe to a new PCR tube.

---

29. Library amplification – necessary for samples at this low concentration

a. Place a new PCR tube on ice and prepare the library rxn by adding reagents in
    order

Low EDTA TE	10 ul	42	42	42
Reagent R1	5 ul	21	21	21
Reagent R2	4 ul	16.8	16.8	16.8
Buffer R3	10 ul	42	42	42
Enzyme R4	1 ul	4.2	4.2	4.2
Total Volume	**30 ul**	**126 ul (4.2x)**	**126 ul (4.2x)**	**126 ul (4.2x)**

b. Add 30ul of pre-mixed library rxn to the 20ul eluted library and mix by pipetting.
    Total volume of PCR rxn is now 50ul.

c. Place in the thermal cycler and run pgm:

98°C	30s	
98°C	10s	**12x cycles**
60°C	30s	
68°C	60s	
4°C	Hold	

Proceed immediately to post-PCR SPRI!

30. Post-Library PCR SPRI

This is the only SPRI that recommends using a two-sided SPRI cleanup approach (outlined below) to eliminate small and large fragments for a more uniform library selection.

    a. Ensure the beads are at RT and briefly vortex to homogenize suspension.

    b. Add 32.5ul SPRI beads (0.65:1 ratio) to each 50ul PCR rxn.

    c. Mix by vortexing, quick spin the samples in a tabletop fuge.

    d. Incubate samples for 5' at RT

    e. Place sample on magnetic rack until the solution clears and a pellet is formed.

    f. Transfer supe to a new PCR tube and discard beads. Add 10ul fresh SPRI beads (0.2:1 ratio) to the supe in the new tube.

    g. Mix by vortexing, quick spin the samples in a tabletop fuge.

    h. Incubate the samples for 5' at RT.

    i. Place the sample on a magnetic rack until the solution clears and a pellet is formed.

j. Remove and discard the supe without disturbing the pellet (leave <5ul in the tube).

k. Add 180ul of fresh 80% EtOH to the pellet while it is still on the magnet. Use care not to disturb the pellet. Incubate for 30s, then carefully remove the EtOH.

l. Repeat step k once more for a second was with 80% EtOH

m. Quick spin the samples in a tabletop fuge and place back onto the magnet. Remove any residual EtOH from the bottom of the tube.

n. Air dry the pellet for no more than 5'. *Watch the pellet to avoid cracking or over-drying, which could result in reduced DNA recovery.*

o. Resuspend the beads in 20ul Low EDTA TE buffer. Mix well by pipetting up and down until homogenous.

p. Place beads on a magnetic rack until the solution clears and a pellet is formed. Transfer supe to a new PCR tube. Use a p10 to remove final bit of solution without taking any beads.

q. Use library quantification kit for Next-generation sequencing to quantify the library

r. Libraries can be stored at -20°C for long-term storage. They are ready for sequencing on the Illumina platforms!

---

31. Sequencing: Submit to a core facility – if youneed guidelines for run setup and sample sheet preparation with MiSeq, HiSeq2500, and NextSeq500 platforms, see www.activemotif.com/nextgen.

References

1. Wiesel, T. N. & Hubel, D. H. Single-cell responses in striate cortex of kittens deprived of vision in one eye. *J. Neurophysiol.* **26,** 1003–1017 (1963).

2. Wiesel, T. N. & Hubel, D. H. Comparison of the effects of unilateral and bilateral eye closure on cortical unit responses in kittens. *J. Neurophysiol.* **28,** 1029–1040 (1965).

3. Wiesel, T. N. & Hubel, D. H. Extent of recovery from the effects of visual deprivation in kittens. *J. Neurophysiol.* **28,** 1060–1072 (1965).

4. Fox, K. A critical period for experience-dependent synaptic plasticity in rat barrel cortex. *J. Neurosci.* **12,** 1826–1838 (1992).

5. Hardingham, N. *et al.* Neocortical Long-Term Potentiation and Experience-Dependent Synaptic Plasticity Require α-Calcium/Calmodulin-Dependent Protein Kinase II Autophosphorylation. *J. Neurosci.* **23,** 4428–4436 (2003).

6. Liu, Q. *et al.* Branch-specific plasticity of a bifunctional dopamine circuit encodes protein hunger. *Science* **356,** 534–539 (2017).

7. Bliss, T. V. P. & Lømo, T. Long-lasting potentiation of synaptic transmission in the dentate area of the anaesthetized rabbit following stimulation of the perforant path. *J. Physiol.* **232,** 331–356 (1973).

8. Steward, O. & Levy, W. B. Preferential localization of polyribosomes under the base of dendritic spines in granule cells of the dentate gyrus. *J. Neurosci.* **2,** 284–291 (1982).

9. Feig, S. & Lipton, P. Pairing the cholinergic agonist carbachol with patterned Schaffer collateral stimulation initiates protein synthesis in hippocampal CA1 pyramidal cell dendrites via a muscarinic, NMDA-dependent mechanism. *J. Neurosci.* **13,** 1010–1021 (1993).

10. Giuditta, A., Dettbarn, W. D. & Brzin, M. Protein synthesis in the isolated giant axon of the squid. *Proc. Natl. Acad. Sci. U. S. A.* **59,** 1284–1287 (1968).

11. Koenig, E. Synthetic mechanisms in the axon—iv. In vitro incorporation of [3h]precursors into axonal protein and RNA. *J. Neurochem.* **14,** 437–446 (1967).

12. Torre, E. R. & Steward, O. Demonstration of local protein synthesis within dendrites using a new cell culture system that permits the isolation of living axons and dendrites from their cell bodies. *J. Neurosci.* **12,** 762–772 (1992).

13. Martin, K. C. *et al.* Synapse-Specific, Long-Term Facilitation of Aplysia Sensory to Motor Synapses: A Function for Local Protein Synthesis in Memory Storage. *Cell* **91,** 927–938 (1997).

14. Frey U, Frey S, Schollmeier F & Krug M. Influence of actinomycin D, a RNA synthesis inhibitor, on long-term potentiation in rat hippocampal neurons in vivo and in vitro. *J. Physiol.* **490,** 703–711 (1996).

15. Dash, P. K., Hochner, B. & Kandel, E. R. Injection of the cAMP-responsive element into the nucleus of Aplysia sensory neurons blocks long-term facilitation. *Nature* **345,** 718–721 (1990).

16. Bartsch, D., Casadio, A., Karl, K. A., Serodio, P. & Kandel, E. R. CREB1 Encodes a Nuclear Activator, a Repressor, and a Cytoplasmic Modulator that Form a Regulatory Unit Critical for Long-Term Facilitation. *Cell* **95,** 211–223 (1998).

17. Davis HP, Squire LR. Protein synthesis and memory: a review. Psychol Bull 96: 518-559 (1984).

18. Bourtchuladze, R. *et al.* Deficient long-term memory in mice with a targeted mutation of the cAMP-responsive element-binding protein. *Cell* **79,** 59–68 (1994).

19. Dong, Y. *et al.* CREB modulates excitability of nucleus accumbens neurons. *Nat. Neurosci.* **9,** 475–477 (2006).

20. Han, M.-H. *et al.* Role of cAMP Response Element-Binding Protein in the Rat Locus Ceruleus: Regulation of Neuronal Activity and Opiate Withdrawal Behaviors. *J. Neurosci.* **26,** 4624–4629 (2006).

21. Viosca, J., Armentia, M. L. de, Jancic, D. & Barco, A. Enhanced CREB-dependent gene expression increases the excitability of neurons in the basal amygdala and primes the consolidation of contextual and cued fear memory. *Learn. Mem.* **16,** 193–197 (2009).

22. Impey, S. *et al.* Induction of CRE-Mediated Gene Expression by Stimuli That Generate Long-Lasting LTP in Area CA1 of the Hippocampus. *Neuron* **16,** 973–982 (1996).

23. Armentia, M. L. de *et al.* cAMP Response Element-Binding Protein-Mediated Gene Expression Increases the Intrinsic Excitability of CA1 Pyramidal Neurons. *J. Neurosci.* **27,** 13909–13918 (2007).

24. Telese, F. *et al.* LRP8-Reelin-regulated Neuronal (LRN) Enhancer Signature Underlying Learning and Memory Formation. *Neuron* **86,** 696–710 (2015).

25. Kim, T.-K. *et al.* Widespread transcription at neuronal activity-regulated enhancers. *Nature* **465,** 182–187 (2010).

26. Mayr, B. & Montminy, M. Transcriptional regulation by the phosphorylation-dependent factor CREB. *Nat. Rev. Mol. Cell Biol.* **2,** 599–609 (2001).

27. Cha-Molstad, H., Keller, D. M., Yochum, G. S., Impey, S. & Goodman, R. H. Cell-type-specific binding of the transcription factor CREB to the cAMP-response element. *Proc. Natl. Acad. Sci.* **101,** 13572–13577 (2004).

28. Thompson, M. A., Ginty, D. D., Bonni, A. & Greenberg, M. E. L-type Voltage-sensitive Ca2+ Channel Activation Regulates c-fos Transcription at Multiple Levels. *J. Biol. Chem.* **270,** 4224–4235 (1995).

29. Matthews, R. P. *et al.* Calcium/calmodulin-dependent protein kinase types II and IV differentially regulate CREB-dependent gene expression. *Mol. Cell. Biol.* **14,** 6107–6116 (1994).

30. Johannessen, M., Delghandi, M. P. & Moens, U. What turns CREB on? *Cell. Signal.* **16,** 1211–1227 (2004).

31. Euskirchen, G. *et al.* CREB Binds to Multiple Loci on Human Chromosome 22. *Mol. Cell. Biol.* **24,** 3804–3814 (2004).

32. Shaywitz, A. J. & Greenberg, and M. E. CREB: A Stimulus-Induced Transcription Factor Activated by A Diverse Array of Extracellular Signals. *Annu. Rev. Biochem.* **68,** 821–861 (1999).

33. Hagiwara, M. *et al.* Coupling of hormonal stimulation and transcription via the cyclic AMP-responsive factor CREB is rate limited by nuclear entry of protein kinase A. *Mol. Cell. Biol.* **13,** 4852–4859 (1993).

34. Nichols, M. *et al.* Phosphorylation of CREB affects its binding to high and low affinity sites: implications for cAMP induced gene transcription. *EMBO J.* **11,** 3337–3346 (1992).

35. Dwarki, V. J., Montminy, M. & Verma, I. M. Both the basic region and the 'leucine zipper' domain of the cyclic AMP response element binding (CREB) protein are essential for transcriptional activation. *EMBO J.* **9,** 225–232

36. Kobayashi, M. & Kawakami, K. ATF-1CREB heterodimer is involved in constitutive expression of the housekeeping Na,K-ATPase alpha 1 subunit gene. *Nucleic Acids Res.* **23,** 2848–2855 (1995).

37. Iourgenko, V. *et al.* Identification of a family of cAMP response element-binding protein coactivators by genome-scale functional analysis in mammalian cells. *Proc. Natl. Acad. Sci.* **100,** 12147–12152 (2003).

38. Altarejos, J. Y. & Montminy, M. CREB and the CRTC co-activators: sensors for hormonal and metabolic signals. *Nat. Rev. Mol. Cell Biol.* **12,** 141–151 (2011).

39. Song, Y. *et al.* CRTC3 links catecholamine signalling to energy balance. *Nature* **468,** 933–939 (2010).

40. Koo, S.-H. *et al.* The CREB coactivator TORC2 is a key regulator of fasting glucose metabolism. *Nature* **437,** 1109–11 (2005).

41. Altarejos, J. Y. *et al.* The Creb1 coactivator Crtc1 is required for energy balance and fertility. *Nat. Med.* **14,** 1112–1117 (2008).

42. Luo, Q. *et al.* Mechanism of CREB recognition and coactivation by the CREB-regulated transcriptional coactivator CRTC2. *Proc. Natl. Acad. Sci.* **109,** 20865–20870 (2012).

43. Hogan, M. F. *et al.* Hepatic Insulin Resistance Following Chronic Activation of the CREB Coactivator CRTC2. *J. Biol. Chem.* (2015).

44. Luan, B. *et al.* CREB pathway links PGE2 signaling with macrophage polarization. *Proc. Natl. Acad. Sci.* **112,** 15642–15647 (2015).

45. Kim, J.-H. *et al.* CREB coactivators CRTC2 and CRTC3 modulate bone marrow hematopoiesis. *Proc. Natl. Acad. Sci.* **114,** 11739–11744 (2017).

46. Mair, W. *et al.* Lifespan extension induced by AMPK and calcineurin is mediated by CRTC-1 and CREB. *Nature* **470,** 404–408 (2011).

47. Shen, R. *et al.* Neuronal energy-sensing pathway promotes energy balance by modulating disease tolerance. *Proc. Natl. Acad. Sci.* **113,** E3307–E3314 (2016).

48. Bell, D. & El-Naggar, A. K. Molecular Heterogeneity in Mucoepidermoid Carcinoma: Conceptual and Practical Implications. *Head Neck Pathol.* **7,** 23–27 (2013).

49. Watts Alan G., Sanchez-Watts Graciela, Liu Ying & Aguilera Greti. The Distribution of Messenger RNAs Encoding the Three Isoforms of the Transducer of Regulated cAMP Responsive Element Binding Protein Activity in the Rat Forebrain. *J. Neuroendocrinol.* **23,** 754–766 (2011).

50. Ch'ng, T. H. *et al.* Activity-dependent transport of the transcriptional coactivator CRTC1 from synapse to nucleus. *Cell* **150,** 207–221 (2012).

51. Ch'ng, T. H. *et al.* Cell biological mechanisms of activity-dependent synapse to nucleus translocation of CRTC1 in neurons. *Front. Mol. Neurosci.* **8,** 48 (2015).

52. Li, S., Zhang, C., Takemori, H., Zhou, Y. & Xiong, Z.-Q. TORC1 Regulates Activity-Dependent CREB-Target Gene Transcription and Dendritic Growth of Developing Cortical Neurons. *J. Neurosci.* **29,** 2334–2343 (2009).

53. Kovács, K. A. *et al.* TORC1 is a calcium- and cAMP-sensitive coincidence detector involved in hippocampal long-term synaptic plasticity. *Proc. Natl. Acad. Sci.* **104,** 4700–4705 (2007).

54. Zhou, Y. *et al.* Requirement of TORC1 for Late-Phase Long-Term Potentiation in the Hippocampus. *PLOS ONE* **1,** e16 (2006).

55. Sekeres, M. J. *et al.* Increasing CRTC1 Function in the Dentate Gyrus during Memory Formation or Reactivation Increases Memory Strength without Compromising Memory Quality. *J. Neurosci.* **32,** 17857–17868 (2012).

56. Reissmann, S. Cell penetration: scope and limitations by the application of cell-penetrating peptides. *J. Pept. Sci. Off. Publ. Eur. Pept. Soc.* **20,** 760–784 (2014).

57. Hirano, Y. *et al.* Fasting launches CRTC to facilitate long-term memory formation in Drosophila. *Science* **339,** 443–446 (2013).

58. Hirano, Y. *et al.* Shifting transcriptional machinery is required for long-term memory maintenance and modification in *Drosophila* mushroom bodies. *Nat. Commun.* **7,** 13471 (2016).

59. Uchida, S. *et al.* CRTC1 Nuclear Translocation Following Learning Modulates Memory Strength via Exchange of Chromatin Remodeling Complexes on the Fgf1 Gene. *Cell Rep.* **18,** 352–366 (2017).

60. Karpova, A. *et al.* Encoding and Transducing the Synaptic or Extrasynaptic Origin of NMDA Receptor Signals to the Nucleus. *Cell* **152,** 1119–1133 (2013).

61. Jansson, D. *et al.* Glucose controls CREB activity in islet cells via regulated phosphorylation of TORC2. *Proc. Natl. Acad. Sci.* **105,** 10161–10166 (2008).

62. Hille, B. *Ionic Channels of Excitable Membranes*. (Oxford University Press, Incorporated, 1992).

63. West, A. E. *et al.* Calcium regulation of neuronal gene expression. *Proc. Natl. Acad. Sci.* **98,** 11024–11031 (2001).

64. Ghosh, A. & Greenberg, M. E. Calcium signaling in neurons: molecular mechanisms and cellular consequences. *Science* **268,** 239–247 (1995).

65. Ghosh *et al.* Calcium regulation of gene expression in neuronal cells. *J Neurobiol.* (1994).

66. Gallin, W. J. & Greenberg, M. E. Calcium regulation of gene expression in neurons: the mode of entry matters. *Curr. Opin. Neurobiol.* **5,** 367–374 (1995).

67. Kornhauser, J. M. *et al.* CREB Transcriptional Activity in Neurons Is Regulated by Multiple, Calcium-Specific Phosphorylation Events. *Neuron* **34,** 221–233 (2002).

68. Huber, K. M., Kayser, M. S. & Bear, M. F. Role for Rapid Dendritic Protein Synthesis in Hippocampal mGluR-Dependent Long-Term Depression. *Science* **288,** 1254–1256 (2000).

69. Niswender, C. M. & Conn, P. J. Metabotropic Glutamate Receptors: Physiology, Pharmacology, and Disease. *Annu. Rev. Pharmacol. Toxicol.* **50,** 295–322 (2010).

70. Hermans, E. & Challiss, R. A. J. Structural, signalling and regulatory properties of the group I metabotropic glutamate receptors: prototypic family C G-protein-coupled receptors. *Biochem. J.* **359,** 465–484 (2001).

71. Li, X.-M. *et al.* JNK1 contributes to metabotropic glutamate receptor-dependent long-term depression and short-term synaptic plasticity in the mice area hippocampal CA1. *Eur. J. Neurosci.* **25,** 391–396 (2007).

72. Page, G. *et al.* Group I metabotropic glutamate receptors activate the p70S6 kinase via both mammalian target of rapamycin (mTOR) and extracellular signal-regulated kinase (ERK 1/2) signaling pathways in rat striatal and hippocampal synaptoneurosomes. *Neurochem. Int.* **49,** 413–421 (2006).

73. Hou, L. & Klann, E. Activation of the Phosphoinositide 3-Kinase-Akt-Mammalian Target of Rapamycin Signaling Pathway Is Required for Metabotropic Glutamate Receptor-Dependent Long-Term Depression. *J. Neurosci.* **24,** 6352–6361 (2004).

74. Delgado, J. Y. & O'Dell, T. J. Long-term potentiation persists in an occult state following mGluR-dependent depotentiation. *Neuropharmacology* **48,** 936–948 (2005).

75. Gallagher, S. M., Daly, C. A., Bear, M. F. & Huber, K. M. Extracellular Signal-Regulated Protein Kinase Activation Is Required for Metabotropic Glutamate Receptor-Dependent Long-Term Depression in Hippocampal Area CA1. *J. Neurosci.* **24,** 4859–4864 (2004).

76. Snyder, E. M. *et al.* Internalization of ionotropic glutamate receptors in response to mGluR activation. *Nat. Neurosci.* **4,** 1079–1085 (2001).

77. Lu, W.-Y. *et al.* Activation of Synaptic NMDA Receptors Induces Membrane Insertion of New AMPA Receptors and LTP in Cultured Hippocampal Neurons. *Neuron* **29,** 243–254 (2001).

78. Bekkers, J. M. & Stevens, C. F. NMDA and non-NMDA receptors are co-localized at individual excitatory synapses in cultured rat hippocampus. *Nature* **341,** 230–233 (1989).

79. Jones, K. A. & Baughman, R. W. Both NMDA and non-NMDA subtypes of glutamate receptors are concentrated at synapses on cerebral cortical neurons in culture. *Neuron* **7,** 593–603 (1991).

80. Rao, A. & Craig, A. M. Activity Regulates the Synaptic Localization of the NMDA Receptor in Hippocampal Neurons. *Neuron* **19,** 801–812 (1997).

81. Collingridge, G. L., Peineau, S., Howland, J. G. & Wang, Y. T. Long-term depression in the CNS. *Nat. Rev. Neurosci.* **11,** 459–473 (2010).

82. Esteban, J. A. *et al.* PKA phosphorylation of AMPA receptor subunits controls synaptic trafficking underlying plasticity. *Nat. Neurosci.* **6,** 136–143 (2003).

83. Deisseroth, K., Heist, E. K. & Tsien, R. W. Translocation of calmodulin to the nucleus supports CREB phosphorylation in hippocampal neurons. *Nature* **392,** 198–202 (1998).

84. Dunlap, K. Forskolin prolongs action potential duration and blocks potassium current in embryonic chick sensory neurons. *Pflüg. Arch.* **403,** 170–174 (1985).

85. Oh, M. C., Derkach, V. A., Guire, E. S. & Soderling, T. R. Extrasynaptic Membrane Trafficking Regulated by GluR1 Serine 845 Phosphorylation Primes AMPA Receptors for Long-term Potentiation. *J. Biol. Chem.* **281,** 752–758 (2006).

86. Pickard, L. *et al.* Transient synaptic activation of NMDA receptors leads to the insertion of native AMPA receptors at hippocampal neuronal plasma membranes. *Neuropharmacology* **41,** 700–713 (2001).

87. Nash Joanne E. *et al.* Disruption of the interaction between myosin VI and SAP97 is associated with a reduction in the number of AMPARs at hippocampal synapses. *J. Neurochem.* **112,** 677–690 (2010).

88. Fitzjohn, S. M. *et al.* An electrophysiological characterisation of long-term potentiation in cultured dissociated hippocampal neurones. *Neuropharmacology* **41,** 693–699 (2001).

89. Molnár, E. Long-term potentiation in cultured hippocampal neurons. *Semin. Cell Dev. Biol.* **22,** 506–513 (2011).

90. Goldin, M., Segal, M. & Avignone, E. Functional Plasticity Triggers Formation and Pruning of Dendritic Spines in Cultured Hippocampal Networks. *J. Neurosci.* **21,** 186–193 (2001).

91. Ewald, R. C. & Cline, H. T. NMDA Receptors and Brain Development. in *Biology of the NMDA Receptor* (ed. Van Dongen, A. M.) (CRC Press/Taylor & Francis, 2009).

92. Eisenman, L. N., Emnett, C. M., Mohan, J., Zorumski, C. F. & Mennerick, S. Quantification of bursting and synchrony in cultured hippocampal neurons. *J. Neurophysiol.* **114,** 1059–1071 (2015).

93. Biffi, E., Regalia, G., Menegon, A., Ferrigno, G. & Pedrocchi, A. The Influence of Neuronal Density and Maturation on Network Activity of Hippocampal Cell Cultures: A Methodological Study. *PLoS ONE* **8,** (2013).

94. Nakamura, T. *et al.* Inositol 1,4,5-Trisphosphate (IP3)-Mediated Ca2+ Release Evoked by Metabotropic Agonists and Backpropagating Action Potentials in Hippocampal CA1 Pyramidal Neurons. *J. Neurosci.* **20,** 8365–8376 (2000).

95. Partridge, J. G., Lewin, A. E., Yasko, J. R. & Vicini, S. Contrasting actions of group I metabotropic glutamate receptors in distinct mouse striatal neurones. *J. Physiol.* **592,** 2721–2733 (2014).

96. Kamsler, A., McHugh, T. J., Gerber, D., Huang, S. Y. & Tonegawa, S. Presynaptic m1 muscarinic receptors are necessary for mGluR long-term depression in the hippocampus. *Proc. Natl. Acad. Sci. U. S. A.* **107,** 1618–1623 (2010).

97. Burack, W. R. & Shaw, A. S. Signal transduction: hanging on a scaffold. *Curr. Opin. Cell Biol.* **12,** 211–216 (2000).

98. Andreae, L. C., Fredj, N. B. & Burrone, J. Independent Vesicle Pools Underlie Different Modes of Release during Neuronal Development. *J. Neurosci.* **32,** 1867–1874 (2012).

99. Cork, K. M., Van Hook, M. J. & Thoreson, W. B. Mechanisms, pools, and sites of spontaneous vesicle release at synapses of rod and cone photoreceptors. *Eur. J. Neurosci.* **44,** 2015–2027 (2016).

100. Chamberland, S. & Tóth, K. Functionally heterogeneous synaptic vesicle pools support diverse synaptic signalling: The functional heterogeneity of synaptic vesicle pools. *J. Physiol.* **594,** 825–835 (2016).

101. Walter, A. M., Haucke, V. & Sigrist, S. J. Neurotransmission: Spontaneous and Evoked Release Filing for Divorce. *Curr. Biol.* **24,** R192–R194 (2014).

102. Hua, Z. *et al.* v-SNARE Composition Distinguishes Synaptic Vesicle Pools. *Neuron* **71,** 474–487 (2011).

103. Melom, J. E., Akbergenova, Y., Gavornik, J. P. & Littleton, J. T. Spontaneous and Evoked Release Are Independently Regulated at Individual Active Zones. *J. Neurosci.* **33,** 17253–17263 (2013).

104. Isaacson, J. S. & Walmsley, B. Counting quanta: Direct measurements of transmitter release at a central synapse. *Neuron* **15,** 875–884 (1995).

105.   Wall, M. J. & Usowicz, M. M. Development of the quantal properties of evoked and spontaneous synaptic currents at a brain synapse. *Nat. Neurosci.* **1,** 675–682 (1998).

106.   Atasoy, D. *et al.* Spontaneous and evoked glutamate release activates two populations of NMDA receptors with limited overlap. *J. Neurosci. Off. J. Soc. Neurosci.* **28,** 10151–10166 (2008).

107.   Ramirez, D. M. O. & Kavalali, E. T. Differential Regulation of Spontaneous and Evoked Neurotransmitter Release at Central Synapses. *Curr. Opin. Neurobiol.* **21,** 275–282 (2011).

108.   Prange, O. & Murphy, T. H. Correlation of Miniature Synaptic Activity and Evoked Release Probability in Cultures of Cortical Neurons. *J. Neurosci.* **19,** 6427–6438 (1999).

109.   Sonntag, T. *et al.* Analysis of a cAMP regulated coactivator family reveals an alternative phosphorylation motif for AMPK family members. *PLOS ONE* **12,** e0173013 (2017).

110.   Collas, P. The Current State of Chromatin Immunoprecipitation. *Mol. Biotechnol.* **45,** 87–100 (2010).

111.   Vann, S. D., Brown, M. W., Erichsen, J. T. & Aggleton, J. P. Fos Imaging Reveals Differential Patterns of Hippocampal and Parahippocampal Subfield Activation in Rats in Response to Different Spatial Memory Tests. *J. Neurosci.* **20,** 2711–2718 (2000).

112.   Liu, X. *et al.* Optogenetic stimulation of a hippocampal engram activates fear memory recall. *Nature* **484,** 381–385 (2012).

113.   Farris, S., Wang, Y., Ward, J. M. & Dudek, S. M. Optimized Method for Robust Transcriptome Profiling of Minute Tissues Using Laser Capture Microdissection and Low-Input RNA-Seq. *Front. Mol. Neurosci.* **10,** (2017).

114.   Ofengeim, D., Giagtzoglou, N., Huh, D., Zou, C. & Yuan, J. Single-Cell RNA Sequencing: Unraveling the Brain One Cell at a Time. *Trends Mol. Med.* **23,** 563–576 (2017).

115.   Chen, P. B.-Y. Temporal gene expression during a critical time window following induction of LTP of mouse hippocampal CA3-CA1 synapses. (UCLA, 2016).

116.   Meng, Q. *et al.* Traumatic Brain Injury Induces Genome-Wide Transcriptomic, Methylomic, and Network Perturbations in Brain and Blood Predicting Neurological Disorders. *EBioMedicine* **16,** 184–194 (2017).

117.   Lipponen, A., Paananen, J., Puhakka, N. & Pitkänen, A. Analysis of Post-Traumatic Brain Injury Gene Expression Signature Reveals Tubulins, *Nfe2l2, Nfkb, Cd44, and S100a4* as Treatment Targets. *Sci. Rep.* **6,** 31570 (2016).

118.   Di Pietro, V. *et al.* Transcriptomics of Traumatic Brain Injury: Gene Expression and Molecular Pathways of Different Grades of Insult in a Rat Organotypic Hippocampal Culture Model. *J. Neurotrauma* **27,** 349–359 (2009).

119.   Lamprecht, M. R. *et al.* Strong Correlation of Genome-Wide Expression after Traumatic Brain Injury In Vitro and In Vivo Implicates a Role for SORLA., Strong Correlation of Genome-Wide Expression after Traumatic Brain Injury In Vitro and In Vivo Implicates a Role for SORLA. *J. Neurotrauma J. Neurotrauma* **34, 34,** 97, 97–108 (2017).

120.   Mathis, D. M., Furman, J. L. & Norris, C. M. Preparation of Acute Hippocampal Slices from Rats and Transgenic Mice for the Study of Synaptic Alterations during Aging and Amyloid Pathology. *J. Vis. Exp. JoVE* (2011). doi:10.3791/2330

121.   Villers, A. & Ris, L. Improved Preparation and Preservation of Hippocampal Mouse Slices for a Very Stable and Reproducible Recording of Long-term Potentiation. *J. Vis. Exp. JoVE* (2013). doi:10.3791/50483

122.   Schurr, A., Reid, K. H., Tseng, M. T. & Edmonds, H. L. The stability of the hippocampal slice preparation: An electrophysiological and ultrastructural analysis. *Brain Res.* **297,** 357–362 (1984).

123.   Kidder, B. L., Hu, G. & Zhao, K. ChIP-Seq: Technical Considerations for Obtaining High Quality Data. *Nat. Immunol.* **12,** 918–922 (2011).

124.   Wardle, F. C. & Tan, H. A ChIP on the shoulder? Chromatin immunoprecipitation and validation strategies for ChIP antibodies. *F1000Research* **4,** (2015).

125.   Nonaka, M. *et al.* Region-Specific Activation of CRTC1-CREB Signaling Mediates Long-Term Fear Memory. *Neuron* **84,** 92–106 (2014).

126.   Arrigoni, L. *et al.* Standardizing chromatin research: a simple and universal method for ChIP-seq. *Nucleic Acids Res.* **44,** e67 (2016).

127.   Arrigoni, L. *et al.* Ultra-parallel ChIP-seq by barcoding of intact nuclei. *bioRxiv* 276469 (2018). doi:10.1101/276469

128.   Roh, H. C. *et al.* Simultaneous Transcriptional and Epigenomic Profiling from Specific Cell Types within Heterogeneous Tissues In Vivo. *Cell Rep.* **18,** 1048–1061 (2017).

129.   Mo, A. *et al.* Epigenomic Signatures of Neuronal Diversity in the Mammalian Brain. *Neuron* **86,** 1369–1384 (2015).

130.   Hallet *et al.* Biochemical Fractionation of Brain Tissue for Studies of Receptor Distribution and Trafficking. *Curr. Prot. Neurosci.* (2008).

131.   Krämer, E.-M., Koch, T., Niehaus, A. & Trotter, J. Oligodendrocytes Direct Glycosyl Phosphatidylinositol-anchored Proteins to the Myelin Sheath in Glycosphingolipid-rich Complexes. *J. Biol. Chem.* **272,** 8937–8945 (1997).

132.   Huang, W., Alessandrini, A., Crews, C. M. & Erikson, R. L. Raf-1 forms a stable complex with Mek1 and activates Mek1 by serine phosphorylation. *Proc. Natl. Acad. Sci.* **90,** 10947–10951 (1993).

133.   Bortolotto, Z. A., Amici, M., Anderson, W. W., Isaac, J. T. R. & Collingridge, G. L. Synaptic Plasticity in the Hippocampal Slice Preparation. *Curr. Protoc. Neurosci.* **54,** 6.13.1-6.13.26 (2011).

134.   Chen, P. B. *et al.* Mapping Gene Expression in Excitatory Neurons during Hippocampal Late-Phase Long-Term Potentiation. *Front. Mol. Neurosci.* **10,** 39 (2017).

135.   Fontes, M. M. *et al.* Activity-Dependent Regulation of Alternative Cleavage and Polyadenylation During Hippocampal Long-Term Potentiation. *Sci. Rep.* **7,** 17377 (2017).

136. Blitzer, R. D., Wong, T., Nouranifar, R., Iyengar, R. & Landau, E. M. Postsynaptic CAMP pathway gates early LTP in hippocampal CA1 region. *Neuron* **15,** 1403–1414 (1995).

137. Winder, D. G., Mansuy, I. M., Osman, M., Moallem, T. M. & Kandel, E. R. Genetic and Pharmacological Evidence for a Novel, Intermediate Phase of Long-Term Potentiation Suppressed by Calcineurin. *Cell* **92,** 25–37 (1998).

138. Thomas, M. J., Moody, T. D., Makhinson, M. & O'Dell, T. J. Activity-Dependent β-Adrenergic Modulation of Low Frequency Stimulation Induced LTP in the Hippocampal CA1 Region. *Neuron* **17,** 475–482 (1996).

139. Chotiner, J. K., Khorasani, H., Nairn, A. C., O'Dell, T. J. & Watson, J. B. Adenylyl cyclase-dependent form of chemical long-term potentiation triggers translational regulation at the elongation step. *Neuroscience* **116,** 743–752 (2003).

140. Makhinson, M., Chotiner, J. K., Watson, J. B. & O'Dell, T. J. Adenylyl Cyclase Activation Modulates Activity-Dependent Changes in Synaptic Strength and Ca2+/Calmodulin-Dependent Kinase II Autophosphorylation. *J. Neurosci.* **19,** 2500–2510 (1999).

141. Morishita, W. *et al.* Regulation of Synaptic Strength by Protein Phosphatase 1. *Neuron* **32,** 1133–1148 (2001).

142. Kameyama, K., Lee, H.-K., Bear, M. F. & Huganir, R. L. Involvement of a Postsynaptic Protein Kinase A Substrate in the Expression of Homosynaptic Long-Term Depression. *Neuron* **21,** 1163–1175 (1998).

143. Kim, J. J., Foy, M. R. & Thompson, R. F. Behavioral stress modifies hippocampal plasticity through N-methyl-D-aspartate receptor activation. *Proc. Natl. Acad. Sci.* **93,** 4750–4753 (1996).

144. Yang, C.-H., Huang, C.-C. & Hsu, K.-S. Behavioral Stress Enhances Hippocampal CA1 Long-Term Depression through the Blockade of the Glutamate Uptake. *J. Neurosci.* **25,** 4288–4293 (2005).

145.   Wong, T. P. *et al.* Hippocampal long-term depression mediates acute stress-induced spatial memory retrieval impairment. *Proc. Natl. Acad. Sci. U. S. A.* **104,** 11471–11476 (2007).

146.   Xu, L., Anwyl, R. & Rowan, M. J. Behavioural stress facilitates the induction of long-term depression in the hippocampus. *Nature* **387,** 497–500 (1997).

147.   Staubli, U. & Scafidi, J. Studies on Long-Term Depression in Area CA1 of the Anesthetized and Freely Moving Rat. *J. Neurosci.* **17,** 4820–4828 (1997).

148.   Babiec, W. E. *et al.* Ionotropic NMDA Receptor Signaling Is Required for the Induction of Long-Term Depression in the Mouse Hippocampal CA1 Region. *J. Neurosci.* **34,** 5285–5290 (2014).

149.   Stanton, P. K., Chattarji, S. & Sejnowski, T. J. 2-Amino-3-phosphonopropionic acid, an inhibitor of glutamate-stimulated phosphoinositide turnover, blocks induction of homosynaptic long-term depression, but not potentiation, in rat hippocampus. *Neurosci. Lett.* **127,** 61–66 (1991).

150.   Collingridge, G. L., Isaac, J. T. R. & Wang, Y. T. Receptor trafficking and synaptic plasticity. *Nat. Rev. Neurosci.* **5,** 952–962 (2004).

151.   Bolshakov, V. Y. & Siegelbaum, S. A. Postsynaptic induction and presynaptic expression of hippocampal long-term depression. *Science* **264,** 1148–1152 (1994).

152.   Massey, P. V. & Bashir, Z. I. Long-term depression: multiple forms and implications for brain function. *Trends Neurosci.* **30,** 176–184 (2007).

153.   Rammes, G. *et al.* Activation of mGlu receptors induces LTD without affecting postsynaptic sensitivity of CA1 neurons in rat hippocampal slices. *J. Physiol.* **546,** 455–460 (2003).

154.   Lindecke, A. *et al.* Long-term depression activates transcription of immediate early transcription factor genes: involvement of serum response factor/Elk-1. *Eur. J. Neurosci.* **24,** 555–563 (2006).

155. Heinz, S. *et al.* Simple Combinations of Lineage-Determining Transcription Factors Prime cis-Regulatory Elements Required for Macrophage and B Cell Identities. *Mol. Cell* **38,** 576–589 (2010).

156. McLean, C. Y. *et al.* GREAT improves functional interpretation of *cis*-regulatory regions. *Nat. Biotechnol.* **28,** 495–501 (2010).

157. Huang, D. W. *et al.* DAVID Bioinformatics Resources: expanded annotation database and novel algorithms to better extract biology from large gene lists. *Nucleic Acids Res.* **35,** W169-175 (2007).

158. Huang, D. W., Sherman, B. T. & Lempicki, R. A. Systematic and integrative analysis of large gene lists using DAVID bioinformatics resources. *Nat. Protoc.* **4,** 44–57 (2009).

159. Lachmann, A. *et al.* ChEA: transcription factor regulation inferred from integrating genome-wide ChIP-X experiments. *Bioinformatics* **26,** 2438–2444 (2010).

160. Miao, F., Wu, X., Zhang, L., Riggs, A. D. & Natarajan, R. Histone Methylation Patterns Are Cell-Type Specific in Human Monocytes and Lymphocytes and Well Maintained at Core Genes. *J. Immunol. Baltim. Md 1950* **180,** 2264–2269 (2008).

161. Mito, M. *et al.* Cell Type-Specific Survey of Epigenetic Modifications by Tandem Chromatin Immunoprecipitation Sequencing. *Sci. Rep.* **8,** 1143 (2018).

162. Maruyama, R. *et al.* Epigenetic Regulation of Cell Type–Specific Expression Patterns in the Human Mammary Epithelium. *PLOS Genet.* **7,** e1001369 (2011).

163. Wang, X., Zhang, C., Szábo, G. & Sun, Q.-Q. Distribution of CaMKIIα expression in the brain in vivo, studied by CaMKIIα-GFP mice. *Brain Res.* **1518,** 9–25 (2013).

164. Mayford, M. *et al.* Control of Memory Formation Through Regulated Expression of a CaMKII Transgene. *Science* **274,** 1678–1683 (1996).

165. Experiment Detail :: Allen Brain Atlas: Mouse Brain. Available at: http://mouse.brain-map.org/experiment/show/79490122. (Accessed: 23rd April 2018)

166. Lalmansingh, A. S., Urekar, C. J. & Reddi, P. P. TDP-43 Is a Transcriptional Repressor. *J. Biol. Chem.* **286,** 10970–10982 (2011).

167. Sun, L. *et al.* Transcriptional repression of SIRT1 by protein inhibitor of activated STAT 4 (PIAS4) in hepatic stellate cells contributes to liver fibrosis. *Sci. Rep.* **6,** 28432 (2016).

168. Bartoszewski, R. *et al.* The Mechanism of Cystic Fibrosis Transmembrane Conductance Regulator Transcriptional Repression during the Unfolded Protein Response. *J. Biol. Chem.* **283,** 12154–12165 (2008).

169. Zeng, L. *et al.* ATF6 modulates SREBP2-mediated lipogenesis. *EMBO J.* **23,** 950–958

170. Knöll, B. & Nordheim, A. Functional versatility of transcription factors in the nervous system: the SRF paradigm. *Trends Neurosci.* **32,** 432–442 (2009).